Targeting Eukaryotic Initiation Factor 4A to Improve Response to Chemotherapy in Acute Myeloid Leukemia

Katie Fooks

Department of Medicine

Division of Experimental Medicine

McGill University, Montreal

December 2021

A thesis submitted to McGill University in partial fulfillment of the requirements of the Degree of Master of Science

Table of Contents

Abstract

Acute myeloid leukemia (AML) is an aggressive hematological cancer characterized by uncontrolled proliferation of myeloid cells blocked in differentiation. AML accounts for the highest proportion of adult leukemia deaths in North America and progresses rapidly without treatment. The standard of care for patients without significant medical comorbidities remains myeloablative chemotherapy with cytarabine and daunorubicin, often followed by hematopoietic stem cell transplantation. However, despite this intensive treatment, more than 50% of patients initially achieving remission relapse within 5 years. Resistance to chemotherapy and relapse remain major problems in the treatment of AML and contribute to the overall poor prognosis. Relapse is thought to originate from a small reservoir of residual AML cells which persist following treatment. Although the mechanisms by which these cells survive chemotherapy are unclear, recent studies examining residual AML cells isolated from cytarabine-treated murine models suggest that persisting AML cells develop metabolic adaptations such as elevated mTORC1 signalling and mitochondrial activity. While mTORC1 signalling is known to regulate several metabolic and pro-survival pathways within cancer cells through control of cap-dependent mRNA translation, inhibitors of mTORC1 have displayed poor clinical efficacy in AML due to intracellular feedback mechanisms. We hypothesized that targeting mRNA translation initiation downstream of mTORC1, through pharmacological inhibition of eukaryotic initiation factor 4A (eIF4A), may produce a better anti-leukemic effect.

To characterize the response of AML to chemotherapy and inhibition of eIF4A, we established syngeneic and xenograft murine models of AML as an experimental platform. We first tested the effect of chemotherapy on AML cells *in vitro* and *in vivo*, and observed increased mTORC1 activity and protein synthesis, in support of an induction of cap-dependent translation initiation in this context. Next, we investigated the effect of the eIF4A-inhibitor CR-1-31-B on AML cell lines *in vitro* and observed an increase in reactive oxygen species and DNA damage, leading to cell cycle arrest and apoptosis and suggesting a critical role of eIF4A in promoting AML survival. We observed that eIF4A inhibition using CR-1-31-B led to downregulation of the anti-apoptotic protein BCL-2, highlighting a possible mechanism of cell death. Further, we treated AML cells with varying doses of cytarabine and CR-1-31-B in combination and found synergy *in vitro*, confirming the role of eIF4A in promoting chemoresistance. *In vivo*, CR-1-31-B significantly reduced leukemic growth in a murine xenotransplantation model of the AML cell line

MOLM-14, suggesting it may have therapeutic potential. To test whether CR-1-31-B was toxic to non-malignant hematopoietic cells, we treated wild-type mice with the same regimen and found no suppression of myelopoiesis, although we observed an isolated impairment in bone marrow derived B-lymphopoiesis. Overall, results from this thesis suggest that eIF4A may be a prospective target to improve response to chemotherapy in AML. This fits in the broader context that persistence of AML cells after chemotherapy remains a significant clinical challenge, and better understanding the dependencies of residual cells could lead to new approaches or therapies to inhibit adaptations and diminish resistance.

Résumé

La leucémie aiguë myéloïde (LAM) est un cancer hématologique agressif caractérisé par une prolifération incontrôlée de cellules myéloïdes bloquées en différenciation. La LAM représente la proportion la plus élevée de décès par leucémie chez l'adulte en Amérique du Nord et progresse rapidement sans traitement. La norme de soins pour les patients sans comorbidités médicales significatives reste la chimiothérapie myéloablative avec la cytarabine et la daunorubicine, souvent suivie d'une greffe de cellules souches hématopoïétiques. Cependant, malgré ce traitement intensif, plus de 50 % des patients en rémission initiale rechutent dans les 5 ans. La résistance à la chimiothérapie et les rechutes restent des problèmes majeurs dans le traitement de la LAM et contribuent au mauvais pronostic global. On pense que la rechute provient d'un petit réservoir de cellules leucémiques résiduelles qui persistent après le traitement. Bien que les mécanismes par lesquels ces cellules survivent à la chimiothérapie ne soient pas clairs, des études récentes examinant les cellules leucémiques résiduelles isolées de modèles murins traités à la cytarabine suggèrent que les cellules LAM persistantes développent des adaptations métaboliques telles qu'une signalisation mTORC1 élevée et une activité mitochondriale. Alors que la signalisation mTORC1 est connue pour réguler plusieurs voies métaboliques et pro-survie dans les cellules cancéreuses par le contrôle de la traduction de l'ARNm, les inhibiteurs de mTORC1 ont montré peu d'efficacité clinique dans la LAM en raison de mécanismes de rétroaction intracellulaire. Nous avons émis l'hypothèse que le ciblage de l'initiation de la traduction de l'ARNm en aval de mTORC1, via l'inhibition pharmacologique du facteur d'initiation eucaryote 4A (eIF4A), peut produire un meilleur effet anti-leucémique.

Pour caractériser la réponse de la LAM à la chimiothérapie et l'inhibition de eIF4A, nous avons établi des modèles murins syngéniques et xénogreffés de la LAM en tant que plate-forme expérimentale. Nous avons d'abord testé l'effet de la chimiothérapie sur les cellules AML in vitro et in vivo, et observé une augmentation de l'activité mTORC1 et de la synthèse des protéines, en faveur d'une induction de l'initiation de la traduction cap-dépendante dans ce contexte. Ensuite, nous avons étudié l'effet de l'inhibiteur eIF4A CR-1-31-B sur les lignées cellulaires AML in vitro et avons découvert qu'il s'agissait d'un puissant inducteur d'espèces réactives de l'oxygène et de dommages à l'ADN, entraînant l'arrêt du cycle cellulaire et l'apoptose et suggérant un rôle de eIF4A dans la promotion de la survie de la LAM. Nous avons observé que la protéine anti-apoptotique

BCL-2 est régulée à la baisse suite à l'inhibition de eIF4A, mettant en évidence un mécanisme possible de mort cellulaire. De plus, nous avons traité des cellules AML avec des doses variables de cytarabine et de CR-1-31-B en combinaison et avons découvert que ces composés sont synergiques, confirmant le rôle d'eIF4A dans la promotion de la chimiorésistance. In vivo, CR-1-31-B a réduit de manière significative la croissance leucémique dans un modèle murin de xénotransplantation de la lignée cellulaire LAM MOLM-14, suggérant qu'il pourrait avoir un potentiel thérapeutique. Pour tester si le CR-1-31-B était toxique pour les cellules hématopoïétiques non malignes, nous avons traité des souris de type sauvage avec le même régime et trouvé que les souris n'avaient pas de perte de poids, bien que nous ayons observé une altération isolée de la lymphopoïèse B dérivée de la moelle osseuse. Dans l'ensemble, les résultats de cette thèse suggèrent que eIF4A peut être une cible pour améliorer la réponse à la chimiothérapie dans la LAM. Cela s'inscrit dans le contexte plus large que la persistance des cellules AML après la chimiothérapie reste un défi clinique important, et une meilleure compréhension des dépendances des cellules résiduelles pourrait conduire à de nouvelles approches ou thérapies pour inhiber les adaptations et diminuer la résistance.

Acknowledgments

First and foremost, I would like to thank my supervisor Dr. Francois Mercier for giving me this opportunity, and for his patience and support. Thank you for believing in me, and for being so generous with your time and advice. I feel lucky to have worked with you.

Thank you to my committee members, Drs. Koren Mann, Stephanie Lehoux, and Nathalie Johnson, for their insightful and constructive input. I would also like to thank Dr. Laura Hulea and Zaynab Nouhi, for all of the guidance and assistance in troubleshooting they provided over the course of this project.

To the wonderful members of the Mercier lab: Maja Jankovic, Wai Lam Poon, Gabriela Galicia-Vazquez, Samantha Worme and Alexandre Bazinet, thank you for always making time to offer encouragement and ideas and to answer my endless questions. This project would not have been completed without your friendship and support. Thank you also to the members of the Orthwein lab for the advice and technical assistance they provided on this project.

To Twin, Megan, and Dad, thank you for encouraging me and for being my life-long cheerleaders. Finally, I would not be the person I am today without the support of my Mom, who has always believed in me and who is always with me.

Contribution of Authors

Dr. Francois Mercier designed and supervised this project, in addition to revising the manuscript. Gabriela Galicia-Vazquez also assisted with experimental planning and manuscript revision. Zaynab Nouhi performed the polysome fractionation experiments and extracted RNA for polysome sequencing. Dr. Laura Hulea and Zaynab Nouhi provided guidance on experimental planning. Western blot assays were performed by Zaynab Nouhi and Raul Flores Gonzalez. Wai Lam Poon and Vincent Luo performed the flow cytometry for bone marrow and spleen samples isolated from healthy C57BL/6 mice treated with CR-1-31-B, and Vincent Luo assisted with analysis of the spleen data. I performed the cell viability assays, viral transfection and transductions, colony-forming assays, and all other flow cytometry assays in addition to data analysis. Francois Mercier and I performed the animal experiments. I performed the immunofluorescence sample preparation and Vincent Luo performed the fluorescence microscopy. Flow cytometry and microscopy were performed at the Lady Davis Institute Flow

Cytometry Core and Cell Imaging Facility managed by Christian Young. Dr. Alexandre Bazinet provided guidance on flow cytometry throughout.

List of Abbreviations

2-HG: D-2-Hydroxyglutarate

4EBP1: 4E-Binding Protein 1

a-KG: alpha-Ketoglutarate

AML: Acute Myeloid Leukemia

APL: Acute Promyelocytic Leukemia

ASXL1: Additional Sex Combs-Like 1

ATM: Ataxia Telangiectasia Mutated kinase

ATR: Ataxia Telangiectasia and Rad3-related protein

BCL-2: B-cell Lymphoma 2

BM: Bone Marrow

CEBPA: CCAAT/Enhancer Binding Protein A

CFU: Colony-Forming Unit

CLP: Common Lymphoid Progenitor

CMP: Common Myeloid Progenitor

CR: Complete Remission

DEPTOR: DEP domain-containing mTOR interacting protein

DMSO: Dimethyl Sulfoxide

DNMT3: DNA methyltransferase

ELN: European Leukemia Net

eIF: Eukaryotic Initiation Factor

FAB: French American British

FBS: Fetal Bovine Serum

FDR: False Discovery Rate

FLT3: Fms-related Tyrosine Kinase 3

GMP: Granulocyte-Macrophage Progenitor

G/C: Guanine & Cytosine

HSC: Hematopoietic Stem Cell

HSF1: Heat Shock Response Factor 1

IRES: Internal Ribosome Entry Site

IDH: Isocitrate Dehydrogenase

LSC: Leukemic Stem Cell

LT-HSC: Long-Term Hematopoietic Stem Cell

MAPK-ERK: Mitogen Activated Protein Kinase-Extracellular Signal-Regulated Kinase

MDR1: Multidrug Resistance Glycoprotein 1

MEP: Megakaryocyte Erythrocyte Progenitor

mLST8: Mammalian Lethal with sec13 protein 8

MMP: Mitochondrial Membrane Potential

MPP: Multipotent Progenitor

mRNA: messenger RNA

mTORC1: Mammalian Target of Rapamycin Complex 1

mTORC2: Mammalian Target of Rapamycin Complex 2

NGS: Next-Generation Sequencing

NOD/Scid: Non-Obese Diabetic/Severe Combined Immunodeficiency

NSG: NOD/Scid /IL-2Rγc^{null}

NSG-S: NOD/Scid /IL-2Rγc^{null}/IL-3/GM-CSF/SCF

NPM1: Nucleophosmin 1

OS: Overall Survival

pAkt: Phosphorylated-Akt

pS6: Phosphorylated-S6

p4EBP1: Phosphorylated-4EBP1

PB: Peripheral Blood

PDA: Pancreatic Ductal Adenocarcinoma

PDX: Patient Derived Xenograft

PI3K: Phosphoinositide 3-Kinase

Poly(A)-binding Protein: PABP

Raptor: Regulatory-Associated Protein of mTOR

Rictor: Rapamycin-Insensitive Companion

RNA: Ribonucleic Acid

ROS: Reactive Oxygen Species

S6: Ribosomal Protein S6

S6K: p70 S6 Kinase

SIN1: Stress-activated protein kinase interacting protein 1

ST-HSC: Short-Term Hematopoietic Stem Cell

TISU: Translation Initiator of Short 5′ UTR

TMRE: Tetramethylrhodamine ethyl ester

TP53: Tumor Protein p53

UTR: Untranslated Region

WHO: World Health Organization

γH2AX: Phosphorylated H2A histone family member X

Chapter 1: Introduction

1.1 Acute Myeloid Leukemia

1.1.1 Introduction to Hematopoiesis

Hematopoiesis is a tightly regulated hierarchical process in which multipotent hematopoietic stem cells (HSCs) self-renew or undergo differentiation to give rise to the lineages of the blood (**Figure 1.1**) [1]. In humans, hematopoiesis first begins in early embryonic development within the yolk sac and later transitions into the bone marrow (BM) [1]. The BM is the primary site of blood cell production in adults and generates up to 500 billion hematopoietic cells per day [2]. Mature blood cells are typically categorized as either myeloid or lymphoid cells, and these lineages are thought to diverge at the progenitor level from HSCs into common lymphoid progenitors (CLPs) or common myeloid progenitors (CMPs) [3, 4]. CLPs differentiate into lymphocytes to produce natural killer cells, B cells, and T cells, which constitute the adaptive immune system [3]. CMPs produce lineage-restricted granulocyte macrophage progenitors (GMPs) or megakaryocyte erythrocyte progenitors (MEPs) [3]. GMPs differentiate into myeloid cell types such as monocytes and granulocytes, which mediate innate immunity, while MEPs differentiate into erythrocytes and megakaryocytes which deliver oxygen throughout the body and generate platelets, respectively. Commitment to these lineages is regulated by key transcription factors which maintain the balance between self-renewal and hematopoietic differentiation [5]. Once blood cells have matured within the BM, they migrate across the endothelium into the circulation. T cell and B cell progenitors derived from CLPs similarly leave the BM to migrate to the secondary lymphoid organs for further development [2].

HSCs were first defined in the 1960s by Till and McCulloch, who demonstrated that intravenous injection of murine BM cells into irradiated mice produced multilineage hematopoietic colonies in the spleen [6]. They later demonstrated that these colonies were formed by single cells with multipotent potential [7]. To better characterize HSCs, subsequent studies focused on developing methods to purify these cells and identify HSC markers. Although much of our understanding of hematopoiesis and HSC function has been derived from mouse models, it is important to note that HSC markers vary between human and mice. In humans, HSCs are enriched within the $CD34^+$, $CD38^-$, $CD90^+$ population, while murine HSCs are often identified as $CD34^-$, $CD38^+$, Sca-1^+ c-KIT^+ cells [8-11]. More recent studies have further defined distinct populations of HSCs within the BM; known as long-term (LT-HSCs) and short-term HSCs (ST-HSCs) [12].

LT-HSCs are largely quiescent but can divide to maintain the pool of HSCs or mature into ST-HSCs, which have a more limited self-renewal capacity. ST-HSCs are responsible for producing multipotent progenitor cells (MPPs), which develop into the CMPs and CLPs [12, 13]. These LT-HSC and ST-HSC subpopulations can also be distinguished by CD34 and CD150 expression in mouse models, as LT-HSCs are $CD34^{-}$ $CD150^{+}$ while ST-HSCs become $CD34^{+}$ $CD150^{-}$ [13, 14].

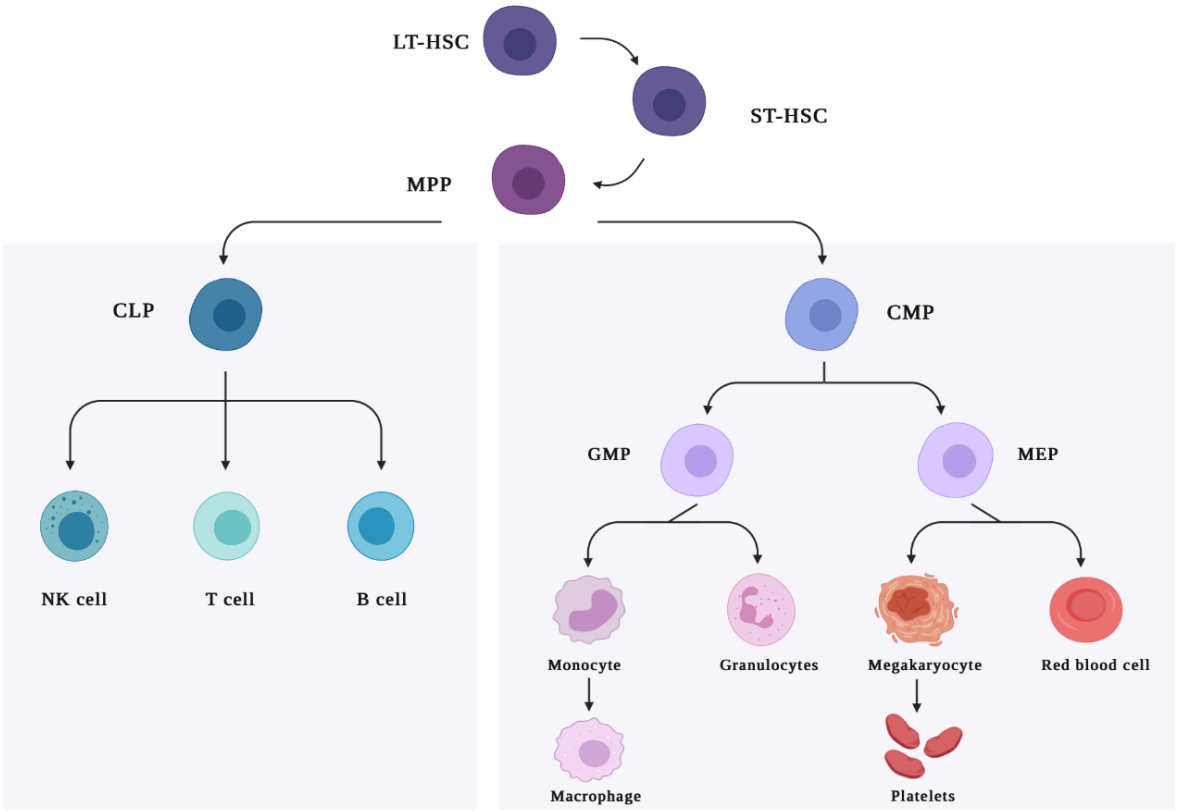

Figure 1.1. Overview of Hematopoietic Differentiation
LT-HSCs sit at the apex of the hematopoietic hierarchy. LT-HSC differentiate in ST-HSCs, which can then mature to MPPs. MPPs can differentiate into CMP or CLPs, representing the earliest lineage commitment. CLPs produce lymphocytes, while CMPs mature into GMPs or MEPs. GMPs can give rise to granulocytes and monocytes/macrophages, and MEPs produce megakaryocytes/platelets and erythrocytes. Abbreviations: LT/ST-HSC: Long/Short-Term Hematopoietic Stem Cell, MPP: Multipotent Progenitor, CLP: Common Lymphocyte Progenitor, CMP: Common Myeloid Progenitor: GMP: granulocyte macrophage progenitor, MEP: Megakaryocyte Erythrocyte Progenitor. Figure adapted from [150] and "Blood Cancers" by BioRender.

1.1.2 Introduction to AML

AML is an aggressive hematological cancer characterized by the rapid growth and accumulation of malignant hematopoietic cells of the myeloid lineage in the BM, blood, and other hematopoietic tissues. AML represents the most common form of acute leukemia and is rapidly fatal if left untreated [15]. In AML, mutations or translocations in myeloid progenitor cells produce immature neoplastic cells which expand within the BM and other organs to impair functional blood cell production. The loss of healthy mature blood cells produces symptoms such as anemia, fatigue, and weight loss, and leaves AML patients highly vulnerable to infections and excessive bleeding [15]. Consequently, AML patients often require urgent therapeutic intervention after the diagnosis is made.

AML is considered a disease of predominately older adults, with the median age of diagnosis being 68 years [16]. Most AML cases develop *de novo*, meaning without known prior disorder of the blood system. However AML may also develop after prior exposure to chemotherapy or radiation (therapy-related AML), prior conditions such as myelodysplastic syndrome or myeloproliferative neoplasms (secondary AML), or Down syndrome [16]. Epidemiological data from the American Cancer Society shows a steady increase in AML incidence with an increase from 3.4 to 6.0 cases per 100,000 persons in the last 10 years [17], which follows aging of the general population. Consequently, the incidence of AML is expected to continue rising in North America [16]. AML has been found to be more common among males for reasons that remain unclear. AML also has a small peak of incidence in the pediatric population, accounting for an estimated 25% of pediatric leukemia. Compared to adult disease, pediatric AML is relatively rare and differs at the molecular level; it has a greater frequency of chromosomal translocations and a lesser burden of somatic mutations [18]. Nevertheless, some chromosomal translocations recur in adult and pediatric cases, albeit at different frequencies (KMT2A-MLLT3, RUNX1-RUNX1T1 translocations are more common in pediatric AML).

1.1.3 Subtypes, Prognosis, and Classification of AML

AML is a highly complex and heterogenous disease with multiple subtypes driven by diverse genetic and epigenetic mutations. The diagnosis of AML is usually made first by a morphological evaluation of a BM biopsy or peripheral blood (PB) smear, demonstrating the presence of leukemic cells called blasts. However, a full diagnostic evaluation requires multiple

tests, including cytogenetic studies and fluorescence *in situ* hybridization to identify chromosomal translocations, DNA sequencing to detect somatic mutations, and immunophenotyping by flow cytometry to characterize the subtype of AML and maturation stage [19]. A BM or PB blast cell count of greater than or equal to 20% is required for an AML diagnosis, except in cases of specific chromosomal translocations (e.g., t(8;21), t(15;17)) that are pathognomonic of AML, in which cases lower blast counts are permitted [19].

Until 2001, AML was primarily classified according to the French-American-British (FAB) system with eight subtypes ranging from M0 – M7 [20]. These subtypes were based on the lineage and stage of differentiation of leukemic cells, as determined by cytochemical staining of a BM aspirate. For example, M0 AML originates in progenitor cells with no evidence of myeloid differentiation (minimally differentiated AML) while M6 AML arises from red blood cell precursors (acute erythroblastic AML). Treatment of the different FAB subtypes is similar, apart from the M3 subtype known as acute promyelocytic leukemia (APL) that is treated with all-trans retinoic acid and arsenic trioxide. Following the identification of recurrent AML mutations, the World Health Organization (WHO) created a new AML categorization system in 2008, which integrated cytogenetic, prognostic, and clinical factors with cell morphology and immunophenotype [21]. The WHO classification system was recently revised in 2016 and includes six broad AML subtypes: AML with recurrent genetic abnormalities, AML with myelodysplasia-related changes, therapy-related myeloid neoplasms, AML not otherwise specified, myeloid sarcoma, and myeloid proliferations related to Down syndrome [22]. AML is also often classified using the prognostic risk groups defined by the European Leukemia Net (ELN; favorable, intermediate, and adverse risk), which are based on a combination of cytogenetic alterations and specific genetic mutations (**Table 1.1**) [19]. These prognostic groups are predictive of patient overall survival (OS) across age groups and are often used to identify the most appropriate treatment.

In recent years, the development of next-generation sequencing (NGS) technologies has transformed the molecular understanding of AML and informed more precise classification practices. Prior to the application of NGS platforms, AML was conventionally classified using cytogenetics. However, almost 50% of AML cases exhibit a normal karyotype or intermediate cytogenetic risk, which represents a heterogeneous group of patients with a range of clinical outcomes [23]. Profiling by NGS of large AML patient cohorts facilitated the identification of

multiple recurrent driver mutations, and has validated the concept that competing clones may develop or coexist within patients and lead to clonal evolution [24]. The characterization of recurrent mutations has improved the classification of AML cases by identifying further subgroups with prognostic significance. These commonly identified genetic mutations in AML are often grouped by function (**Table 1.2**) and include mutations in myeloid transcription factors, epigenetic regulators, nucleophosmin (NPM1), signaling genes, tumor-suppressor genes, spliceosome-complex genes, and cohesin-complex genes [23]. The most frequently identified mutations in AML include Fms-related tyrosine kinase 3 (FLT3) and NPM1, which are altered in 30% of AML patients, as well as mutations in isocitrate dehydrogenase (IDH1/IDH2) and DNA methyltransferase 3A (DNMT3A), which are detected in an estimated 20% of AML patients [25]. The improved characterization of recurrent mutations additionally led the 2017 ELN guidelines to recognize mutations in NPM1, FLT3, CCAAT/enhancer binding protein a (CEBPA), additional sex combs-like 1 (ASXL1), and tumor protein p53 (TP53) as having prognostic relevance and influencing response to treatment [19]. Notably, the co-occurrence of specific mutations in AML cells can further change prognosis and treatment efficacy. For example, mutations in NPM1 alone confer a favorable prognostic risk while co-occurring NPM1 and FLT3-ITD mutations signify a poor risk prognosis [19]. Thus, understanding a patient's complete genomic landscape is important in providing an accurate diagnosis and guiding decisions about treatment. Additional genetic markers are likely to be incorporated into AML clinical classification guidelines with improved understanding of how distinct molecular subgroups and co-occurring mutations inform disease evolution and prognostic stratification [19]. However, despite these advances in the understanding of AML genetics, there have been few improvements in the treatment of AML until recently and the prognosis of many AML patient groups has remained poor.

Table 1.1. 2017 ELN Genetic Risk Stratification

Risk Category	Key Mutations
Favorable	RUNX1-RUNX1T1
	CBFB-MYH11
	Mutated NPM1 without FLT3-ITD or with FLT3-ITD^{low}
	Biallelic mutated CEBPA
Intermediate	Mutated NPM1 and FLT3-ITD^{high}
	Wild-type NPM1 without FLT3-ITD or with FLT3-ITD^{low} (without adverse-risk genetic lesions)
	Mutated NPM1 and FLT3-ITD^{high} MLLT3-KMT2A
	Cytogenetic abnormalities not classified as favorable or adverse
Adverse	DEK-NUP214
	KMT2A rearranged
	BCR-ABL1
	GATA2, MECOM(EVI1)
	−5 or del(5q); −7; −17/abn(17p)
	Complex karyotype, monosomal karyotype
	Wild-type NPM1 and FLT3-ITD^{high}
	Mutated RUNX1 or ASXL1, except if co-occurring with favorable-risk AML subtypes
	Mutated TP53

Table adapted from [19]

Table 1.2. Recurrent AML Mutations by Functional Group

Functional Category	Key Mutations	Estimated Frequency
Signaling genes	*FLT3, KRAS, NRAS, KIT,*	*59%*
DNA-methylation genes	*DNMT3A/DNMT3B, IDH/ IDH2, TET1/TET2,*	*44%*
Chromatin modifying genes	*ASXL1, MLL fusions*	*30%*
Nucleophosmin	*NPM1*	*27%*
Myeloid transcription factors	*CEBPA, RUNX1, GATA2*	*22%*
Transcription factor fusions	*PML-RARA, MYH11-CBFB,*	*18%*
Tumor-suppressor genes	*TP53, WT1*	*16%*
Spliceosome-complex genes	*SRSF2, U2AF1, METTL3, ZRSR2*	*14%*
Cohesin-complex genes	*RAD21, STAG1/STG2, SMC3*	*13%*

Table adapted from [23] and [25]

1.1.4 Current Therapies

Most AML patients eligible for chemotherapy are treated using a combination of cytarabine with an anthracycline, administered in several cycles of "induction" followed by "consolidation". The intensive induction chemotherapy regimen consists of a continuous infusion of cytarabine given for seven days with the anthracycline (e.g. daunorubicin) given concurrently for the first three days; thus, this regimen is often referred as "7+3". With this induction regimen, 60-80% of patients under the age of 60 years and 40-60% of older patients achieve complete remission (CR), defined by the disappearance of blasts on a BM aspirate smear and restoration of normal PB cell counts [19]. After induction chemotherapy, consolidation treatment is generally advised to prevent regrowth of rare AML cells and relapse. Consolidation can be administered as additional cycles of cytarabine for patients with favourable prognostic scores, or allogeneic BM transplantation for patients with greater risk of relapse. Still, despite these intensive regimens, more than 50% of AML patients reaching CR relapse within five years and OS remains poor for these patients [19]. AML

patients identified as adverse risk using ELN criteria respond particularly poorly to treatment, exhibiting overall 5-year survival rates of 12% and only 6% in patients over 60 [26]. In addition, intensive chemotherapy is often not suitable for older adults and those with significant comorbidities, making treatment of these groups a challenge. As such, defining mechanisms of resistance and identifying novel therapeutic targets is crucial to improving AML patient outcomes.

A range of therapies have been approved within the past 10 years as combination or monotherapies, including for patients ineligible for intensive chemotherapy or with specific genetic mutations. The improved understanding of the genetic and epigenetic landscape of AML has enabled the development of targeted therapies directed against key pathways or driver mutations. These include small molecule inhibitors targeting mutated FLT3 (eg. gilteritinib, midostaurin) and IDH1/2 (eg. ivosidenib, enasidenib) that can be used to improve response to induction chemotherapy or as alternate palliative monotherapy [27]. However, when used as single agents, these targeted therapies almost always select for resistant AML clones and their overall use remains limited to patients with these specific abnormalities (16-20% of cases with IDH1/2 mutations and 30% of cases with FLT3 mutations). The combination of a DNA hypomethylating agent (eg. azacitidine) with the BCL-2 inhibitor venetoclax has recently been shown to prolong survival in elderly AML patients or those unfit for intensive chemotherapy [28]. The mechanism underlying this synergy is still unclear. The inhibition by venetoclax of the anti-apoptotic B-cell lymphoma 2 (BCL-2) protein has been shown in AML cells to suppress mitochondrial polarization, highlighting a possible role of this organelle in cell survival and chemoresistance [29]. The mechanism by which hypomethylating agents act against AML is not completely understood, however they are thought to reactivate the expression of tumor suppressor genes or antigens [30]. Although this regimen may become the novel standard of care for AML patients not fit for chemotherapy, it remains non-curative and modestly extends survival (14.7 months versus 9.6 months in the control arm) [28].

For patients with relapsed or refractory AML, treatment remains a significant challenge and prognostic factors must be evaluated to determine whether additional treatment may have a benefit. For younger patients, an estimated 55% can achieve a second CR with salvage chemotherapy. However, for older adults or those with second or third relapses, there are very few treatment options and median survival is estimated to be only 3 months [19]. The intrinsic heterogeneity of AML makes it difficult to develop drugs effective for patients of diverse molecular subtypes and

ages. For these reasons, the development of novel therapies to improve response rates and reduce the risk of relapse is critically needed.

1.1.5 Leukemic Stem Cells (LSCs) in AML

LSCs were first described in AML in seminal studies from the group of Professor John Dick at the University of Toronto, who demonstrated that AML is organized as a hierarchy that originates from rare populations of LSCs [31]. Similar to normal hematopoiesis, LSCs are thought to self-renew as well as partially differentiate into AML blasts that constitute the bulk of the leukemic burden. LSCs were first identified by fractionating AML cells according to the expression of cell surface markers variably expressed on normal hematopoietic and leukemic cells (CD34, CD38), and then demonstrating that only specific fractions could engraft and recapitulate the disease into immunodeficient mice [31].

As LSCs are essential in initiating and propagating AML, there is much interest in identifying therapies targeting them. However, while LSCs give rise to AML blasts, they are thought to have unique biological properties that make them resistant to many forms of traditional therapies [32]. Characterizing or targeting LSCs has proven difficult, as LSCs represent a very minor fraction of leukemic cells and are largely defined by their ability to xenograft disease into immunodeficient mouse models [33]. Cell surface markers often used to identify HSCs or myeloid progenitors also do not consistently identify LSC populations across AML patients, and LSC marker expression has been observed to change within patients over time or following treatment. Although LSCs were initially thought to originate exclusively from the immature $CD34^{+}CD38^{-}$ population, it has since been shown that many AML patients also display $CD34^{+}CD38^{+}$ cells with LSC abilities [34, 35]. Further, rare patient samples lacking $CD34^{+}$ cells have been shown to display engraftment capabilities in immunodeficient mice [35, 36]. Nevertheless, LSCs are still most frequently found within the $CD34^{+}CD38^{-}$ population in the majority of AML patients. Despite this variability in immunophenotype, several antigens have been identified as commonly expressed by LSCs, including CD123, CD200, CD32, TIM3, and CD93 [37-41]. Understanding the phenotypic heterogeneity of LSCs between and within AML patients is essential to the development of therapies eliminating these populations.

Importantly, several groups have demonstrated that LSCs and blast cells often share the same genetic mutations, while only LSCs can engraft in immunocompromised mice and propagate

the disease [32, 42]. This suggests that functional differences between LSCs and their blast progeny arise from epigenetic or gene expression changes, and not mutations alone. To interrogate LSC gene expression, one study identified genes differentially expressed between LSC and bulk AML blast fractions from primary samples validated by xenotransplantation [43]. The differentially expressed genes were then used to perform a multivariate regression analysis and identify a 17-gene expression signature (LSC-17) predictive of AML patient survival. When the LSC-17 signature was applied to other AML patient cohorts, it was found to be consistently associated with survival, as well as with chemotherapy resistance and relapse. This work suggests that a high frequency of LSCs at diagnosis is prognostically relevant and supports the model that relapse in AML originates from surviving LSCs.

There has been significant interest in identifying the metabolic dependencies of LSCs and targeting the adaptations which facilitate their survival. Analogous to HSCs, LSCs are thought to be metabolically dormant as cells derived from primary AML samples capable of engrafting in immunodeficient mice are largely in the G0 phase of the cell cycle [44]. Supporting this notion, LSC-enriched populations also exhibit low levels of oxygen consumption, cellular ATP, and reactive oxygen species (ROS) [29]. This quiescence has been proposed to drive resistance to chemotherapeutic agents which target dividing cells, as well as the metabolic stress induced by chemotherapy. Interestingly, while quiescent HSCs primarily rely on glycolysis for maintenance, several studies have demonstrated that LSCs are highly dependent on oxidative phosphorylation and are unable to switch to glycolysis following inhibition of oxidative phosphorylation [29, 45]. The same studies also established that LSCs rely on mitochondrial integrity and upregulated BCL-2 expression for survival. These findings were consistent with other reports demonstrating that inhibition of mitochondrial translation or mitophagy targets LSCs in primary AML samples [46, 47]. This metabolic vulnerability was consistent across varied primary samples, suggesting applicability across AML patient groups. As healthy HSC and progenitor cells do not depend as heavily on oxidative metabolism or mitochondrial activity, these pathways represent potential strategies for developing LSC-targeted therapies.

1.1.6 Experimental Models of AML

1.1.6.1 *In Vitro* Models

Human cell lines constitute the most used model systems of AML and represent immortalized cells derived from AML patients that proliferate indefinitely in culture. A variety of AML cell lines have been established and can be selected as models for patients of specific age groups, AML subtypes, or response to treatment. Widely used AML cell lines include U937, HL-60, KG1a, MOLM-14, THP-1, and MV4-11, and these are highly useful as model systems for examining the response of AML to novel drug treatments. A notable success of these models is the discovery that retinoic acid induces differentiation of the HL-60 cell line, derived from a patient with APL [48]. Following reports demonstrating that retinoid derivatives induced functional and morphological differentiation of HL-60 cells, it was soon found that the *in vitro* response of this cell line paralleled the response of primary APL samples [49] and subsequently the clinical response of APL patients to retinoic acid [50]. Retinoic acid therapy was then rapidly translated into clinical practice, and changed the clinical course of the APL subtype from most fatal to most curable (greater than 90% cure rates) [51].

In addition to the *in vitro* culture of AML cell lines, novel *ex vivo* culture and co-culture systems have recently made it possible to temporarily culture primary AML samples. By supplementing culture media with certain small molecules [52, 53] or co-culturing AML cells with BM stromal cells [54, 55], primary AML samples can be expanded for a short time *in vitro*. Testing novel drugs or drug combinations on primary samples *in vitro* can validate the benefits of a potential treatment or contribute to understanding the mechanisms of drug resistance. However, despite these new culture methods, patient samples remain difficult to study using *in vitro* methods and cannot be maintained for more than a few weeks.

1.1.6.2 *In Vivo Models*

Murine models have long been used to study cancer initiation, progression, and response to treatment. In AML, murine models have greatly contributed to the understanding of leukemogenesis and are invaluable in studying the mechanisms involved in chemoresistance and the development of new therapies [56]. Although *in vitro* culture systems are useful tools for pre-clinical studies, the short-term culture of primary samples or study of immortalized AML cell lines represent artificial environments with significant limitations. Cell lines often acquire additional

mutations during prolonged periods of culture, while patient samples can be very difficult to acquire and cannot be maintained for more than several weeks *in vitro* despite new culture methods [57]. Furthermore, the primary AML samples that can be expanded in culture are often biased towards more aggressive AML subtypes [58]. While *in vitro* methods are still important tools, murine AML models more accurately replicate the disease complexity as well as the significant involvement of the BM microenvironment [56, 59].

Murine models of AML are generally categorized as syngeneic, transgenic, or xenograft models. Syngeneic AML engraftment involves the transplant of murine AML cells into mice of the same genetic background. Syngeneic AML may be induced through the expression of mutations that drive the development of different human AML subtypes. For example, leukemias driven by mixed lineage leukemia (MLL, also known as KMT2A) fusion proteins (eg. MLL-ENL, MLL-AF4, MLL-AF9) are known to be aggressive and resistant to chemotherapy [60]. Similar to the methods used in this thesis, a commonly used approach to generate these models involves isolating HSCs, CMPs, or GMPs from a mouse, retrovirally transducing the cells with a MLL fusion protein, and re-transplanting the cells into syngeneic recipients to induce AML. The MLL-AF9 fusion protein in particular has been widely used in the study of leukemogenesis and has a well-characterized immunophenotype and LSC compartment [61-63]. Syngeneic murine models also maintain the involvement of a functional immune system.

Transgenic mice are also commonly used to study AML *in vivo*. In these models, specific gene targets are altered to constitutively express an oncogene or prevent expression of a tumor-suppressor gene. Transgenic mice have been engineered to produce a variety of AML models, including mice with MLL fusion proteins [64], FLT3-ITD mutations [65], or defective myeloid transcription factors [66]. Transgenic and syngeneic AML models remain immunocompetent. Transgenic models have the advantage of facilitating the study of leukemogenesis, as the disease is not transplanted and arises spontaneously. Improvements in the engineering of transgenic mice have made it possible to selectively express a transgene in specific cell types, using specific promoters only active in targeted cells, and limit the effects on other lineages and tissues. However, these models are the most difficult to engineer and remain costly.

In xenografted murine models of AML, human cell lines or primary patient samples are transplanted into immunodeficient mice which facilitate engraftment of human hematopoietic cells [31]. Early model used genetic backgrounds such as non-obese diabetic/severe combined

immunodeficiency (NOD/Scid). These models have been further improved to generate strains such as NOD-Scid-IL-2Rγc^{null} (NSG) and NOD-Scid-IL-2Rγc^{null}/IL-3/GM-CSF/SCF (NSG-S mice) [67, 68]. NSG mice carry mutations in the Prkdc DNA repair enzyme and IL-2 receptor gamma chain, preventing the development of functional lymphocytes and possible allograft rejection [67]. NSG-S mice represent NSG mice modified to express the human cytokines IL-3, G-CSF, and SCF, which strongly promote engraftment of human hematopoietic cells [68]. Although these models are highly immunocompromised and do not completely reproduce the human BM microenvironment, they are highly valuable for studying the response of human cells to treatment and can replicate the disease phenotype and heterogeneity of the original patient [31, 35].

1.1.7 Therapeutic Resistance and Relapse in AML

Despite advances in the treatment of AML, relapse remains a leading cause of death. Although several mechanisms have been proposed to explain why some cells may develop chemoresistance, it is not completely understood how AML cells escape chemotherapy and expand to cause relapse. Furthermore, the heterogeneity of AML patients makes it difficult to characterize mechanisms driving therapeutic resistance. Until recently, it was believed that LSCs regenerate AML following chemotherapy as a result of their intrinsic capacity to self-renew and propagate the disease [31, 69]. Additionally, there is evidence that LSCs may be preferentially quiescent, putatively allowing them to resist cell-cycle specific chemotherapy [44]. Several clinical studies have further shown that a higher LSC burden at diagnosis is associated with poor survival and the presence of residual disease in AML patients [70]. Challenging these assumptions however, two recent studies found that residual human AML cells isolated from cytarabine-treated patient-derived xenograft (PDX) models were not enriched in LSCs and exhibited functional adaptations [71, 72]. Previously published LSC transcriptional signatures were downregulated after treatment, indicating that LSCs are not preferentially chemoresistant. Residual cells were found to exhibit a metabolic signature with increased mitochondrial activity (increased oxidative phosphorylation, fatty acid oxidation) and elevated ROS production. Both studies additionally proposed that leukemic re-growth depends on factors or interactions present within the BM microenvironment. This data is in keeping with earlier PDX-based studies describing mitochondrial transfer from BM stromal cells to leukemic cells to maintain oxidative metabolism during chemotherapy [73], as well as upregulation of CD36 expression and fatty acid oxidation in chemoresistant AML cells

[74]. As these pathways were not found to be enriched at the time of overt relapse, it is possible that they are transiently upregulated to confer protection during treatment and promote chemoresistance [71, 72]. These findings suggest that targeting these metabolic adaptations has the potential to prevent the development of chemoresistant clones.

In addition to the abovementioned metabolic pathways, new data suggest that mammalian target of rapamycin (mTOR) kinase signalling may also play a role in the re-growth of AML post-chemotherapy [75]. The mTOR complex 1 (mTORC1) is a master cell growth regulator which responds to environmental signals to control processes such as cell survival, metabolism, and mRNA translation. mTORC1 also plays a role in the regulation of mitochondrial activity by driving translation of proteins involved in mitochondrial metabolism and repair. mTOR is constitutively activated in nearly all AML patient samples [76, 77] and mTOR inhibition has been shown to improve the *in vitro* response of AML cells to chemotherapy [78]. Unfortunately, clinical trials evaluating mTORC1 inhibition in AML have had limited or mixed success [79, 80]. However, recent evidence suggests that mTORC1 activation in AML may be dynamic and context dependent. In a murine model of AML driven by the leukemogenic fusion protein MLL-AF9, Oki, Mercier, *et al.* found that while mTORC1 activity inversely correlates with AML burden *in vivo*, mTORC1 signalling is re-activated within five days following treatment with cytarabine [75]. In this murine model, timed genetic inhibition of mTORC1 enhanced the efficacy of chemotherapy. Thus, while dysregulation of mTORC1 and its downstream pathways supports the rapid growth of AML, their level of activation may also be dynamic and contribute to adaptation to treatment.

1.2 mTORC1-regulated mRNA Translation

1.2.1 The Eukaryotic Initiation Factor (eIF) 4F Complex

Eukaryotic translation is a tightly controlled process which occurs in four stages: translation initiation, elongation, termination, and ribosome recycling [81]. Translational regulation significantly influences gene expression and cellular protein abundance [82]. Translation initiation is the most highly regulated of these phases and represents the rate-limiting step in protein synthesis [83]. Following mRNA transcription, a crucial step in translation initiation is the formation of the heterotrimeric eIF4F initiation complex, composed of eIF4E, eIF4A, and eIF4G (**Figure 1.2**). eIF4E acts as the cap-binding protein to mediate binding of the initiation complex to the 5’ cap of mRNA transcripts. eIF4E is the least abundant initiation factor and is

therefore rate limiting to translation initiation. eIF4A is an ATP-dependent RNA helicase which unwinds secondary structures of mRNA to facilitate ribosome binding and is the most abundant initiation factor within the cell [83]. Finally, eIF4G is a scaffolding protein which interacts with eIF4A, eIF4E, and the poly(A)-binding protein (PABP) on the poly(A) tail of mRNA transcripts to promote recruitment of the 43S pre-initiation complex [84]. Once the 43S pre-initiation complex, comprised of the small 40S ribosomal subunit and other eIFs, is recruited to the mRNA, it proceeds to scan the 5' untranslated region (UTR) until a start codon is reached and the complete 80S ribosome is then assembled [81].

After the ribosome vacates the initiation site, additional ribosomes may also bind to an individual mRNA transcript and form a group of actively translating ribosomes known as a polysome. Gene expression and translation levels are often measured through examining polysome activity using a technique known as polysome profiling [85]. This technique allows for the isolation and examination of highly translated versus poorly translated mRNA transcripts within a cell, and better describes global gene expression than transcriptomics alone.

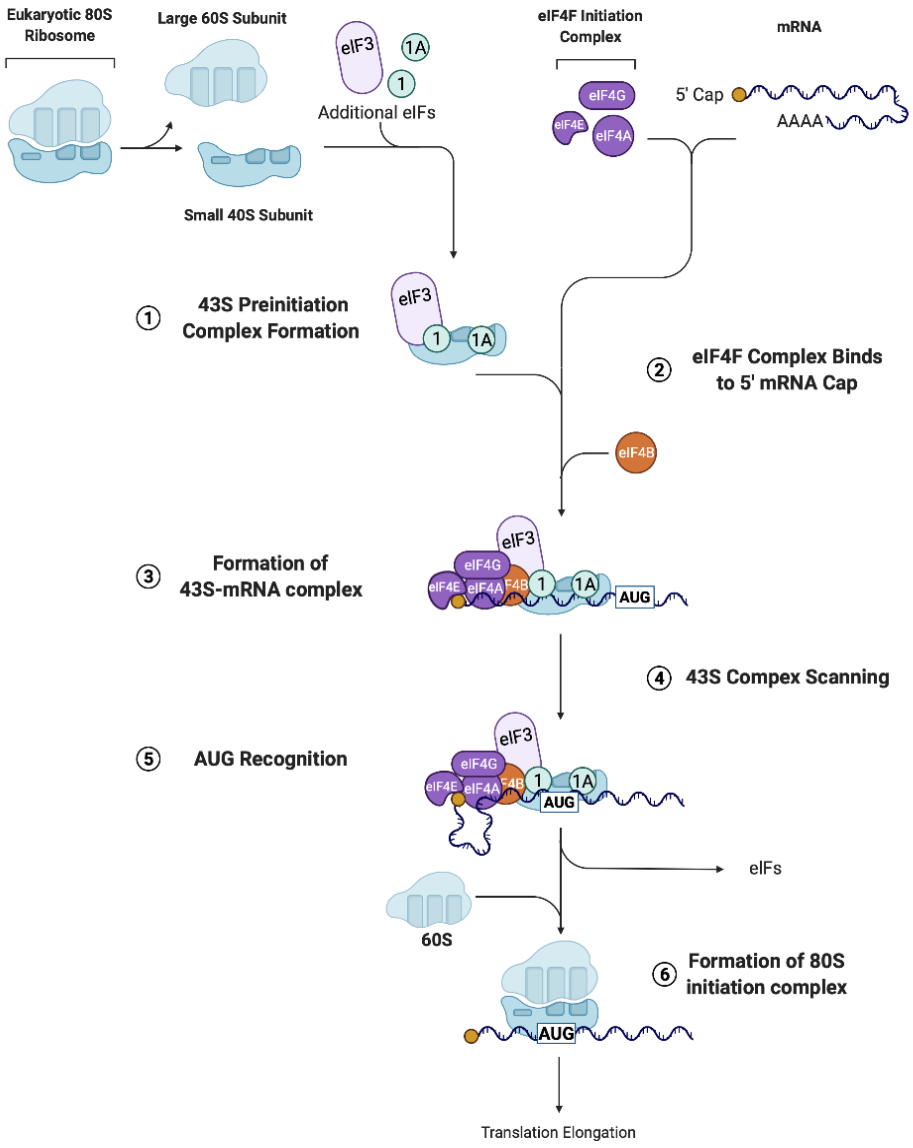

Figure 1.2. **Overview of Eukaryotic Cap-dependent Translation Initiation**
Following ribosome recycling, the 43S-preintiation complex is formed by the small 40S ribosomal subunit and additional eIFs (eIF1, eIF1A and eIF3) (1). At the same time, the assembled eIF4F initiation complex binds to the 5' cap of an mRNA transcript (2). The eIF4F complex then recruits the 43S-preintiation complex to the 5' mRNA cap. Once the 43S-preintiation complex is bound to the mRNA (3), it scans from 5'-3' until a start (AUG) codon is found (4). Recognition of the start codon then induces release of the eIFs and stops the 5'-3'scanning (5). The 60S ribosomal subunit is then recruited to the mRNA, to form the 80S initiation complex (6), which can proceed to the elongation phase of translation. Figure adapted from [81] and "Protein Translation Cascade" by BioRender.

The availability of eIF4F plays an important role in protein synthesis and determining which mRNAs are efficiently translated. Although a minor group of mRNAs are translated in eukaryotes through an internal ribosome entry site (IRES), the overwhelming majority are translated via cap-dependent translation initiation [81]. For these mRNAs, the primary and secondary structure strongly influences how frequently the eIF4F complex is recruited to the 5' cap of the transcript [82]. Given that eIF4F levels are limiting within the cell, mRNAs with relatively short or simple 5' UTRs are translated at the highest rates as they are most accessible to the initiation complex and translational machinery. mRNA transcripts with complex or extended 5' UTRs must be unwound to allow for ribosome recruitment and consequently require higher levels of eIF4F to be efficiently produced. The guanine and cytosine (G/C) content of the 5' UTR also impacts translation as higher G/C content mRNAs form more stable secondary structures [86]. As a result of this mRNA discrimination by eIF4F, increasing eIF4F levels results in only a minor increase in global cellular protein levels but a strong increase in the levels of a select subset of mRNAs [87]. Interestingly, ribosome and polysome profiling analyses have revealed that eIF4F-sensitive transcripts largely encode proteins which regulate cell growth and survival, or cell cycle progression (Eg. MYC, BCL-2, CCDN1). In contrast, housekeeping genes (Eg. GAPDH) with shorter 5'UTRs are less responsive to eIF4F availability [87]. As such, control of translation initiation is increasingly being recognized as an important regulator in malignant transformation as eIF4F can selectively upregulate the expression of a subset of pro-oncogenic and metastatic transcripts [87].

There is significant interest in characterizing eIF4F-sensitive transcripts, as well as the role of individual complex components in translational regulation and tumorigenesis. Two landmark studies examining eIF4A and eIF4E activity established that the degree of mRNA secondary structure is directly proportional to how heavily these initiation factors are required for translation [88, 89]. While the dependency of these transcripts on eIF4A for their translation is likely due to the requirement of eIF4A helicase activity, the mechanisms underlying sensitivity to eIF4E are less clear. It is thought that eIF4E may stimulate eIF4A unwinding activity in addition to helping recruit eIF4A to the 5' mRNA cap [90]. This increase in eIF4A activity is mediated through eIF4G, which can only stimulate eIF4A helicase activity following eIF4E binding. Additionally, phosphorylation of eIF4E (peIF4E) occurs after formation of the eIF4F complex and promotes the expression of tumorigenic mRNAs without affecting global translation [91]. Consistent with this

data, eIF4E and eIF4A have been found to be overexpressed in many types of human cancers, including lymphoma, leukemia, and breast cancer [92-94]. This has led to increasing interest in developing drugs inhibiting these proteins as a potential targeted therapy for these malignancies.

Although targeting of eIF4A and eIF4E similarly acts to impair formation of the eIF4F complex and translation initiation, minor differences have been observed in the translational response when comparing inhibition of these factors. Inhibition of eIF4E is thought to have less of an effect on global protein synthesis in contrast to targeting eIF4A activity [87, 95, 96]. In addition, transcripts with highly structured and G/C-rich 5' UTRs, such as those containing G-quadruplex structures, are more sensitive to eIF4A inhibition. G-quadruplexes, or $(CGG)_4$ sequences, are highly stable secondary RNA structures composed of paired guanine nucleotides linked by an additional nucleotide [97]. Importantly, G-quadruplexes are frequently observed in mRNA transcripts encoding oncogenes, such as NRAS, VEGFA, MYC, BCL-2, and NOTCH. Inhibition of eIF4A may therefore be highly effective in eliminating cancer cells which depend on these proteins. Finally, a small group of mRNAs containing Translation Initiator of Short 5' UTR (TISU) sequences are highly dependent on eIF4E but not on eIF4A activity due to their unusually short 5' UTRs [98, 99]. Notably, TISU-containing mRNAs are enriched for proteins encoding for mitochondrial functions [98].

1.2.2 Regulation of Cap-dependent mRNA translation by mTOR signalling

mTOR signalling is one of the major cellular pathways that controls cap-dependent translation initiation. The mTOR kinase itself forms two functionally distinct signalling complexes; mTORC1 and mTOR complex 2 (mTORC2) [100]. mTOR signalling is positioned downstream of the oncogenic phosphoinositide 3-kinase (PI3K)-Akt and mitogen-activated protein kinase-extracellular signal-regulated kinase (MAPK-ERK) pathways and responds to both intracellular and extracellular signals to regulate cell growth or survival. The mTORC1 complex is composed of the proteins mTOR, regulatory-associated protein of mTOR (Raptor), mammalian lethal with sec13 protein 8 (mLST8), and DEP domain-containing mTOR interacting protein (DEPTOR). mTORC2 is made up of mTOR, rapamycin-insensitive companion (Rictor), stress-activated protein kinase interacting protein 1 (SIN1), mLST8, and DEPTOR [100]. mTORC1 and mTORC2 play discrete roles in cell metabolism and proliferation, with mTORC1 largely promoting cell growth and proliferation and mTORC2 regulating cell survival and cytoskeleton

organization [100]. A complete description of the complex signaling networks involving mTOR is outside of the scope of this thesis, which will focus on mTORC1-dependent signalling and mRNA translation.

mTORC1 is stimulated by a variety of environmental cues, including growth factors, energy and oxygen levels, and amino acid availability. Once activated, mTORC1 regulates cell growth and metabolism through cap-dependent translation initiation and upregulation of processes such as nucleotide synthesis, lipid metabolism, and mitochondrial activities [100]. mTORC1 activity is highly dependent on growth factors and nutrient availability within the BM microenvironment [75, 101]. mTORC1 controls protein synthesis by moderating formation of the eIF4F initiation complex via phosphorylation of the eIF4E-binding protein 1 (4E-BP1) and p70 S6 kinase (S6K). 4E-BP1 is a negative regulator of eIF4E that competitively inhibits eIF4E:eIF4G binding [87]. Phosphorylation of 4E-BP1 by mTORC1 causes dissociation of eIF4E to allow its recruitment to the eIF4F complex. Similarly, activation of S6K results in the phosphorylation of the eIF4A-inhibitor programmed cell death protein 4 (PDCD4), which controls cellular eIF4A levels by competing with eIF4G to bind eIF4A [102]. Phosphorylation of PDCD4 marks the protein for degradation and enables formation of the initiation complex. Activated S6K also stimulates additional proteins involved in translation such as ribosomal protein S6 (S6), and eukaryotic initiation factor 4B (eIF4B) which further enhances eIF4A activity [87].

1.2.3 Targeting Cap-dependent Translation in AML

Elevated mTORC1 signaling has frequently been observed in AML patients, and is thought to contribute to leukemogenesis, chemoresistance, and poor OS [75-77]. Unfortunately, prior attempts to target mTORC1 directly in AML have displayed limited clinical efficacy. Allosteric mTORC1 inhibitors, termed rapalogs (for “analogues of rapamycin”), were found to largely be cytostatic to AML cells and had little benefit as single agents [103] or in combination with chemotherapy for AML patients [80]. This was thought to be in part due to release of negative feedback loops and activation of alternate upstream pathways achieving mTORC1 signaling [104]. Although combinations of PI3K and mTOR inhibitors show greater cytotoxic effects [105], targeting of downstream mTORC1 pathways may be an alternate way to circumvent this resistance. mTORC1-regulated mRNA translation represents an attractive downstream target as protein synthesis is a key pathway regulating cell proliferation and survival in AML. Furthermore,

elevated eIF4F complex levels are associated with chemoresistance in other hematological malignancies [106, 107]. In AML, targeting of eIF4E and eIF4A potently inhibits cell growth *in vitro* and in PDX models [87, 92, 108-110]. In support of targeting eIF4A, studies aimed at characterizing the response to inhibition of eIF4F in contrast to mTORC1 inhibition have identified mRNAs differentially regulated by these complexes. Inhibition of mTORC1 and eIF4E is believed to impair translation of mRNAs with both short and long 5' UTRs, while targeting of eIF4A predominantly reduces translation of structured 5' UTR proteins [106, 111]. Thus, eIF4A inhibition targets proteins with pro-growth or survival functions while sparing proteins involved in mitochondrial activity and respiration, damaging mitochondrial integrity and inducing apoptosis [111-113]. eIF4A inhibition has also been shown to impair the autophagic clearance of damaged mitochondria, known as mitophagy, to additionally promote apoptosis [112].

In response to growing evidence for targeting mTORC1-regulated translation in AML, two clinical trials (NCT00559091 and NCT01056523) explored targeting eIF4E for patients with relapsed or refractory disease or otherwise unfit for induction chemotherapy using the FDA-approved drug ribavirin [114, 115]. Ribavirin is a synthetic guanosine analog which has historically been used as a broad-spectrum antiviral agent. The precise mechanisms by which ribavirin acts are incompletely understood; however, it was proposed that the drug functions in part by structurally mimicking the guanine nucleotide within the 5' mRNA cap to directly bind to eIF4E and inhibit translation [116, 117]. This discovery resulted in the first clinical trial targeting eIF4E, where ribavirin was found to be clinically beneficial as a monotherapy for some patients with poor-prognosis AML [114]. However, many other patients did not respond to ribavirin treatment and patients initially achieving clinical responses developed drug resistance within 4 months of treatment initiation. A subsequent trial combining ribavirin with low dose cytarabine to improve the frequency and duration of clinical response unfortunately produced disappointing results. Cytarabine was found to impair the absorption of ribavirin, interfere with ribavirin activity, and patients similarly developed resistance [115]. In both trials, clinical relapse was associated with glucuronidation of ribavirin, modifying the activity of the drug and preventing the interaction between eIF4E and ribavirin [114, 118]. Further, refractory and several relapsed patients also exhibited notably low levels of the nucleoside transporter ENT1 and the enzyme adenosine kinase, which are required for ribavirin uptake into the cell and pro-drug metabolism [115]. Although these trials had limited clinical benefit, the loss of response and mechanisms facilitating resistance

appeared to be specific to the mechanism of action and/or metabolism of ribavirin and not to targeting of eIF4E. Thus, inhibiting the eIF4F complex using other translation inhibitors could still prove effective in AML.

More specific small-molecule inhibitors which selectively and potently target eIF4A *in vitro* and *in vivo* have only been developed in recent years. Encouragingly, in hematological malignancies, these inhibitors seem to induce cell death in AML blasts while sparing normal HSCs and progenitor cells [108]. Furthermore, in addition to pre-clinical data supporting the use of eIF4A inhibitors as single agent therapies in AML, targeting eIF4A may also potentiate response to chemotherapy [95, 107, 109, 110, 119]. As previously discussed, the mitochondria and anti-apoptotic BCL-2 family proteins are associated with AML cell survival and chemoresistance. Several BCL-2 family members (Eg. BCL-2) are well-characterized as eIF4F-responsive transcripts and are depleted following eIF4A inhibition, presenting the possibility that eIF4A inhibitors synergize with chemotherapy in AML [107, 108].

1.2.4 Targeting Translation Initiation using Rocaglates

The rocaglate family of eIF4A inhibitors were originally isolated from the *Aglaia* tree genus and have demonstrated the highest selectivity and potency of existing eIF4A inhibitors [120-122]. Rocaglates act by stimulating the interaction between eIF4A and mRNA, sequestering eIF4A from the eIF4F complex and leading to translational arrest (**Figure 1.3**). Silvestrol is one of the most well-characterized rocaglates and was previously found to exhibit favorable pharmacokinetic properties and *in vivo* efficacy at nanomolar concentrations [108, 123]. However, silvestrol has since been recognized as a substrate of the multidrug resistance glycoprotein (MDR1) transporter, potentially limiting its efficacy as an anti-cancer agent [124]. To eliminate this resistance, synthetic derivatives of silvestrol have subsequently been developed through organic chemistry such as WGD-57-59 and CR-1-31-B [121, 125].

Although all rocaglates function to similarly induce eIF4A-RNA binding, they exhibit distinct binding affinities for purine versus pyrimidine motifs within the 5' UTRs of mRNAs [120, 125]. This observation has led to the understanding that different rocaglates modify the translation of different groups of mRNA transcripts. For example, the compound CR-1-31-B was found to selectively bind purine bases within 5' UTRs while silvestrol and WGD-57-59 exhibited no preference for polypurine verses polypyrimidine motifs [125]. These studies imply that individual

rocaglates may target unique subsets of mRNA transcripts and differentially alter protein synthesis.

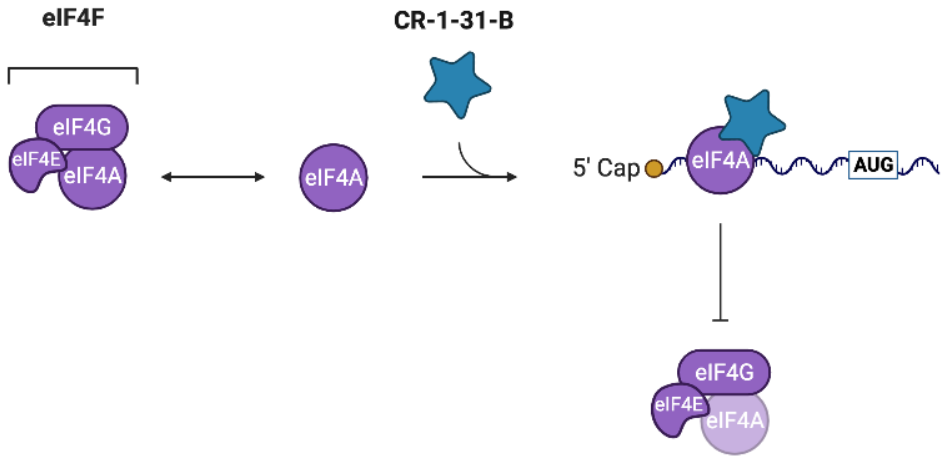

Figure 1.3. **CR-1-31-B Enhances eIF4A-RNA-Binding**
Mechanism of action of CR-1-31-B. CR-1-31-B binds to free initiation factor eIF4A and strongly stimulates the binding between eIF4A and mRNA. This produces a highly stable interaction between eIF4A-RNA and prevents eIF4A from incorporating into the eIF4F translation initiation complex. Figure adapted from [151] with information from [120] and created with BioRender.

Chapter 2: Hypothesis and Aims

Prior observations suggest that following chemotherapy exposure, AML cells rely on mTORC1-dependent metabolic adaptations and elevated protein synthesis for survival [72, 75, 110]. In experimental murine models, mTORC1 is downregulated in densely packed leukemic bone marrow but is reactivated by chemotherapy. mTORC1 signalling has been linked to chemoresistance in other malignancies through multiple mechanisms, including promoting metabolic reprogramming and anti-apoptotic signalling [126, 127]. This pro-survival signaling is largely mediated through mTORC1-mediated control of the eIF4F initiation complex and dysregulation of protein translation. As high levels of eIF4F are also associated with poor prognosis and drug resistance in other hematological cancers, inhibition of this downstream effector of mTORC1 represents an attractive target [106, 107]. In addition, previous work suggests that targeting of eIF4A inhibits the translation of a subset of eIF4A-dependent mRNA transcripts, which includes proteins critical to AML growth and metabolism (Eg. Myc, cyclins, BCL-2 family proteins) [107, 108, 128]. Thus, we hypothesize that inhibiting eIF4A in AML cells may target pro-survival adaptations induced by chemotherapy and limit regrowth.

The overarching goal of this thesis was to characterize the metabolic and translatomic changes driving therapeutic resistance in AML to facilitate the development of therapies targeting these adaptations. Specifically, our two experimental aims were:

Aim 1: Characterize the metabolic and translatomic adaptations of AML to chemotherapy

We studied chemoresistance in experimental models of AML, *in vitro* and *in vivo*, using techniques such as polysome profiling, O-propargyl-puromycin (OP-Puro) labeling, and flow cytometry.

Aim 2: Investigate the effects of targeting eIF4A in chemoresistant AML

We examined if targeting of eIF4A inhibits the adaptation of AML to treatment, by treating AML cell lines or leukemic mice with chemotherapy and/or the translation inhibitor CR-1-31-B, coupled with metabolic and translatomic functional characterizations on residual cells.

Chapter 3: Materials and Methods

Reagents

Cytarabine, doxorubicin and CR-1-31-B were obtained from MedChemExpress. Cytarabine and CR-1-31-B were resuspended in DMSO, doxorubicin was suspended in sterile water, and all drugs were stored in multiple aliquots at -80°C.

Cell lines

The human AML cell lines MOLM-14, U937, and KG1a were ordered from the American Type Culture Collection (ATCC). Human AML cells were maintained in RPMI-1640 supplemented with 10% FBS (Wisent Bio Products) and 100 units/ml penicillin/streptomycin at 37°C with 5% CO_2. The murine AML cell line FM4 was generated by Dr. Francois Mercier through retroviral transduction of the MLL-AF9 oncogene and fluorescent protein iRFP into granulocyte-macrophage progenitors sorted from a CD45.1 C57BL/6 congenic mouse [75]. FM4 cells were cultured in RPMI-1640 supplemented with 10% FBS, 5 ng/ml IL-3, 10 ng/ml SCF, and 100 units/ml penicillin/streptomycin. All cells were routinely tested for Mycoplasma.

Lentivirus production and cell transduction

The pLenti CMV puro LUC plasmid containing firefly luciferase was gifted by the laboratory of Dr. Alexandre Orthwein (McGill University). The LeGO Venus (LeGO-V2) plasmid was gifted by Dr. Boris Fehse. HEK293 cells were transfected with lentiviral plasmid, envelope plasmid VSV-G and gag/pol plasmid delta 8.9 using the FuGENE 6 transfection reagent as per manufacturer's instructions, and the viral supernatant was harvested 24 hours post-transfection. $5x10^5$ MOLM-14 cells were then seeded into 6-well plates with 0.5 mL of pLenti CMV puro LUC lentivirus, 0.5 mL of LeGO-V2 lentivirus, and 4 μg/ml of polybrene. MOLM-14 cells were then spinfected at 1000g for 1 hour at 32°C. Fluorescent cells were sorted using a FACSAria Fusion in the LDI Flow Cytometry Core. Venus+ cells were selected with puromycin for luciferase expression. Stable luciferase expression was confirmed using the Promega GloMax 20/20 Luminometer and D-Luciferin prior to transplant.

MOLM-14 xenograft murine model

All *in vivo* experiments were approved by the animal care committee of McGill University. NOD.Cg-Prkdc^{scid}IL2Rg^{tm1Wjil}/SzJ (NSG) mice were gifted from the laboratory of Dr. Mark Basik (McGill University). 8-12-week-old male NSG mice were sub-lethally irradiated with 2.5 Gy 24

hours prior to transplant and given enrofloxacin in their drinking water for 14 days. Venus luciferase-expressing MOLM-14 cells (MOLM-14-Luc) were washed twice in PBS, re-suspended in PBS at $1x10^7$ cells/ml, and 200 uL ($2x10^6$) cells were intravenously injected. Mice were assessed for engraftment at 10-12 days post-transplant by bioluminescent imaging using a Perkin Elmer IVIS Spectrum at the LDI animal phenotyping core (detailed below). NSG mice were treated with 50 mg/kg cytarabine injected intraperitoneally (i.p.) daily for 5 days, 0.20 mg/kg CR-1-31-B i.p. daily for 7 days, or with both drugs administered concomitantly. Cytarabine was diluted in sterile PBS, and CR-1-31-B was diluted in 5.2% TWEEN 80/5.2% PEG400. As controls, mice were treated with 5.2% TWEEN 80/5.2% PEG400 vehicle alone. On day 8, mice were euthanized and mononuclear cells were purified from crushed BM using Ficoll-Paque density centrifugation.

***In Vivo* Bioluminescent imaging**

At 10-12 days post-transplant, NSG mice were given one i.p. injection of 150 mg/kg D-luciferin in PBS. Mice were then anesthetized with 2% isoflurane and imaged using the IVIS Spectrum In Vivo system. Kinetic curves were optimized for the MOLM-14-Luc cell line prior to treatment by imaging transplanted mice every 2 minutes for 45 minutes beginning 1 minute after D-luciferin injection. Images were captured using Living Image analysis software and total flux values (photons/second) were determined using regions of interest (ROI) of the same size for each mouse. The total flux values of each image over the 45-minute time course were plotted and the point of maximum luminescence was chosen as the optimal time point for imaging. Mice were imaged on Days 1 and 8 of treatment and the final total flux value for each mouse was calculated by normalizing to the Day 1 value.

FM4 murine model

C57BL/6J founders were obtained from Charles River Laboratories and bred at the Lady Davis Institute. 8-12-week-old male C57BL/6J mice were sub-lethally irradiated with 4.5 Gy 24 hours before transplant. FM4 cells were washed twice in PB, re-suspended in PBS at $2.5x10^7$ cells/ml, and 200 uL ($5x10^6$) cells were intravenously injected. To quantify engraftment starting at 14 days post-transplant and weekly thereafter, 50-100 µl of peripheral blood was collected from the saphenous vein, the red blood cells were lysed using Gibco ACK Lysing Buffer, and iRFP+ FM4 cells were quantified as percentage of white blood cells (WBC) using a BD Fortessa instrument in the LDI Flow Cytometry Core. When FM4 cells reached a level greater than 1% of WBC, representative of at least 50% BM burden, C57BL/6J mice were treated with 50 mg/kg

cytarabine i.p. daily for 5 days with 3 mg/kg doxorubicin i.p. daily concomitantly from days 1-3, with 0.20 mg/kg CR-1-31-B i.p. daily for 7 days, or with the combination of all three drugs. Cytarabine and doxorubicin were diluted in sterile PBS, and CR-1-31-B was diluted in 5.2% TWEEN 80/5.2% PEG400. As controls, mice were treated with vehicle alone. On day 8 mice were euthanized and mononuclear cells were purified from BM using Ficoll-Paque density centrifugation.

CR-1-31-B Toxicity *In Vivo*

Healthy C57BL/6J mice were treated with 0.20 mg/kg CR-1-31-B i.p. daily for 7 days. On day 8 mice were euthanized and mononuclear cells were purified from BM using Ficoll-Paque density centrifugation. Spleens were crushed and treated with ACK lysing buffer.

***In vitro* drug treatment**

MOLM-14 cells were washed in PBS and then re-suspended in cell culture media with vehicle (0.00021 % DMSO), 250 nM cytarabine, and/or 2.5 nM CR-1-31-B. $1x10^6$ cells were plated into the wells of 6-well plates in 4 mL of media and all treatments were plated in triplicates. All stock solutions of drugs were freshly diluted 1:1000 in PBS and added to cell culture media to make the final concentrations.

Polysome Profiling

For *in vitro* samples, $2x10^7$ cell MOLM-14 cells were resuspended in cell culture media with DMSO diluted in sterile PBS or 250 nM cytarabine in T175 flasks. After 24-hours, half of the cytarabine treated cells were then resuspended in media with 10 nM CR-1-31-B for 1 hour. An additional sample was treated with 10 nM CR-1-31-B alone. All drugs were freshly diluted 1:1000 in PBS and then added to cell culture media to make the final dilutions. AML cells were then counted and lysed in hypotonic buffer (5mM Tris-HCL at pH 7.5, 2.5 mM $MgCl_2$, 1.5 mM KCl, 0.5% Triton-X100, 200 U/ml RNase Inhibitor, 1X protease inhibitor, 100 ug/ml cycloheximide and 2 mM DTT). Polysome profiling was performed by the laboratory of Dr. Laura Hulea (Centre de recherche de l'Hôpital Maisonneuve-Rosemont) as previously described [129].

***In Vitro* Colony-Forming Assays**

Mononuclear cells were purified from whole mouse BM using Ficoll-Paque density centrifugation. For AML experiments, mouse CD45.1 (FM4) and human CD45 cells (MOLM-14) were purified using Miltenyi Biotec's MACs cell separation system. 500 AML cells were plated into 2 mL of MethoCult M3434 or H3434 methylcellulose media. Colonies were then counted at

day 7. For non-AML experiments, $2x10^4$ cells were plated into hematopoietic progenitor-supporting MethoCult M3434 methylcellulose medium and $1x10^5$ cells were plated into MethoCult M3630 B-progenitor cell supporting methylcellulose. Colonies were propagated in culture for 12 and 7 days respectively, before being counted.

***O*-propargyl-puromycin labelling**

MOLM-14 cells were treated with vehicle, 250 nM cytarabine, and/or 2.5 nM CR-1-31-B for 48-hours. O-propargyl-puromycin (OP-Puro) reagent was added to pre-warmed cell media (20 uM) and incubated for 30 minutes. Click-iT chemistry reactions were then performed according to the Click-iT Plus OPP Protein Synthesis Assay Kit. Cells were fixed in 3.7% formaldehyde and permeabilized in ice-cold methanol. The level of OP-Puro incorporation was detected using the LDI's BD LSR Fortessa Cytometer.

Phosphoprotein Analysis

AML cells recovered from murine models or following *in vitro* treatment were washed and incubated with BD Fixable Viability Stain 700. The cells were then fixed in 3.7% formaldehyde and permeabilized in ice-cold methanol. Samples were resuspended in PBS and incubated in anti-pS6 (1:250, Cell Signaling Technology; Alexa Fluor 594 conjugate #9468), anti-p4EBP1 (1:1000, Cell Signaling Technology; Alexa Fluor 488 conjugate #2846), or anti-pAKT (1:400, Cell Signaling Technology; PE conjugate #5315), before being analyzed on the LDI's BD LSR Fortessa Cytometer.

Mitochondrial Membrane Potential & ROS Production

Mitochondrial membrane potential and ROS production were assessed by flow cytometry using 50 nM TMRE and 2.5 uM mitoSOX red staining performed as per the manufacturer's protocol. Dead cells and debris were excluded using DAPI staining.

Cell Cycle and Annexin-V Staining

$1x10^6$ MOLM-14 cells were seeded into 6-well plates and treated with vehicle, 250 nm cytarabine and/or 2.5 nm CR-1-31-B. 24- and 48-hours post treatment, the cells were collected and stained using Annexin-V/PI or fixed with ethanol and incubated with RNase A, Triton X-100, and PI. Experiments were performed in triplicates and three independent experiments were conducted.

Synergy Analysis

To examine the relationship between cytarabine and CR-1-31-B, and venetoclax and CR-1-31-1B, 5,000 MOLM-14 cells were seeded in triplicates in 96-well plates and treated with

increasing drug concentrations**.** 24-hours later, viability was assessed using the CellTiter-Glo luminescent viability assay. Readouts were normalized to untreated cells and viability values were used to perform a Bliss analysis using the SynergyFinder application.

Western Blot

$1x10^7$ MOLM-14 cells were seeded into T-75 flasks and treated with vehicle or 250 nm cytarabine for 24-hours. After 24-hours, $5x10^7$ cells were taken from each flask and treated with 10 nm CR-1-31-B for 1 hour. Samples were then washed twice in PBS and immediately placed on ice, before being lysed in RIPA buffer for Western blotting.

Immunofluorescence

$1x10^6$ MOLM-14 cells were treated with vehicle or 10 nm CR-1-31-B for 1 hour. Samples were then washed and resuspended at $1x10^6$/mL in PBS, and 200 ul of each were aliquoted into the wells of a cytospin. Samples were spun at 800 rpm for 5 minutes before the slides were briefly allowed to air dry. Samples were then fixed in formaldehyde and permeabilized in ice-cold methanol. Slides were blocked for 1 hour at room temperature in 1% BSA in PBS with 0.1% TritonX-100. Without washing, anti-pH2AX antibody diluted at 1:1000 in 5% BSA in PBS was added and slides were stained overnight in a humid chamber at 4°C. The following day, the slides were washed in PBS, counterstained with 2.5 ug/ml DAPI, and washed again. The slides were then mounted in 10 ul warm 0.5% N-propyl gallate in 90% glycerol + 1X phosphate buffer (pH 8.0), and imaged.

Chapter 4: Results

4.1 Development of two pre-clinical models of chemoresistant AML.

We first sought to generate and validate two *in vivo* models of AML to treat with chemotherapy and subsequently characterize the response. The human MOLM-14 cell line expresses the FLT3-ITD mutation, found in an estimated 30% of AML patients. MOLM-14 cells also express the MLL/AF9 fusion protein, the product of a translocation between chromosomes 9 and 11 which is found in 30% of pediatric AML and 5% of adult AML cases. Both genetic alterations are associated with adverse clinical outcomes in AML patients. To ensure adequate tracking of the cells *in vivo*, we transduced the cells with lentiviruses driving the constitutive expression of firefly luciferase and the fluorescent protein mVenus. This cell line is referred thereafter as MOLM-14-Luc and results obtained using this model are colored in blue in **Figure 4.1, Figure 4.3**, **Figures 4.5-4.8**, **Figure 4.10**, and **Figure 4.11A**.

To develop a syngeneic murine model of AML, we used the FM4 cell line developed by Dr. Mercier [75]. FM4 cells are driven by the constitutive retroviral expression of the MLL/AF9 fusion protein in murine myeloid progenitors. To track and isolate the cells *in vivo*, the FM4 line was derived from a congenic mouse strain expressing the variant CD45.1 on hematopoietic cells (whereas recipient C57Bl/6 mice express CD45.2) and previously transduced with a lentivirus driving the constitutive expression of the fluorescent protein iRFP. Results obtained with the FM4 line are colored in red in **Figure 4.1**, **Figures 4.4-4.8**, and **Figure 4.10**.

To establish the sensitivity of our AML models to cytarabine *in vitro*, MOLM-14 cells were treated with 0 to 5 uM cytarabine and FM4 cells with 0 to 2 uM cytarabine. For both cell lines, cell viability was assessed 48 hours later using the CellTiter-Glo viability assay. IC50 values were calculated with a four-parameter logistic regression model using GraphPad Prism software and were found to be 0.955 uM for MOLM-14 and 0.163 uM for FM4 (**Figure 4.1)**. For MOLM-14 cells, these results are consistent with prior reports where MOLM-14 was found to be relatively resistant among a panel of AML cell lines [72, 130, 131]. The FM4 model is chemotherapy naïve, which may explain its greater sensitivity.

Next, we transplanted both models into mice and examined the effects of treatment with chemotherapy regimens adapted from the standard treatment of human AML. We transplanted 2 million MOLM-14-Luc cells into sub lethally irradiated NSG mice and began monitoring leukemic

burden using bioluminescence at day 10. We confirmed that bioluminescent imaging accurately reflected MOLM-14-Luc leukemic burden by plotting the percent BM leukemic burden as determined by flow cytometry gating of live mVenus+ cells in the BM against total flux values in all mice analyzed (**Figure 4.2).** Following confirmation of AML engraftment, we stratified recipients into experimental groups to ensure equivalent pre-treatment leukemic burden. We then treated mice with 50 mg/kg cytarabine i.p. daily for 5 days or vehicle control (see methods). This dose was established in our laboratory as the maximum tolerated dose for the NSG strain (data not shown) and is in accordance with reports from other groups that used the same regimens [71, 72]. Doxorubicin was not administered as NSG mice are highly sensitive to DNA-damaging agents and often do not tolerate treatment with multiple chemotherapies. To monitor the effect of treatment on leukemic burden *in vivo*, we repeated luciferase imaging on day 8 post-treatment initiation and normalized to pre-treatment values (day 1). In this model, chemotherapy failed to significantly reduce leukemic burden, seen by normalized luminescence values (**Figure 4.3A**) and no significant difference in spleen weight between treated and untreated mice (**Figure 4.3B**).

Using a similar design, we transplanted 5 million murine AML FM4 cells into sub lethally irradiated C57BL/6 mice. Starting at 2 weeks post-transplant and weekly thereafter, we collected PB from the recipient mice and measured the presence of iRFP-positive cells in the PB using flow cytometry to demonstrate leukemic engraftment. Once most recipient mice had greater than 1% circulating AML cells among peripheral white blood cells, representative in this model of greater than 50% abundance in the BM which was reached typically 2-3 weeks post-transplant, we stratified mice into experimental groups and treated with cytarabine for 5 days and doxorubicin concomitantly on days 1-3 ("5+3" regimen) or vehicle control as previously described for this model [75]. On day 8 of treatment, we euthanized the mice and harvested BM cells for analysis. As shown in **Figure 4.4A**, chemotherapy significantly lowered leukemic burden with the mean fraction of AML cells within the BM reduced to 49% from 96% in the vehicle-treated group ($p = 0.0317$). Additionally, spleen weight was also largely reduced in treated C57BL/6 mice (**Figure 4.4B**).

The differential response to chemotherapy between the MOLM-14-Luc and FM4 AML models, both driven by the same MLL/AF9 translocation, mirrors the different sensitivities to cytarabine *in vitro*. However, the C57Bl6 recipient mice transplanted with FM4 cells were also treated with a higher dose of cytarabine combined with an anthracycline to better reflect human

therapy ("7+3 regimen"). Nevertheless, our 5+3 regimen did not eliminate the FM4 cells *in vivo*, consistent with prior reports.

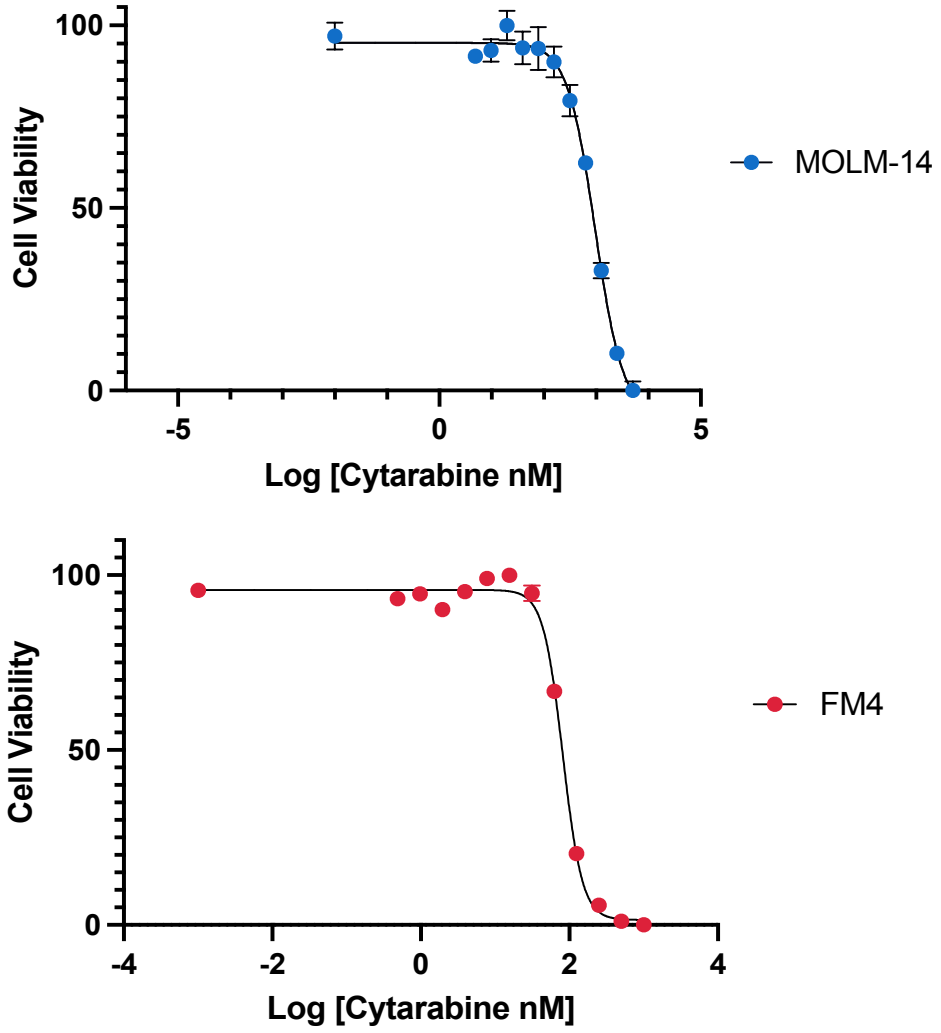

Figure 4.1. **Effect of cytarabine treatment on human and murine AML Cells *in vitro***
MOLM-14 cells (blue) were treated with cytarabine (0 - 5 uM) for 48 hours. Cell viability was assessed using the CellTiter-Glo luminescent viability assay. Data represents 3 independent experiments with SEM shown. FM4 cells (red) were treated with cytarabine (0 – 2 uM) for 48 hours. Data represents triplicates with SEM shown.

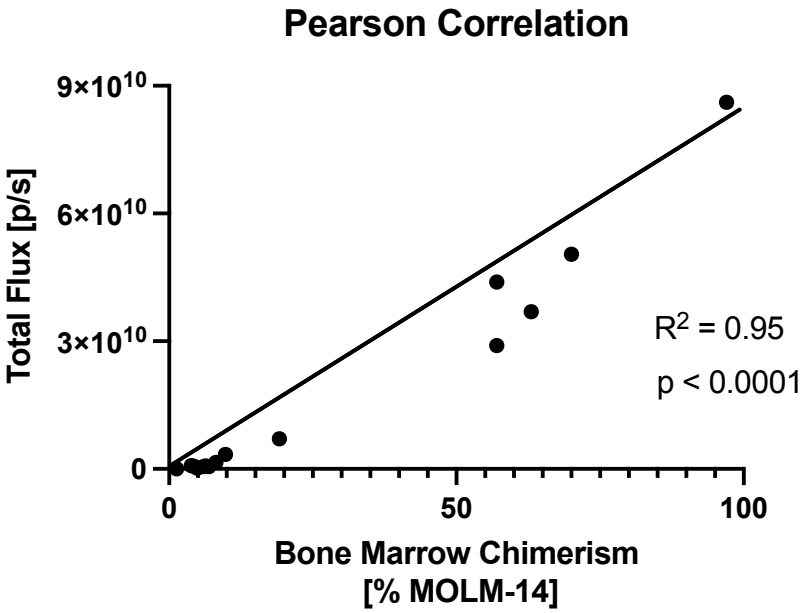

Figure 4.2. Pearson correlation of human AML burden and luciferase flux values *in vivo*
BM chimerism determined by the fraction of live mVenus+ MOLM-14 cells using flow cytometry was plotted against total flux values determined from bioluminescent imaging values for each animal and used to perform a Pearson correlation analysis.

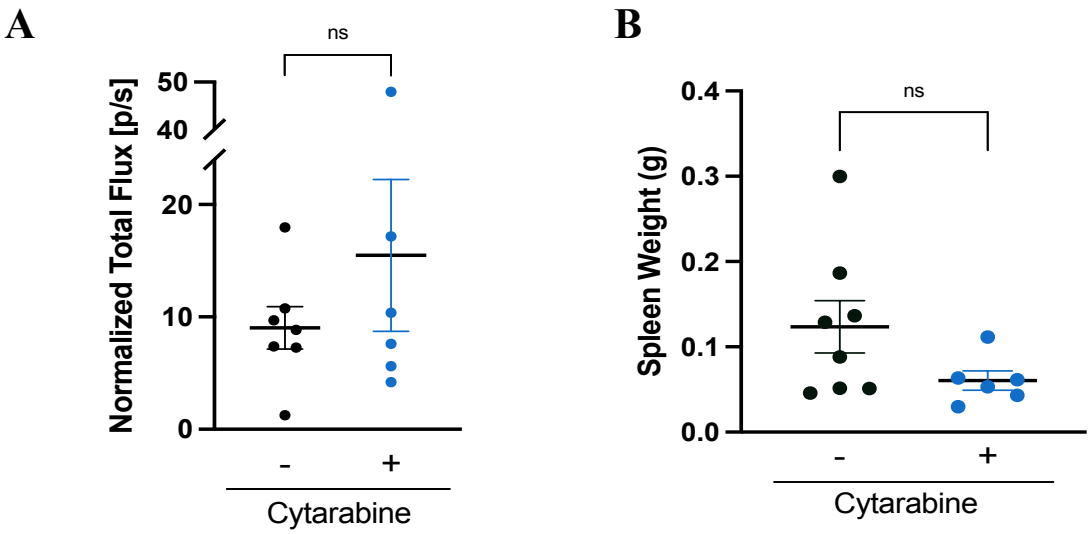

Figure 4.3. Cytarabine treatment does not reduce AML burden of MOLM-14 engrafted mice *in vivo*
(**A**) NSG mice normalized post-treatment total flux values (t-test, n = 13, p = 0.3447). (**B**) Spleen weight in grams of vehicle and cytarabine-treated mice (t-test, n = 14, p = 0.1155).

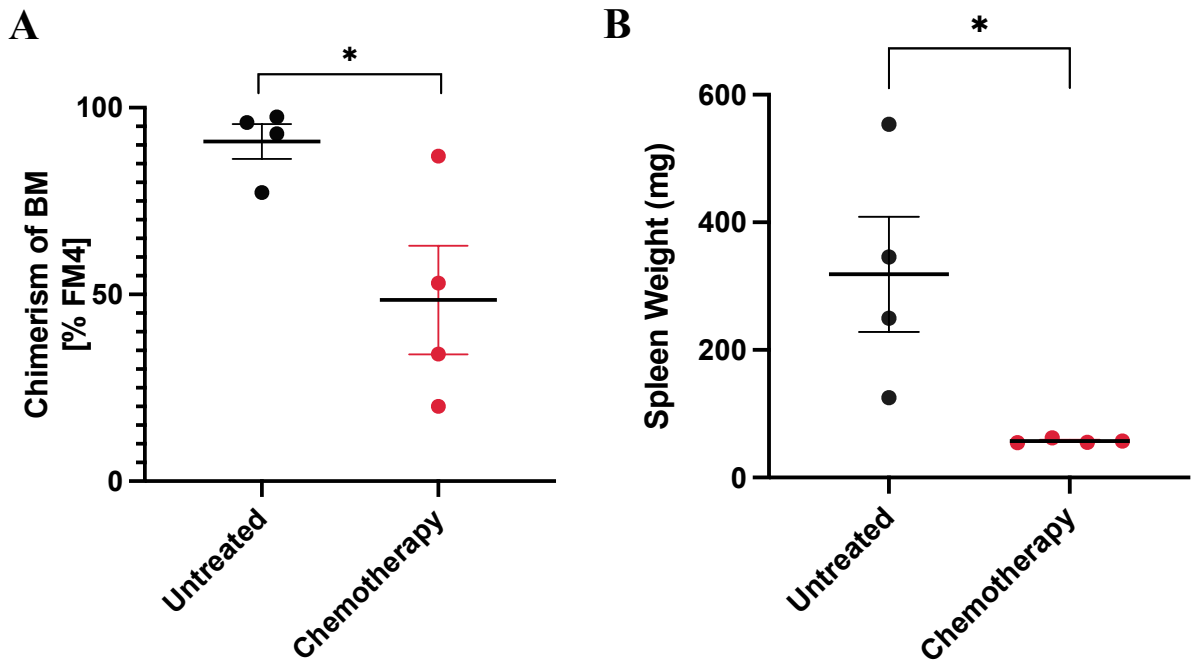

Figure 4.4. Chemotherapy treatment reduces murine AML burden *in vivo*
(**A**) Bone marrow chimerism (percent of iRFP+ FM4 cells of total live mononuclear cells) determined by flow cytometry (t-test, n = 8, p = 0.0317). (**B**) Spleen weight of vehicle and chemotherapy-treated mice (t-test, n = 8, p = 0.0278).

4.2 Chemotherapy increases mitochondrial activity and ROS production *in vitro* and *in vivo*

As previous work has proposed that increased mitochondrial activity contributes to chemoresistance in AML (see Introduction, section 1.1.7 Therapeutic Resistance and Relapse in AML), we examined two functional features of this process, mitochondrial membrane potential (MMP) and mitochondrial ROS production, in our AML cell lines in response to chemotherapy *in vitro* and *in vivo*. We examined MMP using the fluorescent mitochondrial dye tetramethylrhodamine ethyl ester (TMRE), which accumulates in active mitochondria relative to membrane potential. We then examined mitochondrial ROS production using the mitoSOX probe, which is similarly sequestered into the mitochondrial matrix due to its positive charge and reacts with superoxide to become fluorescent.

For experiments in the MOLM-14 cell line treated *in vitro* with cytarabine, we used the estimated IC25 dose for 48 hours (250 nM). We observed increased TMRE staining compared to

vehicle-controls, indicating a more polarized mitochondrion (**Figure 4.5A**). Consistent with the TMRE staining, we observed increased ROS production following cytarabine treatment (**Figure 4.5B**). We repeated these analyses on our FM4 cell line and we found a similar increase in mitochondrial ROS production (**Figure 4.5C**).

Next, we tested whether chemotherapy alters MMP *in vivo.* In parallel with the *in vitro* profile of mitochondrial activity, FM4 cells isolated from mice treated with the 5+3 regimen exhibited increased MMP and mitochondrial ROS production (**Figure 4.6A, Figure 4.6B**). In the MOLM-14-Luc model, we analyzed MMP and ROS production using TMRE and mitoSOX staining in the mVenus+ AML cells and observed a trend ($p = 0.4588$, $p = 0.4383$) towards increase in the cytarabine-treated animals (**Figure 4.6C, Figure 4.6D**). In this model, the absence of effect on mitochondrial activity with cytarabine may be a related to sub-therapeutic dosing *in vivo* (see section 4.1, **Figure 4.3**), thus limiting the conclusions that we can derive from this experiment.

In summary, we observed upregulation of MMP and ROS production in two AML models following exposure to cytarabine *in vitro* and in the *in vivo* FM4 model. This consistent increase in mitochondrial activity confirms what others have previously shown [72] and suggests a potential role of the mitochondria, specifically mitochondrial MMP and ROS homeostasis, in chemoresistance in AML.

4.3 Cytarabine treatment does not select for LSCs *in vivo*

As there has been conflicting reports that chemotherapy in AML may enrich for a dormant population of LSCs, we next examined the effect of chemotherapy on the clonogenic potential *ex vivo* of residual AML cells. While LSCs are defined operationally by their ability to re-initiate the disease in secondary recipients, the ability of single AML cells to give rise to colonies *ex vivo* is a surrogate functional readout of self-renewal. To perform the assay, we plated FM4 and MOLM-14-Luc cells isolated from the BM of chemotherapy-treated mice versus controls in methylcellulose and quantified the number of colony-forming units (CFUs). We found that the CFU ability of chemotherapy-treated samples was markedly decreased compared to untreated samples in both murine and humanized AML cells retrieved from mouse BM (**Figure 4.7A, Figure 4.7B**). This data supports the hypothesis that chemotherapy targets both self-renewing and mature AML populations.

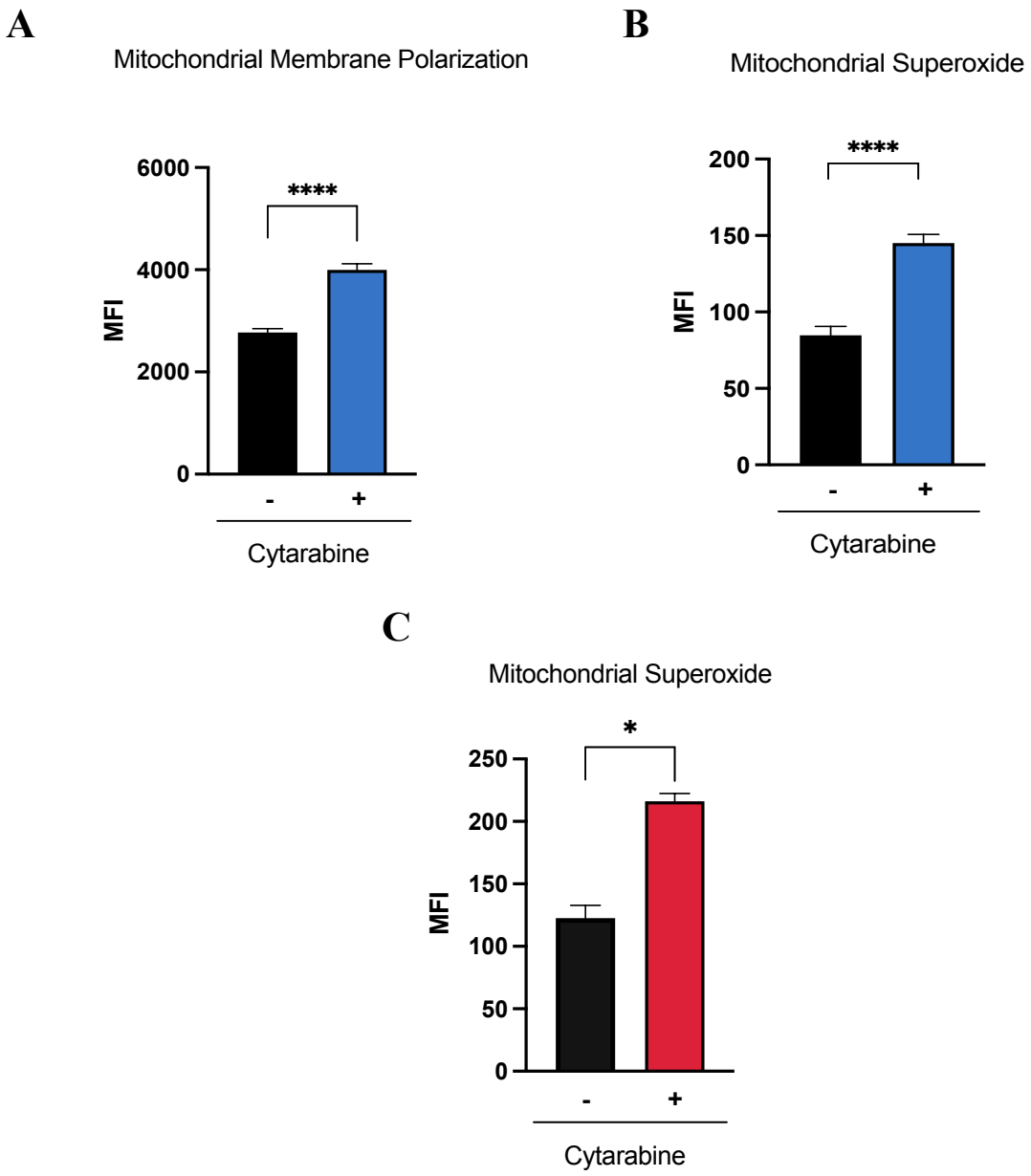

Figure 4.5. **Cytarabine treatment increases mitochondrial activity and ROS production *in vitro*** (**A**) MMP was assessed in vehicle and cytarabine treated MOLM-14 cells (250 nM for 48 hours) using TMRE. Data represents 3 independent experiments with 3 replicates (t-test, n = 18, p = < 0.0001). (**B**) Mitochondrial ROS production was assessed in vehicle and cytarabine-treated MOLM-14 cells using mitoSOX. Data represents 3 independent experiments with 3 replicates (t-test, n = 18, p = < 0.0001). (**C**) Mitochondrial ROS production was assessed in vehicle and cytarabine-treated FM4 cells treated (116 nM for 48 hours) using mitoSOX (t-test, n = 6, p = 0.0160).

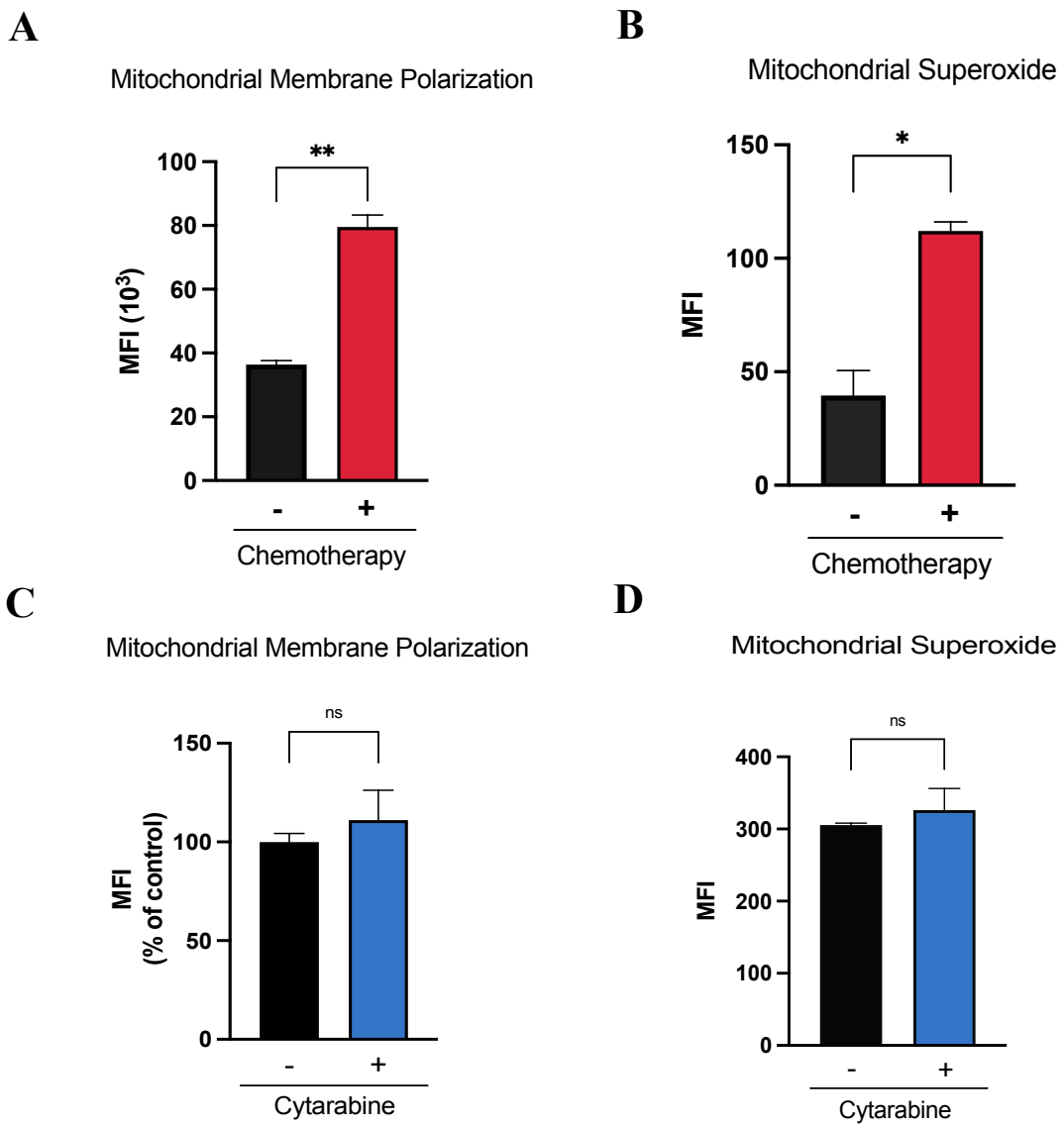

Figure 4.6. **Chemotherapy induces mitochondrial activity and ROS production *in vivo***
(**A**) MMP was assessed in vehicle and chemotherapy-treated FM4-engrafted mouse BM using TMRE (t-test, n = 5, p = 0.0083). (**B**) Mitochondrial ROS production was assessed in vehicle and chemotherapy-treated FM4-engrafted mouse BM using mitoSOX (t-test, n = 5, p = 0.025). (**C**) MMP was assessed in vehicle and cytarabine-treated MOLM-14-Luc engrafted BM using TMRE. Data represents 2 independent experiments expressed as a percentage of untreated control mice for each experiment (t-test, n = 11, p = 0.1279). (**D**) Mitochondrial ROS production in vehicle and cytarabine-treated MOLM-14-Luc engrafted BM using mitoSOX (t-test, n = 5, p = 0.4283).

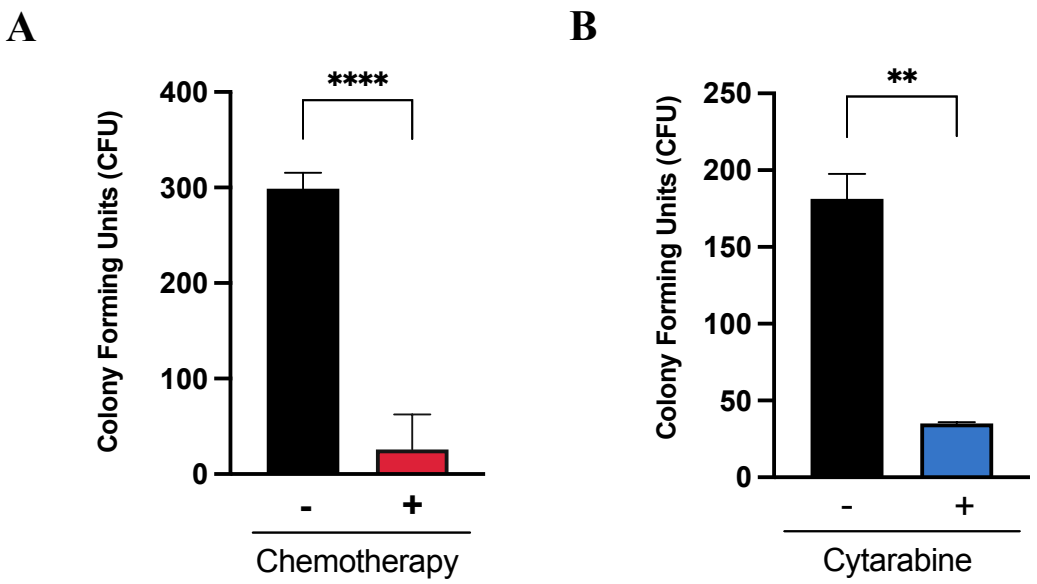

Figure 4.7. Chemotherapy does not enrich for AML LSCs *in vivo*
(A) Colony forming assays for mouse CD45.1 FM4 cells purified from whole mouse BM. 500 cells were plated into 2 mL of M3434 methylcellulose media and incubated for 7 days. Colonies were then counted. (t-test, n = 8, $p < 0.0001$). **(B)** Colony forming assays for hCD45 MOLM-14 cells purified from whole mouse BM. 500 cells were plated into 2 mL of H3434 methylcellulose media and incubated for 7 days before colonies were counted (t-test, n = 5, $p = 0.0061$).

4.4 AML cells upregulate mTORC1 signalling and cap-dependent translation following chemotherapy

As mTORC1 is known to be involved in the regulation of oxidative metabolism and a previous report showed that mTORC1 activity is induced following chemotherapy [75], we next assessed mTORC1 activity through analysis by flow cytometry of phosphorylation on two direct targets: phosphorylated-S6 (pS6) at Ser240/244 and phosphorylated-4EBP1 (p4EBP1) at Thr37/46. In FM4 AML cells isolated from the BM of mice at day 8 of treatment, we observed considerable upregulation of both p4EBP1 and pS6 (**Figure 4.8A, Figure 4.8B**), suggesting that mTORC1 is hyper-activated in this model after chemotherapy. In the MOLM-14-Luc model, we observed a non-significant trend toward increased p4EBP1 and pS6 levels ($p = 0.25$ and $p = 0.24$, **Figure 4.8C, Figure 4.8D**). As previously mentioned, this absence of significant change in

mTORC1 activity in the *in vivo* MOLM-14-Luc model may be related to the lack of significant AML killing (**Figure 4.3**) and difference in mitochondrial activity (**Figure 4.6**).

To assess whether the role of the BM microenvironment is essential for the upregulation of mTORC1 signalling following chemotherapy (see Introduction, section 1.1.7 Therapeutic Resistance and Relapse in AML), we examined mTORC1 activity following 48 hours of cytarabine treatment of the MOLM-14 cell line *in vitro.* Surprisingly, we detected increased levels of pS6 and p4EBP1 following cytarabine treatment *in vitro* (**Figure 4.8E, Figure 4.8F**), suggesting that the microenvironment may not be required for these effects. To determine whether this increase in mTORC1 activity was mediated by the PI3K-Akt pathway, we also examined cytarabine-treated MOLM-14 cells for phosphorylated-Akt (pAkt) levels at Ser473. pAkt levels were correspondingly elevated in treated samples, suggesting that the PI3K-Akt pathway is involved in upregulating mTORC1 signalling post-chemotherapy (**Figure 4.8G**).

To validate these results, we performed, in collaboration with the laboratory of Dr. Sonia Del Rincon, an immunoblotting analysis of the PI3K-Akt-mTORC1/2 pathway in MOLM-14 cells exposed for 24 hours to cytarabine or vehicle controls (**Figure 4.9**). This experiment was performed only once due to time constraints, and the results are presented to demonstrate validity of the technique and in support of the flow cytometry findings. While we observed no difference of phosphorylation on mTOR at serine 2481, it appeared increased at S2448 after cytarabine, suggesting activation of the mTORC1 complex and not mTORC2 [132]. Further supportive of mTORC1 activation, we observed increased p4EBP1 accompanied by a relative shift of total 4EBP1 towards the faster migrating bands, another finding representative of 4EBP1 phosphorylation [133], and we detected a possible increase in the levels of peIF4E. Of note, the levels of total eIF4A were unchanged between conditions and we observed no change in total or phosphorylated S6 or S6K protein expression in contrast to the change in pS6 levels detected by flow cytometry; this finding may be related to different durations of exposure to cytarabine (48-hour versus 24-hour) or sensitivities of both techniques. If confirmed, these findings may suggest a greater activation of the mTORC1-4EBP1-eIF4E axis and less signalling through mTORC1-S6K-PDCD4-eIF4A. Collectively, these findings support the hypothesis that AML cells upregulate mTORC1 in response to chemotherapy. Interestingly, this was again observed *in vitro*, which suggests an effect occurring independently of the BM microenvironment.

As we observed mTORC1 activation following chemotherapy *in vitro* and *in vivo*, we hypothesized that chemoresistant AML may depend on increased mTORC1-regulated protein synthesis for re-growth. To examine rates of protein synthesis in cytarabine-treated samples and controls, we used the OP-Puro reagent that is incorporated in nascent peptide chains. MOLM-14 cells were first treated *in vitro* for 48-hours with cytarabine or vehicle. Following drug treatment, the cells were incubated with the OP-Puro compound and conjugated to a fluorescent azide using click chemistry. We observed a strong increase in OP-Puro incorporation in cytarabine-treated samples (**Figure 4.10A**), suggesting elevated levels of translation. We similarly assessed translation levels using OP-Puro in FM4 cells retrieved from the BM of mice treated with chemotherapy and observed an upward trend ($p = 0.063$) in protein synthesis (**Figure 4.10B**). Altogether, our data suggests that AML cells induce mTORC1-signalling following chemotherapy to increase protein synthesis and support metabolic adaptation and regrowth.

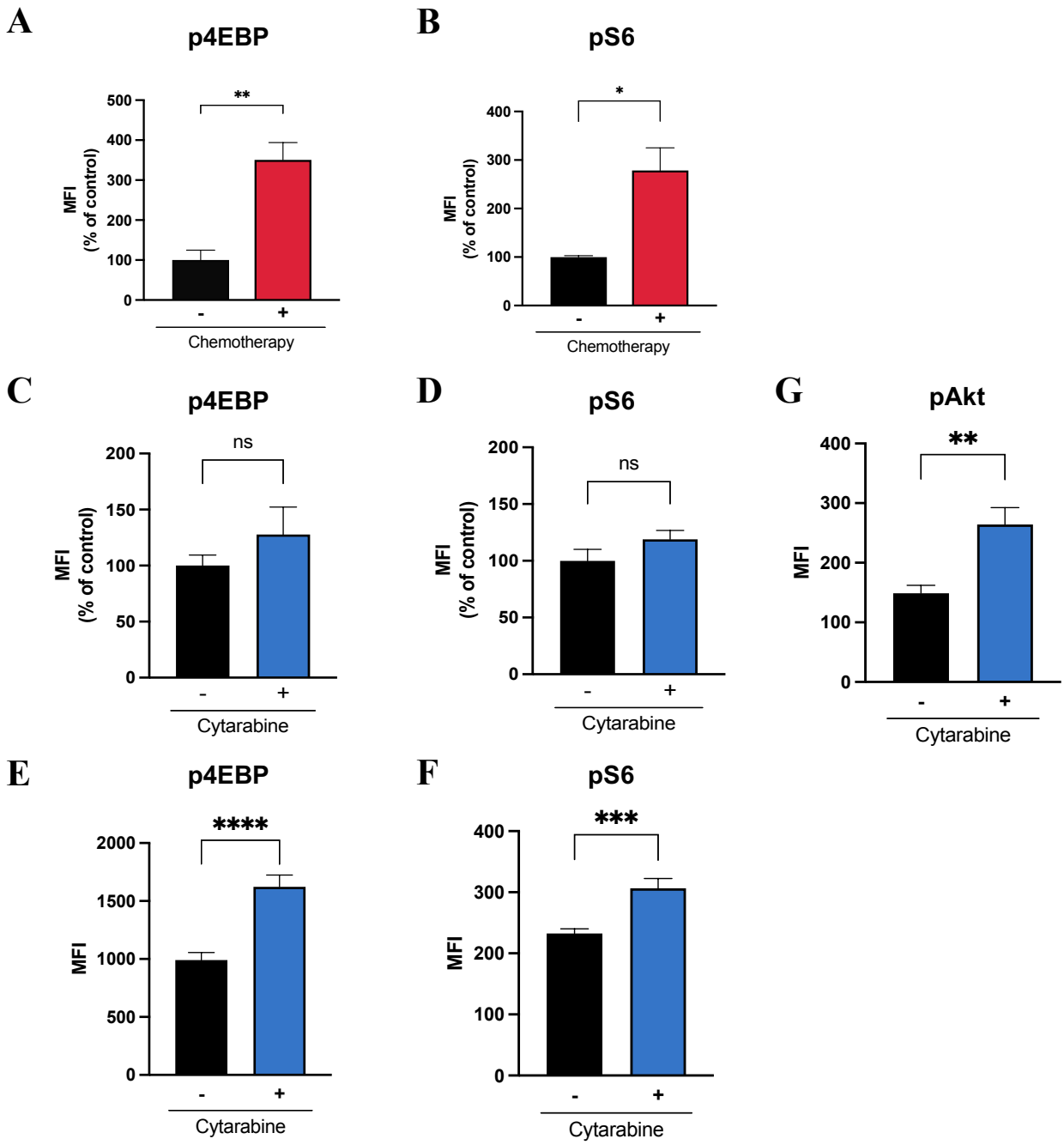

Figure 4.8. **Cytarabine treatment induces mTORC1 signaling *in vitro* and *in vivo***

(A-F) p4EBP and pS6 levels in untreated vs cytarabine treated samples. (**A-B**) FM4 isolated from the BM of C57BL/6 mice. Data represents 2 independent experiments expressed as a percentage of untreated control mice for each experiment (**A**: t-test, n = 7, p = 0.0063, **B**: t-test, n = 7, p = 0.0233). (**C-D**) MOLM-14-Luc isolated from the BM of NSG mice. Data represents 2 independent experiments expressed as a percentage of untreated control mice for each experiment (**C**: t-test, n = 8, p = 0.1487, **D**: t-test, n = 8, p = 0.2418). (**E-F**) MOLM-14 cells treated *in vitro* (250 nM for 48 hours). Data represents 3 independent experiments with 3 replicates (**E**: t-test, n = 18, p = <0.0001, **F**: t-test, n = 18, p = 0.0007). (**G**) pAkt levels in untreated vs cytarabine MOLM-14 cells treated *in vitro*. Data represents 2 independent experiments with 2-3 replicates (t-test, n = 10, p = <0.0061).

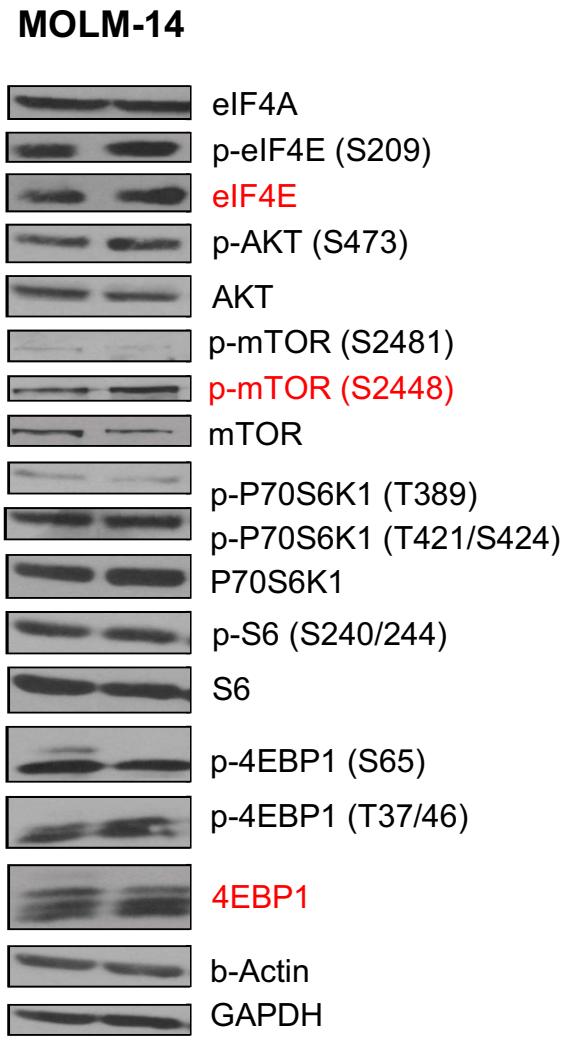

Figure 4.9. **mTORC1 activity is upregulated following cytarabine treatment *in vitro***

Western blotting showing eIF4A, peIF4E, eIF4E, pAKT, Akt, pmTOR, mTOR, pS6K, S6K, pS6, S6, p4EBP1, and 4EBP1in MOLM-14 cells after 24-hour treatment with 250 nM of cytarabine. Beta-Actin and GAPDH were used as loading controls. Evident changes after treatment are highlighted in red.

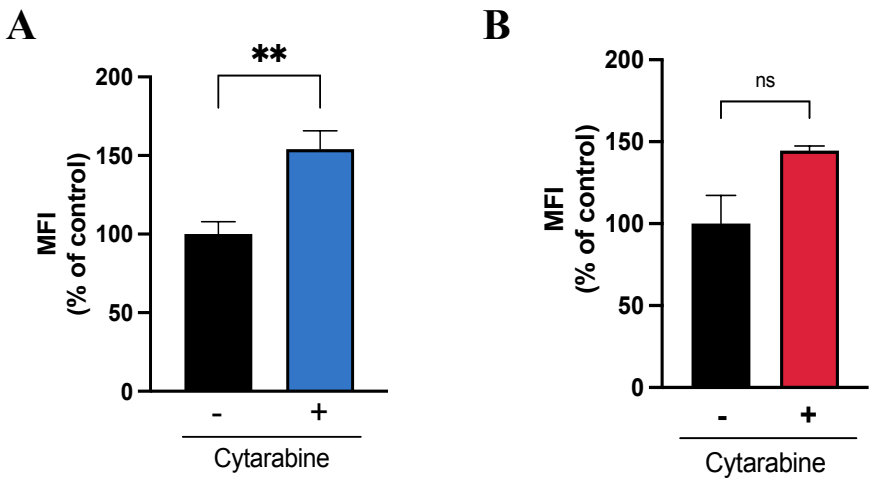

Figure 4.10. **AML cells upregulate protein synthesis following chemotherapy *in vitro* and *in vivo*** (**A**) Level of OP-Puro conjugation in MOLM-14 cells treated with cytarabine or vehicle-controls (250 nM for 28 hours). Data represents 3 independent experiments expressed as a percentage of untreated controls for each experiment (t-test, n = 12, p = 0.0033). (**B**) Level of OP-Puro conjugation in FM4 cells from the BM of cytarabine or vehicle-treated C57BL/6 mice. Data represents 2 independent experiments expressed as a percentage of untreated controls for each experiment (t-test, n = 6, p = 0.063).

4.5. Pharmacological inhibition of eIF4A using CR-1-31-B is synergistic with cytarabine in AML cells *in vitro*

As eIF4A-driven cap-dependent mRNA translation is a mechanism through which mTORC1 promotes protein synthesis, and our previous data suggested that this activity is increased in the context of chemotherapy, we sought to test whether blocking this pathway would enhance the chemo-sensitivity of AML. To do this, we used the potent and selective inhibitor of eIF4A CR-1-31-B. First, we determined the sensitivity of the AML lines MOLM-14, U937, and KG1-a to single-agent CR-1-31-B. We observed marked reduction of viability at nanomolar concentrations (**Figure 4.11A**). At 48-hours, the IC50 values were determined to be 0.65 nM for MOLM-14, 1.7 nM for U937, and 1 nM for KG1-a.

To determine whether treatment with CR-1-31-B would synergize with chemotherapy, we treated MOLM-14 cells with CR-1-31-B or cytarabine in dose matrices to test multiple pairings of serially diluted single and combination agent doses, quantified viability using the CellTiter-Glo assay, and analyzed drug synergy using the Synergyfinder application to assess the effect of cytarabine in combination with CR-1-31-B (**Figure 4.11C**). We chose to perform this analysis

with the MOLM-14 cell line, as MOLM-14 cells appeared to be more resistant to chemotherapy and were a more relevant human model in comparison to the FM4 mouse cell line. The Synergyfinder analysis indicated a Bliss score of 11.923 in the MOLM-14 cell line, signifying a synergistic relationship between the two compounds [134]. We also constructed an isobologram and found that samples treated with both agents produced IC50 and IC70 values which fell below those corresponding to single agents, indicating drug synergy (**Figure 4.11D**).

Next, to further examine the interaction between CR-1-31-B and chemotherapy, we treated MOLM-14 cells with cytarabine, CR-1-31-B, or both, and assessed for levels of cell death using annexin-V/PI staining 24 and 48 hours later. The cells were treated with the estimated IC25 dose of cytarabine (250 nM), and a concentration of CR-1-31-B which was calculated as highly synergistic with this dose of cytarabine (2.5 nM) based on the Bliss synergy analysis. At 24 hours, cells treated with cytarabine or CR-1-31-B alone displayed approximately 10% and 18% cell death, respectively, whereas cells treated with both agents displayed a significant increase in cell death with 32% of cells undergoing apoptosis (**Figure 4.11B**, One-way ANOVA with Tukey's HSD, $p < 0.0001$). At 48 hours, 15% of cells treated with cytarabine alone were apoptotic while both CR-1-31-B and the combination treatment displayed considerably higher levels of cell death (80%, 91%). At 48 hours, samples treated with the combination of cytarabine and CR-1-31-B exhibited significantly greater cell death than CR-1-31-B alone (One-way ANOVA with Tukey's HSD, $p < 0.0001$).

4.6. CR-1-31-B treatment induces cell cycle arrest, DNA damage, and apoptosis in AML cells *in vitro*

As studies with older rocaglates (Eg. Silvestrol) demonstrate inhibition of cell-cycle related genes and stalling in either the G1 or G2 phase [135, 136], we performed cell cycle analyses to determine if the mechanism of CR-1-31-B cytotoxicity alone or in combination with cytarabine involves cell cycle arrest. We treated MOLM-14 cells for 24 hours with cytarabine, CR-1-31-B, or both drugs. Cytarabine alone resulted in a significant increase in the fraction of cells in S-phase (**Figure 4.12**, Two-way ANOVA with FDR correction, $p < 0.0001$) compared to control samples, which is consistent with the mechanism of a nucleoside analog. In contrast, in samples treated with CR-1-31-B the proportion of MOLM-14 cells in G0/G1 was significantly increased (Two-way ANOVA with FDR correction, $p < 0.05$) compared to vehicle controls. Samples given the

combination treatment exhibited significantly fewer cells in G0/G1 (Two-way ANOVA with FDR correction, $p < 0.0001$).

To better understand the mechanisms underlying how CR-1-31-B alone and in combination with cytarabine induces cell death in AML, we performed polysome profiling on the MOLM-14 cell line. MOLM-14 cells were treated for 24 hours with 250 nM of cytarabine or vehicle controls. At 23 hours, half of the cytarabine treated cells were treated with 10 nM of CR-1-31-B for 1 hour. An additional sample was treated with 10 nM of CR-1-31-B alone for 1 hour before proceeding to polysome fractionation. 3 independent experiments were performed to create replicates for RNA sequencing, with a representative polysome profile displayed in **Figure 4.13A**. As expected, vehicle-treated MOLM-14 cells displayed the highest levels of translation, with the lowest monosome peak and highest polysome peaks, while samples treated with CR-1-31-B and cytarabine and CR-1-31-B exhibited the lowest protein synthesis. Counter to our earlier data, cytarabine-treated samples did not show elevated translation levels but remained at a greater level than samples treated with CR-1-31-B. Aliquots were also taken from each condition for analysis by western blot (**Figure 4.13B**).

Interestingly, we observed increased levels of phosphorylated H2A histone family member X (γH2AX), a marker of double-strand DNA breaks, after CR-1-31-B treatment (**Figure 4.13B**). To confirm this finding, we visualized γH2AX foci in MOLM-14 cells treated with CR-1-31-B using immunofluorescence (**Figure 4.13C**). An increase in γH2AX fluorescence was observed in the CR-1-31-B treated cells, suggesting that CR-1-31-B either impairs the DNA damage response of the cell or otherwise promotes double-strand DNA breaks.

Finally, to further examine protein synthesis in CR-1-31-B and combination treated AML cells, we performed OP-puro labeling in MOLM-14 cells treated *in vitro* for 48-hours (250 nM cytarabine and 2.5 nM CR-1-31-B) (**Figure 4.13D**). In agreement with our polysome data, we found CR-1-31-B treated samples displayed reduced OP-puro incorporation, indicating decreased translation. Samples treated with both cytarabine and CR-1-31-B were interestingly not significantly reduced compared to vehicle controls in contrast to our polysome analysis, although the SEM for this group was elevated.

In agreement with previous reports examining translation inhibition in acute lymphoblastic leukemia and in AML which demonstrated decreased expression of BCL-2 family proteins *in vitro* [108, 128], we observed that BCL-2 expression was increased following cytarabine treatment and

decreased after CR-1-31-B treatment. To further support this, we reasoned that CR-1-31-B might synergize with venetoclax (a clinically approved BCL-2 inhibitor commonly used to treat older AML patients) due to their putative complementary mechanisms. To examine the interaction of CR-1-31-B and venetoclax *in vitro*, MOLM-14 cells were exposed to increasing concentrations of both drugs alone or in combination in dose matrices and the cell viability was assessed 24-hours later using CellTiter-Glo. A Bliss independence model was again applied to analyze synergy through the Synergyfinder application, and the Bliss score was calculated to be 19.80 indicating strong synergy (**Figure 4.14**). These results support the notion that eIF4A inhibition potently targets AML cells and acts at least in part due to induction of DNA damage and suppression of the anti-apoptotic protein BCL-2.

A

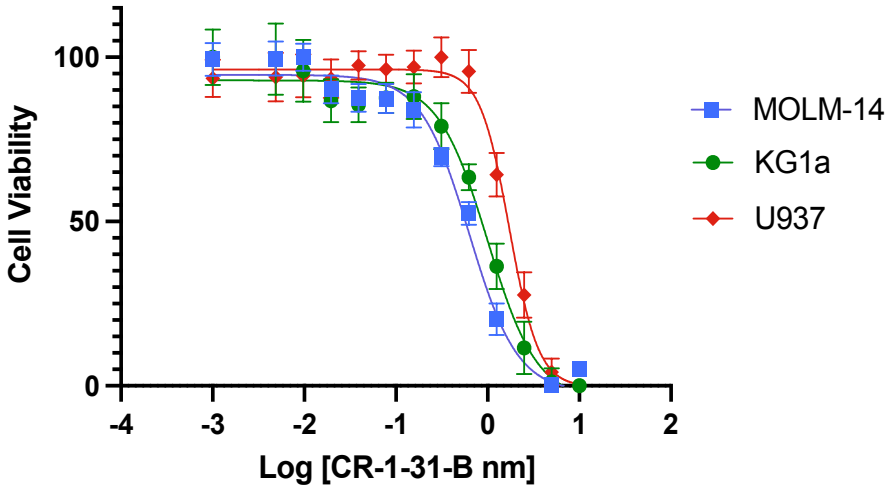
Cell Viability
100
50
0
-4
-3
-2
-1
0
1
2
Log [CR-1-31-B nm]
MOLM-14
KG1a
U937

B

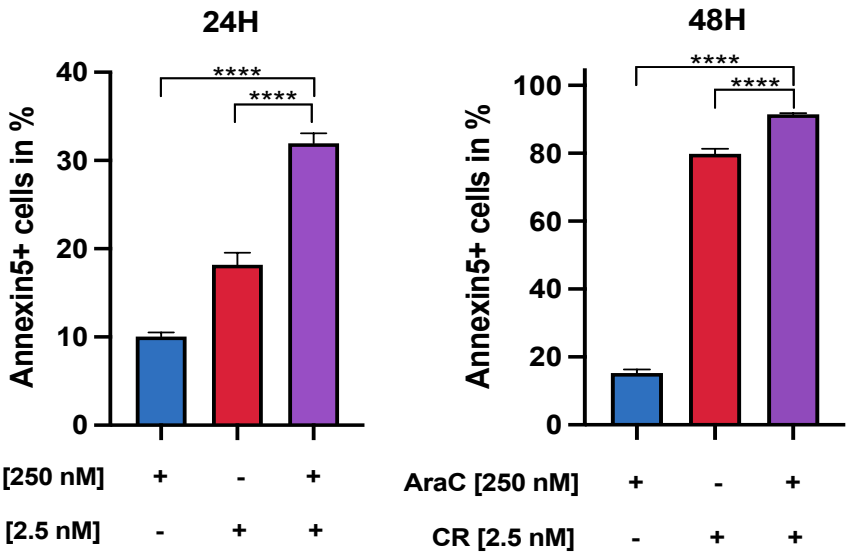
24H
48H
Annexin5+ cells in %
****
****
AraC [250 nM]
CR [2.5 nM]

C

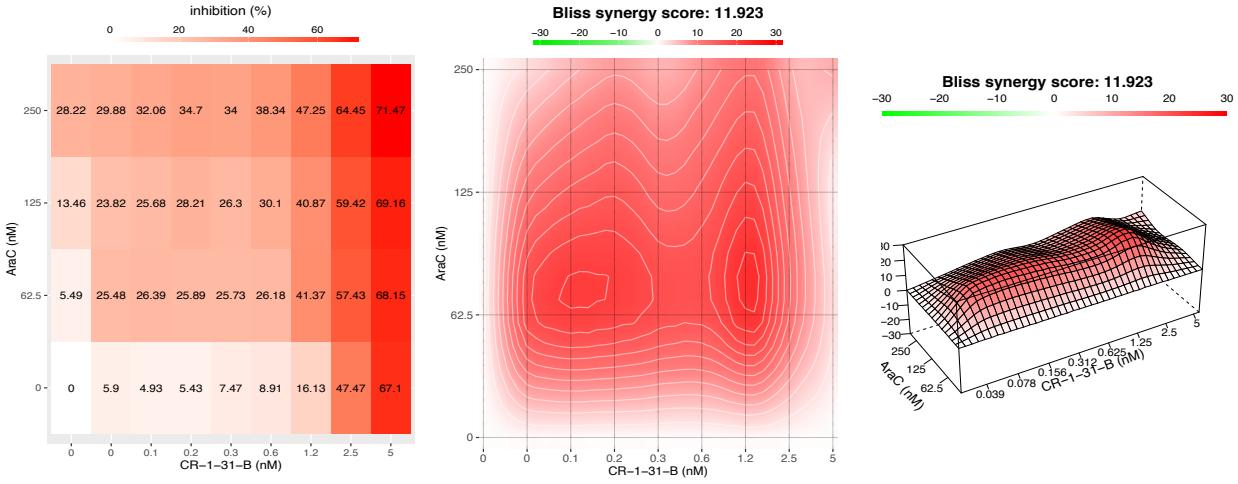
inhibition (%)
Bliss synergy score: 11.923
AraC (nM)
CR−1−31−B (nM)

D

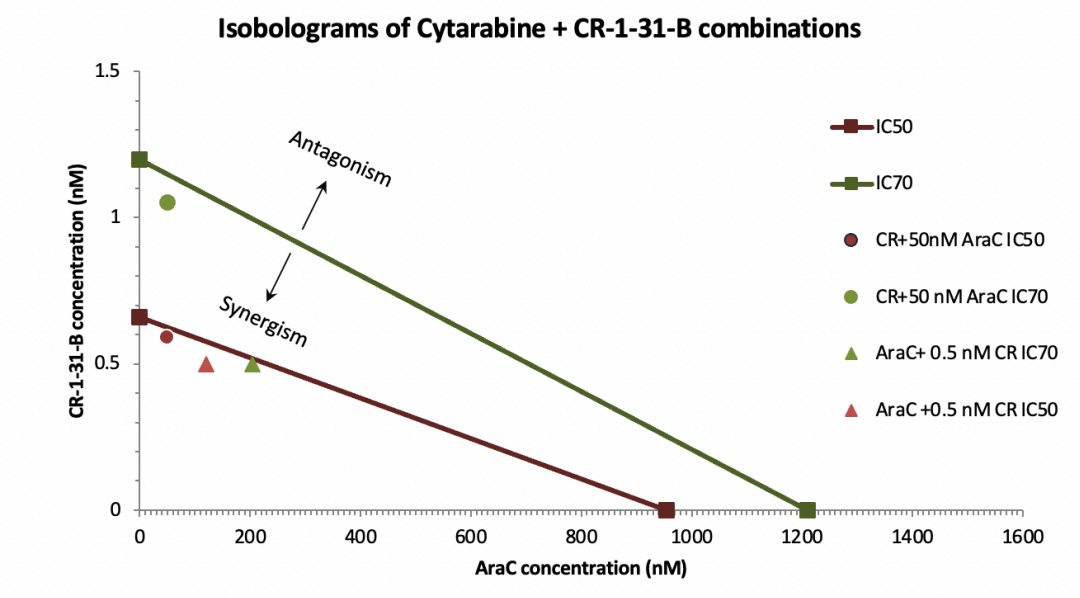

Figure 4.11. **CR-1-31-B and cytarabine synergize *in vitro***
(**A**) AML cell lines were seeded in 96-well plates in increasing concentrations of CR-1-31-B. Cell viability was measured 48-hours later using the CellTitre-Glo reagent. Data represents 3 independent experiments with 3 replicates with SEM shown. (**B**) Percent of AnnexinV+ MOLM-14 cells 24 and 48-hours after drug treatment. Data represents 3 independent experiments with 3 replicates (One-way ANOVA with Tukey's HSD). (**C**) Bliss Synergy analysis for the combination of CR-1-31-B and cytarabine 24-hours after treatment. Plots produced by the Synergyfinder application. Data represents 3 independent experiments with 2 replicates. (**D**) An isobologram was constructed to examine the interaction between cytarabine and CR-1-31-B. The IC50 and IC70 values of each drug determined in the MOLM-14 cell line were plotted on the axes with individual points representing the IC70 and IC50 of the combination treatments. Points falling below the line indicate drug synergy, while points above indicate antagonism.

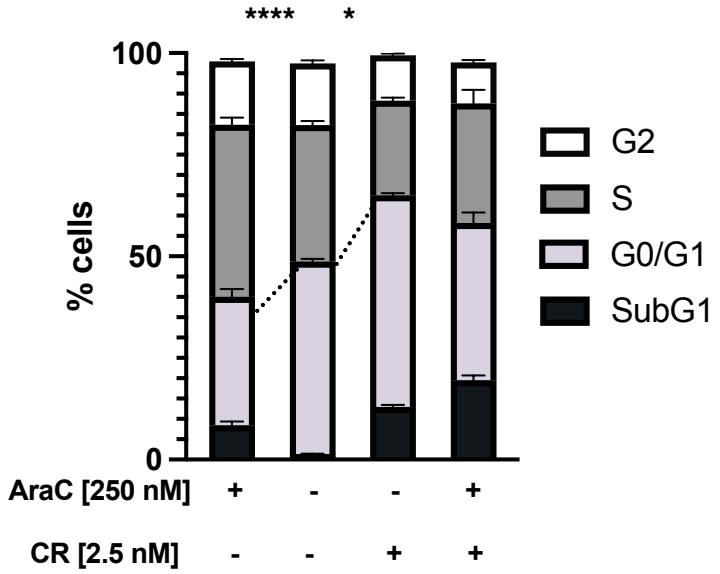

Figure 4.12. **CR-1-31-B alters cell cycle progression *in vitro***
Cell cycle distribution of MOLM-14 cells 24-hours after treatment. Data represents 3 independent experiments with 3 replicates (Two-way ANOVA with FDR correction).

A

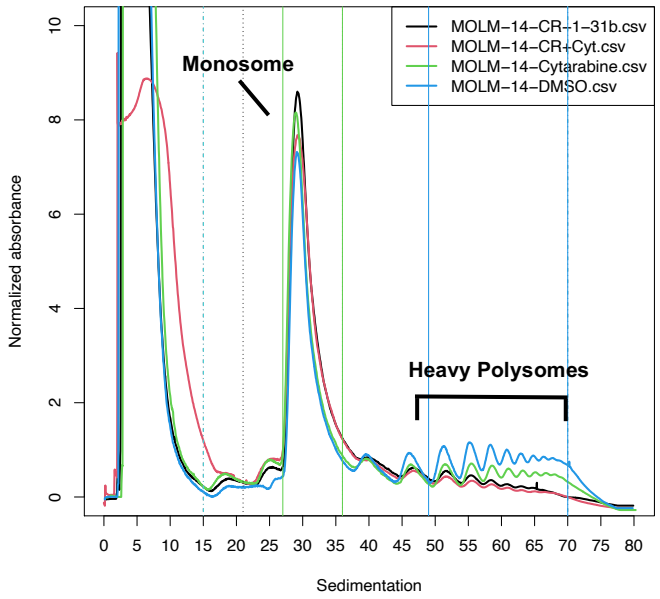
MOLM−14−CR−1−31b.csv
MOLM−14−CR+Cyt.csv
MOLM−14−Cytarabine.csv
MOLM−14−DMSO.csv
Monosome
Heavy Polysomes
Normalized absorbance
Sedimentation
0
2
4
6
8
10
0 5 10 15 20 25 30 35 40 45 50 55 60 65 70 75 80

B

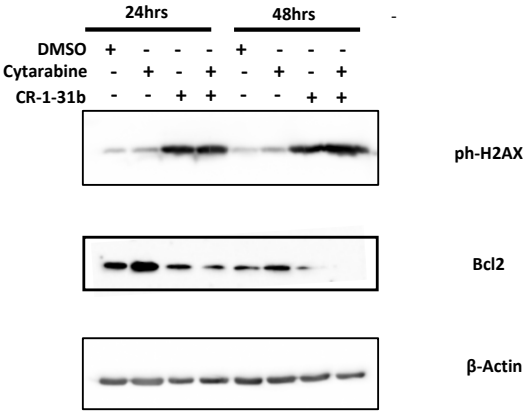
24hrs
48hrs
DMSO + - - - + - - -
Cytarabine - + - + - + - +
CR-1-31b - - + + - - + +
ph-H2AX
Bcl2
β-Actin

C

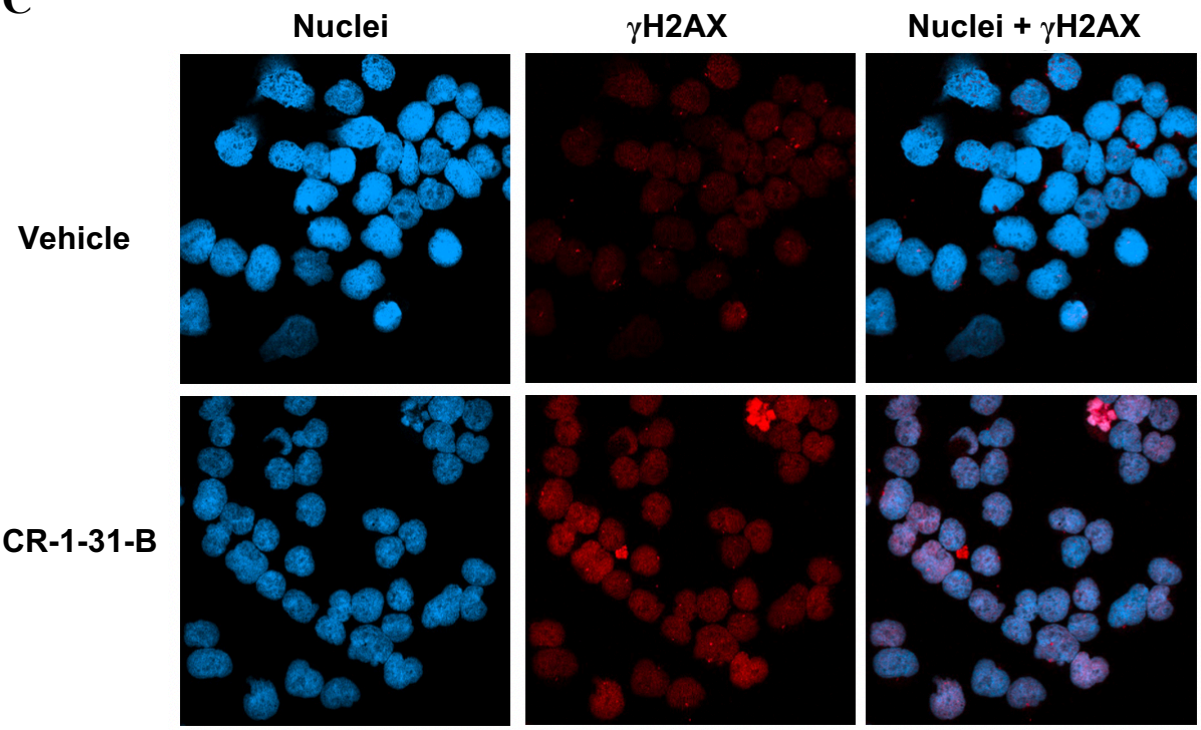
Nuclei
γH2AX
Nuclei + γH2AX
Vehicle
CR-1-31-B

D

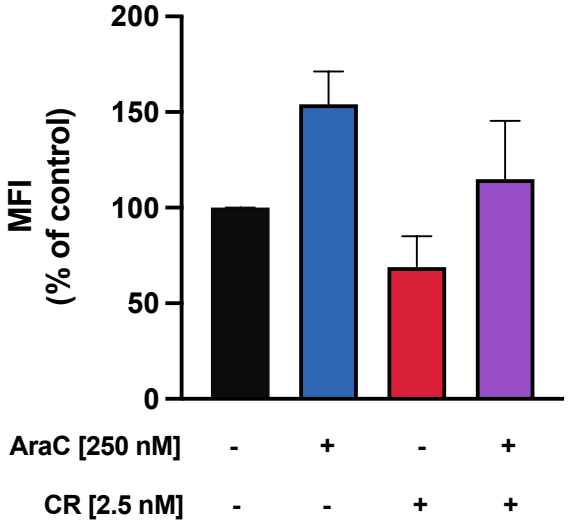

Figure 4.13. **CR-1-31-B activity *in vitro***
(**A**) Polysome profile of MOLM-14 cells after treatment with cytarabine (250 nM for 24 hours), CR-1-31-B (10 nM for 1 hour), or both agents. Polysome profiling was performed in 3 independent experiments and a representative profile is shown. (**B**) Western blot of γH2AX and BCL-2 in MOLM-14 cells after treatment with cytarabine, CR-1-31-B or both drugs. Beta-actin was used as a loading control. (**C**) Immunofluorescence of γH2AX foci (red) in MOLM-14 cells treated with vehicle or 10 nM CR-1-31-B for 1 hour. DNA was stained with DAPI (blue). (**D**) Level of OP-Puro conjugation in MOLM-14 cells treated with vehicle, cytarabine (250 nM for 48 hours), CR-1-31-B (250 nM for 48 hours), or both drugs. Data represents 3 independent experiments with 2 replicates expressed as a percentage of untreated controls for each experiment.

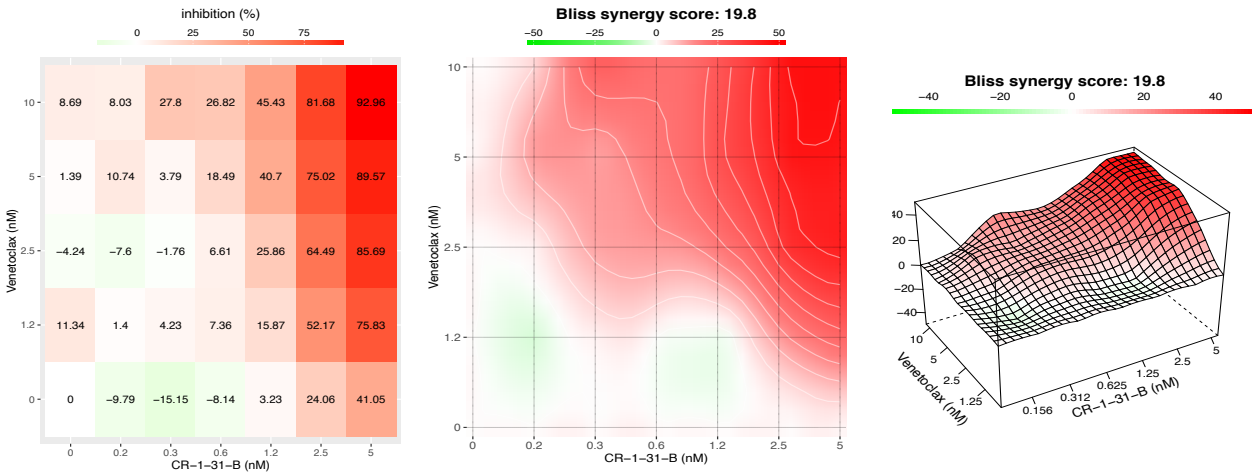

Figure 4.14. Venetoclax and CR-1-31-B treatment synergize *in vitro*
Bliss Synergy analysis for the combination of CR-1-31-B and venetoclax 24-hours after treatment. Plots produced by the Synergyfinder application. Data represents 3 independent experiments with 2 replicates.

4.7 Cytarabine and CR-1-31-B treatment strongly induces mitochondrial depolarization and ROS production *in vitro*

To examine whether the increased mitochondrial function and polarization in AML cells following chemotherapy (Section 4.2) is an adaptation mediated by eIF4A, we treated MOLM-14 cells with CR-1-31-B and/or cytarabine for 48 hours, and again used the TMRE and mitoSOX dyes. CR-1-31-B alone and in combination with cytarabine showed a strong increase in cells with depolarized mitochondria compared to cytarabine alone (**Figure 4.15A**). Interestingly, although CR-1-31-B alone increased mitochondrial ROS production compared to vehicle controls, the combination treatment induced significantly greater ROS than either single agent (**Figure 4.15B**, One-way ANOVA with Tukey's HSD; CR-1-31-B: $p = 0.0002$, cytarabine: $p < 0.0001$). Given that we observed significantly greater levels of mitochondrial ROS in cells treated with cytarabine and CR-1-31-B, we asked whether reducing mitochondrial ROS levels could rescue cell viability *in vitro*. To determine the effect of targeting mitochondrial ROS signalling, cells were incubated with 20 uM of the mitochondrial-specific antioxidant mitoTEMPO for 2 hours prior to drug treatment. After 48-hour treatment, the fraction of apoptotic cells was quantified using annexin-V/PI staining and compared to samples which were not pre-treated with mitoTEMPO. The addition

of the mitoTEMPO buffer did not significantly alleviate cytarabine-induced cell death, but partially rescued CR-1-31-B and the combination treatment induced cytotoxicity (**Figure 4.15C**, One-way ANOVA with Sidak's correction; CR-1-31-B: $p = 0.0002$, cytarabine + CR-1-31-B: $p = 0.0011$). These findings suggest that although CR-1-31-B strongly induces mitochondrial ROS production, rescuing from oxidative stress may not be sufficient to prevent cell death.

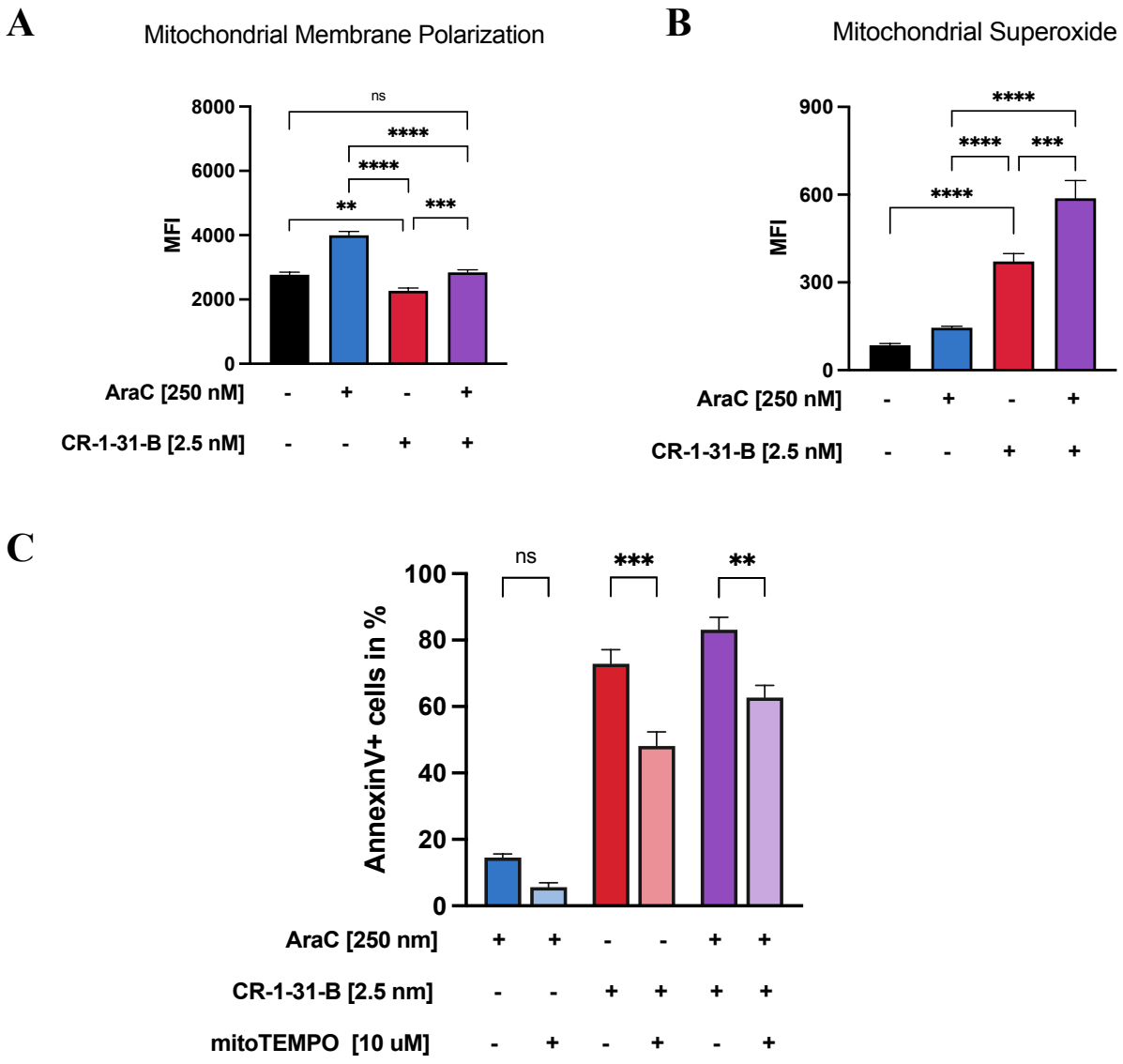

Figure 4.15. **Cytarabine and CR-1-31-B treatment strongly induces mitochondrial depolarization and ROS production *in vitro***

(**A**) MMP in MOLM-14 cells treated with cytarabine, CR-1-31-B, both drugs, or vehicle for 48 hours. Data represents 3 independent experiments of 3 replicates (One-way ANOVA with Tukey's HSD). (**B**) Mitochondrial ROS production in MOLM-14 cells treated with cytarabine, CR-1-31-B, both drugs, or vehicle. Data represents 3 independent experiments of 3 replicates (One-way ANOVA with Tukey's HSD). (**C**) Annexin V+ MOLM-14 cells treated with drugs versus samples incubated with mitoTEMPO prior to drug treatment. Data represents 2 independent experiments with 2 replicates (One-way ANOVA with Sidak's correction; Cytarabine: $p = 0.02085$, CR-1-31-B: $p = 0.0002$, Cytarabine + CR-1-31-B: $p = 0.0011$).

4.8 CR-1-31-B significantly reduces AML burden *in vivo*

To examine if targeting translation initiation inhibits AML growth *in vivo*, we next examined the effects of CR-1-31-B treatment in our mouse model of chemoresistant human AML. In this model, MOLM-14 engrafted mice treated with CR-1-31-B alone and in combination with cytarabine displayed appreciably reduced leukemic burdens (**Figure 4.16A, Figure 4.16C**). It was striking to find that normalized flux values for CR-1-31-B alone were not significantly different in comparison to the combination treatment, indicating CR-1-31-B was equally effective as a single agent in this model. Notably, mice treated with cytarabine or cytarabine and CR-1-31-B had spleens of similar size, however mice treated with CR-1-31-B alone exhibited much larger spleens (**Figure 4.16B**). This increase in spleen weight parallels that of healthy C57BL/6 mice treated with CR-1-31-B (**Figure 4.17C**), suggesting the enlargement does not represent infiltration of the spleen by blasts. MMP analysis of MOLM-14 cells following treatment also did not appear to show a significant change in the MFI of TMRE in untreated compared to cytarabine or CR-1-31-B treated BM (**Figure 4.16D**).

4.9 CR-1-31-B is not cytotoxic to healthy myeloid cells but impairs B-cell development

We next sought to determine if CR-1-31-B treatment displayed toxicity towards healthy myeloid cells or otherwise modified hematopoiesis. Healthy C57BL/6 mice were treated with 0.2 mg/kg CR-1-31-B for 7 days intraperitoneally. This dose was well tolerated and there was no significant weight loss or change in animal activity compared to vehicle-treated controls (**Supplemental Figure 1A**). Additionally, this regimen did not alter the livers of treated mice (**Supplemental Figure 1B**). To determine if CR-1-31-B significantly induced hematopoietic cell death, annexin-V staining was performed on harvested BM cells (**Figure 4.17A**). No difference was observed in the number of cells undergoing apoptosis compared to control BM, suggesting that CR-1-31-B is not strongly cytotoxic to normal hematopoietic cells. We then assessed the effect of CR-1-31-B treatment on hematopoietic lineages in the blood, BM, and spleen. Whole BM cell counts were multiplied by the percent of individual cell types determined by flow cytometry to estimate absolute cell counts for each population.

We first evaluated hematopoietic lineages in the blood, BM, and spleen using well-established cell surface markers for B cell ($B220^+$), T cell ($CD3^+$, $CD4^+$, $CD8^+$) and myeloid cell ($CD11b^+$ $GR\text{-}1^+$, encompassing monocytes, neutrophils, and eosinophils) populations. Strikingly,

we found was an approximate 5-fold reduction in the fraction of $B220^+$ cells within the BM in comparison to control mouse BM (**Figure 4.17B**). Interestingly, we observed a prominent increase in spleen size (**Figure 4.17C**) however we found no difference in the absolute number of $B220^+$ cells within the blood or the spleen (**Figure 4.17D, Figure 4.17E**), suggesting more mature B-cell populations are less affected by CR-1-31-B treatment. When examining other hematopoietic populations, we found no significant difference in the fraction of total $CD3^+$ T cells in any tissue, or in $CD4^+$ or $CD8^+$ T cells in the BM (**Figure 4.17D, Figure 4.17E, Supplemental Figure 2B**). We also detected no change in the absolute number of $CD11b^+$ $GR\text{-}1^+$ cells in the BM but a slight increase in blood and the spleen (**Supplemental Figure 2C, Figure 4.17D, Figure 4.17E**).

To evaluate the effect of CR-1-31-B on earlier hematopoietic development, we then examined vehicle and drug treated mouse BM using an 11-color flow cytometry panel for HSC and progenitor populations (Gating strategy displayed in **Supplemental Figure 2A**). From our progenitor panel, we found a corresponding decrease in CLPs in CR-1-31-B-treated mouse BM compared to control BM (**Figure 4.17F**). However, there was no significant difference in the absolute number of lymphoid-primed MPPs (LMPPs), which represent the first lymphoid-biased progeny of HSCs (**Figure 4.17G**). In contrast to the more mature myeloid cell types, we observed no difference in the fraction of GMPs within the BM (**Supplemental Figure 2D**). Finally, we also found no change in the number of BM HSCs (**Supplemental Figure 2E**).

To delineate the effects of CR-1-31-B on different stages of B-cell development, we further examined the distinct populations of B-cell precursors within the BM in CR-1-31-B and vehicle-treated mice. These B-cell precursor populations, known as "Hardy Fractions" (described in **Supplemental Figure 3)**, represent increasing stages of maturation and range from Hardy Fraction A (Pre-Pro B cells) to Fraction F (Mature B-cells) [137]. Following CR-1-31-B treatment, we found a significant block in Hardy fraction A (Pre-pro B cells) (**Figure 4.17H**), with all succeeding progenitor populations containing significantly fewer cells in comparison to control BM fractions. However, as the absolute number of cells within fraction A in treated BM appeared to trend downward compared to vehicle controls and we observed fewer CLPs in CR-1-31-B treated mice, it is possible a significant difference would be observed in Hardy fraction A with a larger sample size.

To functionally assess the effects of CR-1-31-B treatment on hematopoietic cells, we finally plated cells from the BM of CR-1-31-B and vehicle-treated mice into methylcellulose

media for CFU assays. Consistent with our flow cytometry data, we observed considerably fewer pre-B cell colonies (**Figure 4.17I**) and a greater number of granulocyte-macrophage colonies (CFU-GM) in cells plated from CR-1-31-B -treated BM (**Figure 4.17J)**. We detected no significant change in the number of granulocyte, macrophage, or erythroid CFUs (CFU-G, CFU-M, CFU-GM, CFU-E, CFU-GEMM**)** (**Figure 4.17J**).

A

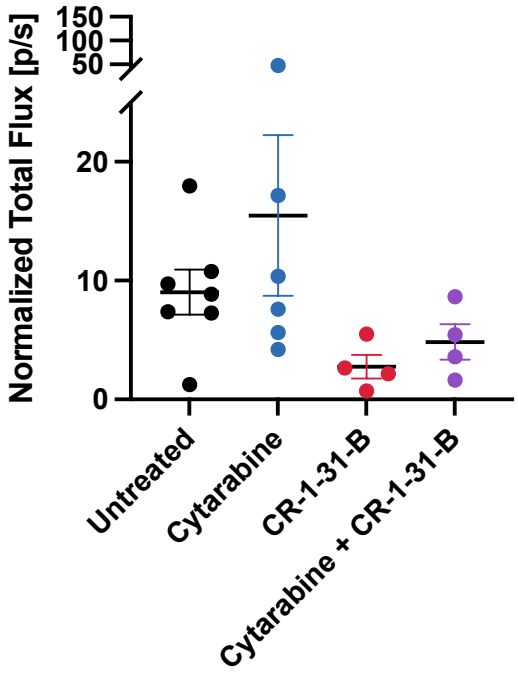
Normalized Total Flux [p/s]
150
100
50
20
10
0
Untreated
Cytarabine
CR-1-31-B
Cytarabine + CR-1-31-B

B

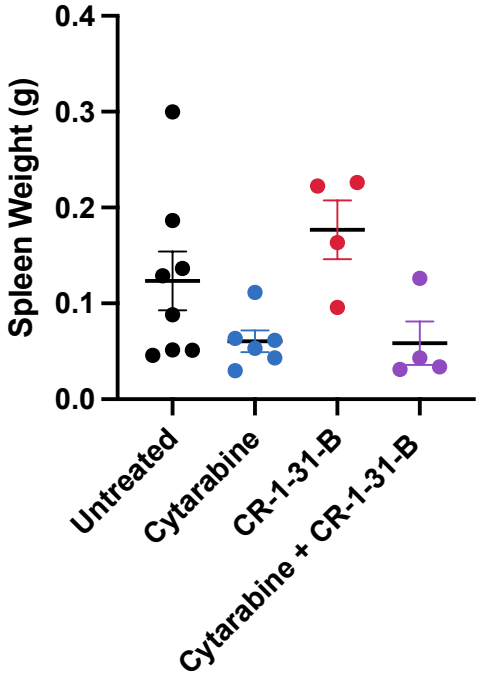
Spleen Weight (g)
0.4
0.3
0.2
0.1
0.0
Untreated
Cytarabine
CR-1-31-B
Cytarabine + CR-1-31-B

C

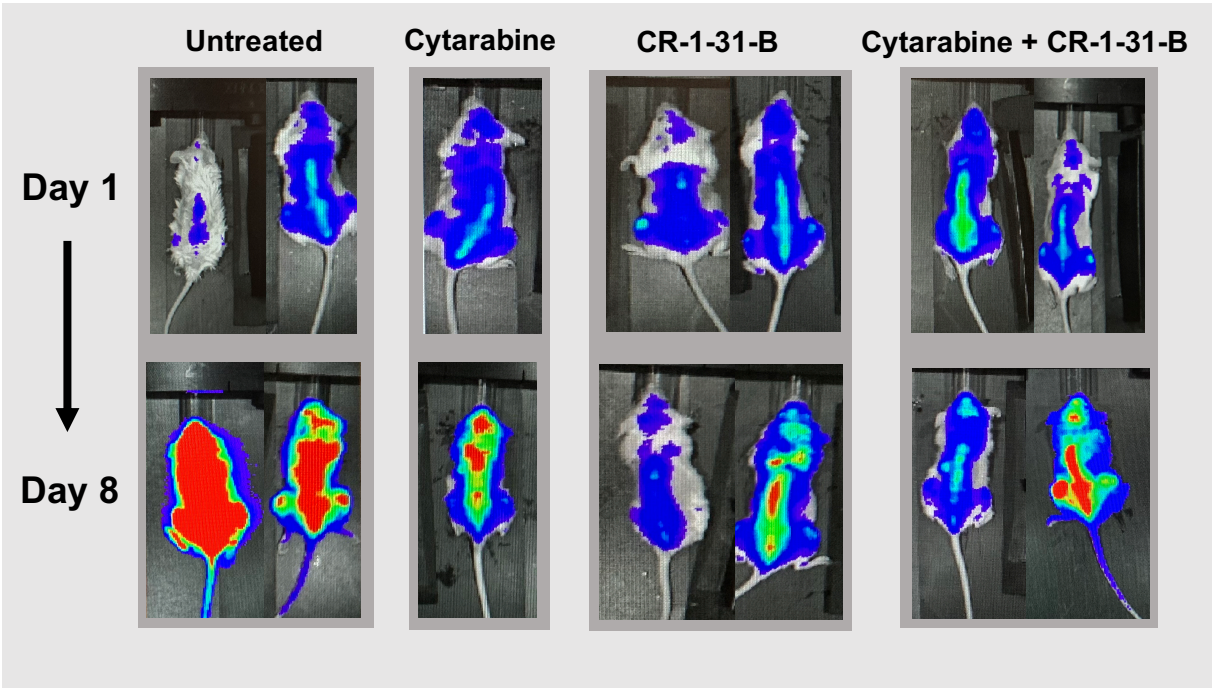
Untreated
Cytarabine
CR-1-31-B
Cytarabine + CR-1-31-B
Day 1
Day 8

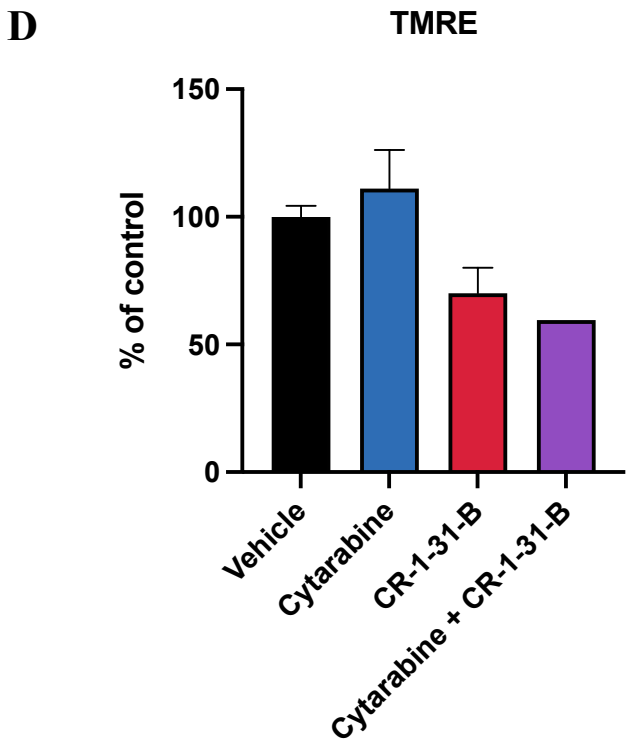

Figure 4.16. Cytarabine and CR-1-31-B combination treatment significantly reduces AML burden *in vivo*

At day 10 post-transplantation of MOLM-14-Luc cells, NSG mice were treated with 50 mg/kg of cytarabine for 5 days and/or 0.2 mg/kg CR-1-31-B for 7 days intraperitoneally. Luciferase imaging was done on day 1 and day 8 of treatment initiation (**A**) NSG mice normalized post-treatment total flux values. (**B**) Mouse spleen weight following treatment (grams). (**C**) Bioluminescent images of NSG mice transplanted with MOLM-14-LUC on Day 1 and Day 8 of treatment. (**D**) MMP was assessed in MOLM-14-Luc isolated from mouse BM after treatment using TMRE. Data represents 2 independent experiments expressed as percentage of control mice for each experiment.

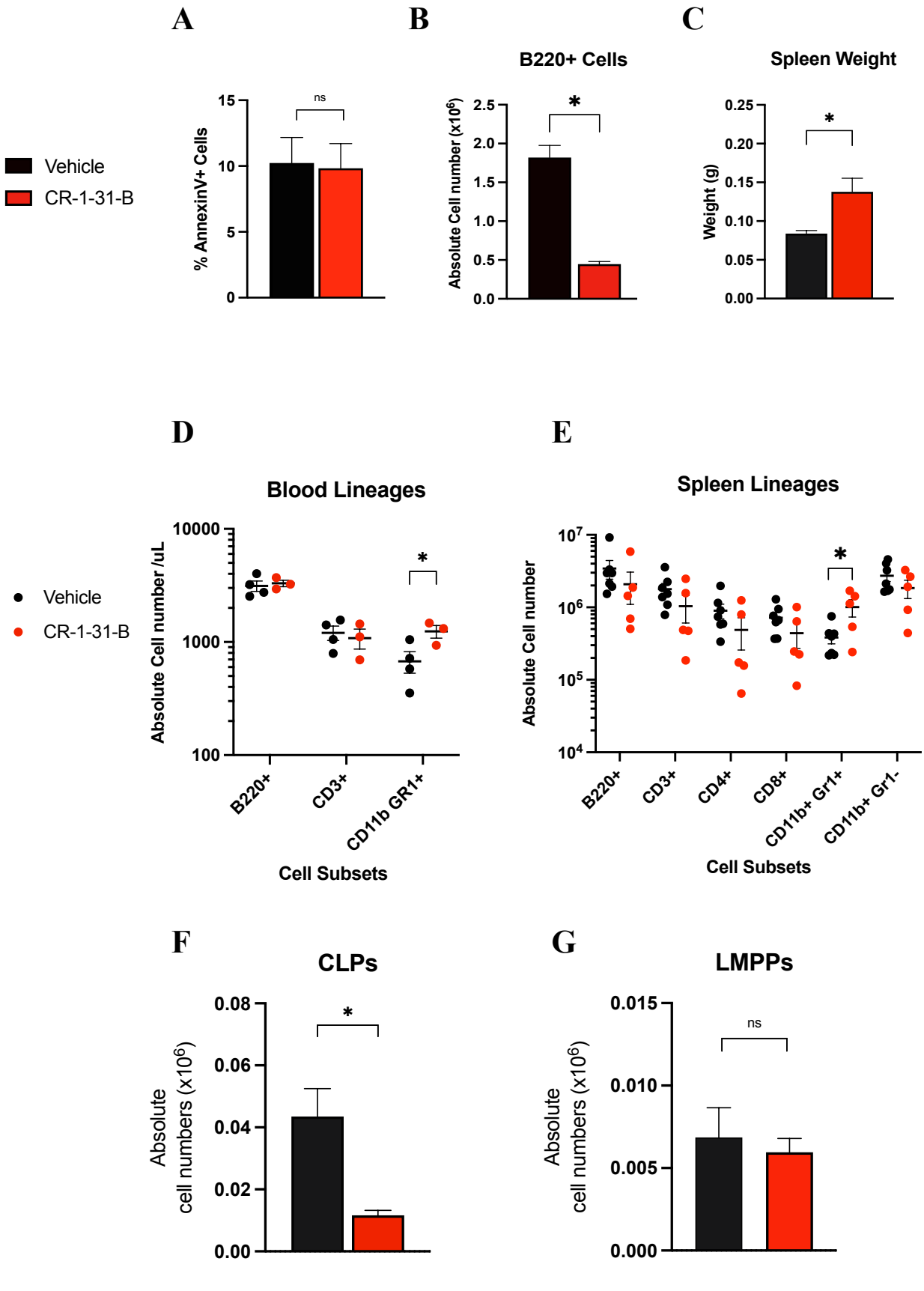
A
B
C
Vehicle
CR-1-31-B
% AnnexinV+ Cells
ns
B220+ Cells
Absolute Cell number (x10^6)
*
Spleen Weight
Weight (g)
*
D
E
Blood Lineages
Absolute Cell number /uL
*
B220+
CD3+
CD11b GR1+
Cell Subsets
Spleen Lineages
Absolute Cell number
*
B220+
CD3+
CD4+
CD8+
CD11b+ Gr1+
CD11b+ Gr1-
Cell Subsets
F
G
CLPs
Absolute cell numbers (x10^6)
*
LMPPs
Absolute cell numbers (x10^6)
ns

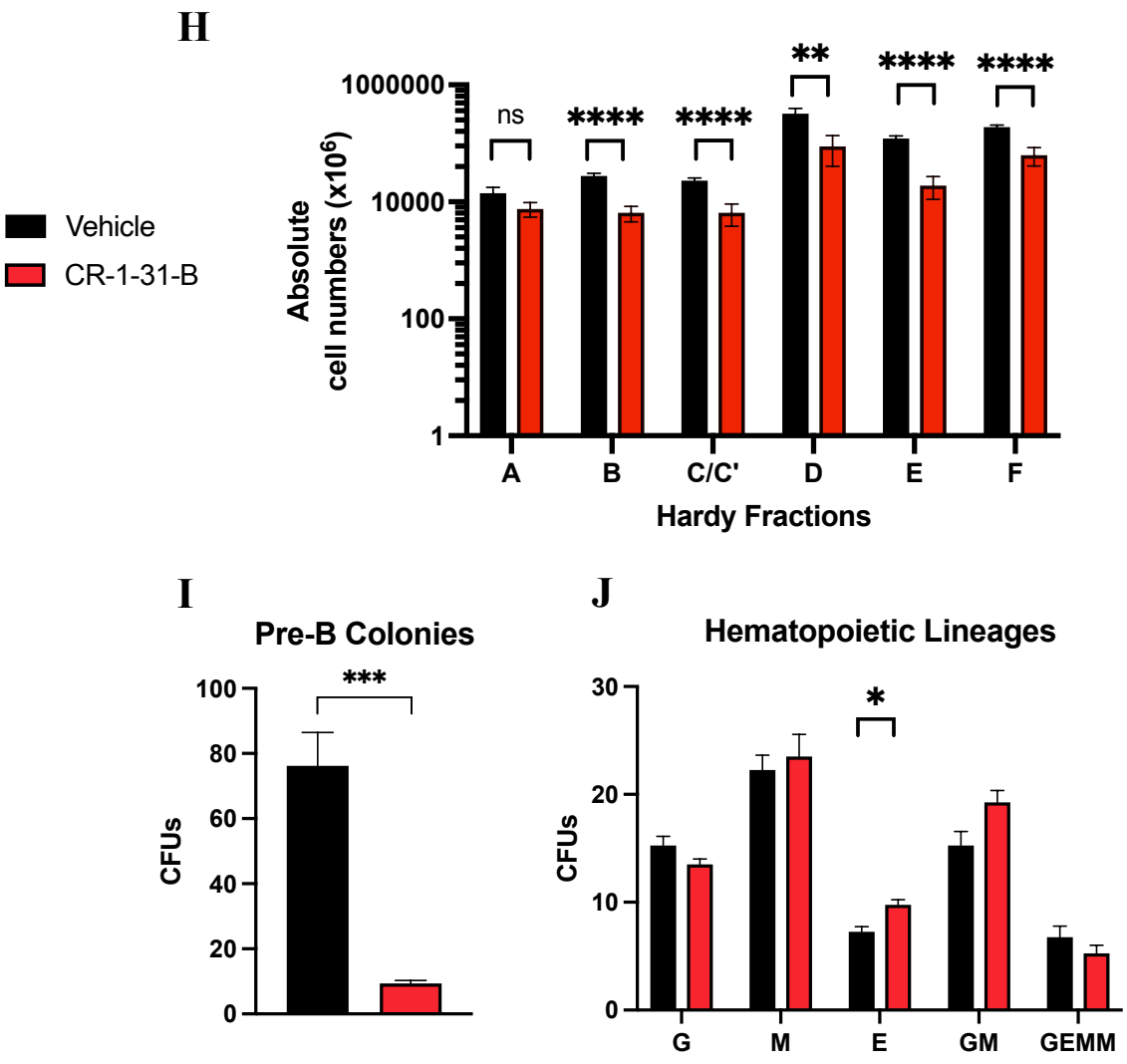

Figure 4.17. CR-1-31-B impairs B-cell development and promotes production of myeloid progenitors

(**A**) AnnexinV$^+$ cells in vehicle and CR-1-31-B treated mouse BM (t-test. n = 6, p = 0.8889). (**B**) Fraction of B220$^+$ B cells in the BM of vehicle and CR-1-31-B-treated mice (Two-way ANOVA with FDR correction). (**C**) Spleen weight in grams of vehicle and CR-1-31-B treated mice (t-test, n = 14, p = 0.0106). (**D**) Lineages in the blood of untreated and CR-1-31-B treated mice. (**E**) Lineages cells in the spleen of vehicle and CR-1-31-B treated mice. (**F**) Fraction of CLPs cells in the BM of vehicle and CR-1-31-B treated mice (t-test, n = 17, p = 0.0104). (**G**) Fraction of LMPPs in the BM of vehicle and CR-1-31-B treated mice (t-test, n = 17, p = 0.5872). (**H**) Absolute number of cells contained within each Hardy Fraction within the BM. (**I**) Colony forming assays for pre-B cells from vehicle and CR-1-31-B treated BM. 100,000 cells were plated into 2 mL M3630 methylcellulose media and incubated for 7 days (t-test, n = 10, p = 0.0002). (**J**) Colony forming assays for hematopoietic progenitor cells from vehicle and CR-1-31-B treated BM. 20,000 cells were plated into 2 mL M3434 methylcellulose media and incubated for 12 days.

Chapter 5: Discussion

Relapse remains common in AML despite advances in the understanding of its pathogenesis. However, most of our understanding of the mechanisms driving AML growth are derived from characterization of samples obtained from patients at diagnosis. Indeed, recent studies aiming to understand the response of AML to therapy have shown that residual cells after treatment exhibit a distinct transcriptional and metabolic profile, which may represent adaptations required to survive in that context [71, 72, 75]. Thus, it is essential to better characterize residual AML cells and the molecular mechanisms underlying their survival for the development of therapies targeting relapse-initiating leukemic cells.

Data from prior studies supports the model that LSCs are not selectively chemoresistant and that AML cells rely on metabolic adaptations to adapt and persist following chemotherapy [71, 72, 75]. Signaling through the master metabolic regulator mTORC1 is often upregulated in AML patient samples and is associated with therapeutic resistance in other malignancies [76, 126, 127]. Unfortunately, mTORC1 inhibitors have proved to be largely ineffective clinically in AML, partly due to compensatory activation of other signaling pathways [75, 76, 80]. Consequently, efforts have shifted towards targeting of downstream effectors of mTORC1, with the subunits of the eIF4F initiation complex recently emerging as attractive targets. As *in vitro* work has demonstrated in other models that inhibition of eIF4A targets a subset of mRNA transcripts that includes proteins associated with pathways implicated in chemoresistance, we therefore proposed that inhibition of eIF4A may target the metabolic adaptations supporting resistance and reduce AML regrowth. We selected the novel rocaglate CR-1-31-B to target eIF4A, as this drug is highly potent and selective, and has demonstrated favorable pharmacokinetic properties in mice.

To investigate the functional adaptations of chemoresistant AML cells and test the effect of specific therapeutic interventions, we developed experimental murine models that recapitulate human treatment regimens. The human MOLM-14 and murine FM4 cell lines were chosen as they represent aggressive models of AML driven by prevalent genetic alterations (FLT3-ITD and MLL/AF9) and have been used by other groups to model chemotherapy *in vivo* [72, 75]. We used the MOLM-14-Luc cell line to develop a xenograft AML model with luciferase expression as a reporter for disease burden. Although we previously established a maximum tolerable cytarabine dose for our NSG mice, we found that in this model chemotherapy did not significantly lower leukemic burden, as measured by spleen weight and bioluminescent imaging. Thus, this dose was

likely sub-therapeutic, and conclusions drawn from our human AML model are limited by the sensitivity of host NSG mice to chemotherapy. In addition, we developed a syngeneic model of AML using the FM4 cell line and found that in this model chemotherapy significantly reduced leukemic burden (assessed by the fraction of AML cells in the BM by flow cytometry and spleen weight) although the mean fraction of AML within the BM post-chemotherapy remained nearly 50%. We plan to use this model for further *in vivo* metabolomic and polysome studies of chemoresistant AML cells, as sufficient quantities of harvestable residual AML cells may be isolated post-treatment. However, a limitation of both *in vivo* models may be that chemotherapy does not truly remove the AML cells or reduce AML to minimal levels within the BM as is often observed following complete remission in humans. Consequently, it is yet unclear how accurately these models reproduce the microenvironment and metabolic or translatomic profiles of regenerating leukemic cells in AML patients. We aim to validate the data derived from our FM4 and MOLM-14 murine models by developing PDX models within the Mercier lab using NSG and/or NSG-S mice and primary AML samples from our institution's biobank, then treating these models with chemotherapy.

Our data obtained from the FM4 and MOLM-14 models is consistent with the emerging theory that LSCs are not selectively chemoresistant as previously assumed. To estimate the proportion of LSCs within the AML population after chemotherapy, we used a functional *in vitro* surrogate of self-renewal potential: colony-forming activity in semi-solid methylcellulose media. Whereas LSC activity is formally measured by the ability to initiate AML in transplanted mice, colonies *in vitro* are nevertheless representative of divisional potential, and have been found to correlate in several studies. We observed that the CFU ability of chemotherapy-treated BM was significantly reduced in both murine models, suggesting that chemotherapy does not enrich for LSCs. Several studies have proposed explanations to describe how non-quiescent AML cells may adapt to chemotherapy; including induction of senescence and transcriptional and metabolic reprogramming [71, 72, 138]. Although further work must be done to establish what population of cells drives chemoresistance in AML, it is rational to propose that targeting of LSCs or stemness genes may not significantly improve response to treatment if these cells are already vulnerable to chemotherapy. In this context, targeting of crucial metabolic adaptations or of proteins highly upregulated by resistant cells may limit leukemic regeneration. In support of this theory, a 2018 study established a gene expression signature of human AML cells at the onset of re-growth post-

treatment and found this signature was expressed only during active response to chemotherapy, and was absent at diagnosis and relapse [71]. When the same group targeted a druggable protein identified from this signature, it was found to delay AML relapse in PDX models. Further characterization of residual human AML cells *in vivo* is necessary to clarify the role of LSCs in chemoresistance and determine whether targeting of the dynamic metabolic adaptations acquired during chemotherapy impairs re-growth.

In this study, we tested a novel inhibitor of eIF4A, CR-1-31-B, as a potential therapy for chemoresistant AML and observed an interesting anti-leukemic effect *in vitro* and *in vivo*. eIF4A is an essential downstream target of mTORC1 signaling that controls the initiation of translation of a subset of pro-oncogenic mRNAs. *In vitro*, brief exposure to CR-1-31-B led to apoptosis of AML cells at low nanomolar concentrations, accompanied by increased levels of ROS as measured by mitoSOX staining. This was also accompanied by decreased mitochondrial potential, cell cycle arrest in the G0/G1 phase, and increased DNA damage as assessed by γH2AX staining. Importantly, CR-1-31-B led to a decrease in heavy polysomes, consistent with its mechanism of action at the level of mRNA translation. While we do not know at present which mRNAs are most responsible for these effects, the same class of inhibitors (rocaglates) have previously been shown to affect the expression of BCL-2 family proteins, MYC, NRAS, and cell cycle regulators such as CDK1 [139, 140]. Several of these targets have already been shown to be relevant to AML and inhibitors of these pathways are in clinical use (eg. the BCL-2 inhibitor venetoclax) or development. It should also be noted that CR-1-31-B sensitivity may vary between AML cases or samples depending on their mutation status, as several prevalent genetic alterations in AML are also thought to impact cellular metabolism. For example, IDH1/IDH2 mutations impair the ability of these enzymes to produce alpha-ketoglutarate (a-KG) and instead drive formation of the oncometabolite D-2-hydroxyglutarate (2-HG). This largely impacts epigenetic signaling as 2-HG inhibits multiple histone and DNA demethylating enzymes within the cell. However, other a-KG dependent metabolic pathways are also affected (e.g. Citric Acid Cycle metabolism), leading to an altered metabolic state in AML cases harboring these mutations [141]. To determine if AML mutation status significantly alters response to CR-1-31-B, we propose to treat primary AML samples with distinct mutation profiles *in vitro* and examine their sensitivity.

To better characterize the complete set of mRNA transcripts targeted by CR-1-31-B and understand which mRNAs are especially important to AML growth, the Mercier and Hulea

laboratories are currently analyzing the mRNA transcripts differentially translated by eIF4A using a combination of polysome fractionation and extraction of bound mRNA for NGS sequencing. Polysome profiling of treated samples will more accurately describes changes in gene expression than traditional transcriptomic analyses, as RNA levels do not always reflect the final protein quantity within a cell [85]. Ultimately, to demonstrate that the anti-leukemic effect of CR-1-31-B occurs through decreased synthesis of specific proteins, rescue experiments where these proteins are overexpressed may be necessary. However, a potential limitation of these experiments is that CR-1-31-B may simultaneously target several important pathways. Thus, the anti-leukemic effect may be related to the global change in cellular metabolism and not the effect of one single protein or pathway.

We believe that CR-1-31-B targets a subset of proteins which are important to AML survival or metabolic reprogramming, such as BCL-2, NRAS, and MYC, on which chemoresistant AML cells rely to adapt and survive. LSCs more heavily depend on oxidative metabolism than healthy HSC and progenitor cells and can exploit various substrates to support this such as amino acids or fatty acids [29, 74, 142, 143]. Encouragingly, a recent report by Chan *et al* testing CR-1-31-B in pancreatic ductal adenocarcinoma (PDA) demonstrated that CR-1-31-B inhibited mRNA transcripts essential to mitochondrial respiration in addition to restricting a compensatory metabolic shift towards glycolysis [144]. Thus, it is possible that CR-1-31-B targets the unique transcriptional changes and metabolic pathways, such as oxidative respiration, supporting chemoresistance. To characterize the effect of CR-1-31-B on these pathways we used reporters of mitochondrial activity such as TMRE which measures MMP, and mitoSOX which measures mitochondrial generation of superoxide. Overall, our observations suggest that mitochondrial activity is inhibited by CR-1-31-B, presumably through its effect on the aforementioned transcripts. To confirm this effect on metabolism, several additional assays are possible, such as the Seahorse assay which measures cellular oxygen consumption and extracellular acidification of treated cells as reporters of oxidative respiration and glycolysis, respectively. Liquid chromatography-based mass spectrometry could also be used to directly measure the levels of several metabolic intermediates and identify dysregulated metabolic pathways. Finally, tracing of carbon metabolism using C^{13}-labeled metabolites can measure the utilization of nutrients by the cells. Using the models that we generated, it is now possible to perform these extensive metabolic characterizations in treated cells in collaboration with laboratory of Dr. Hulea, *in vitro* and *in vivo*,

to better understand the therapeutic effect. Interrogating both the translatome and metabolome will ensure we have a comprehensive picture of the cellular response to chemotherapy and to CR-1-31-B in AML.

In AML cells treated with CR-1-31-B, we also observed signs of upregulation of the DNA damage response. Following the occurrence of DNA double-stranded breaks, the ataxia telangiectasia mutated (ATM) protein kinase senses damaged DNA and phosphorylates the histone H2AX at Ser139 [145] to form γH2AX, which can be measured by immunoblotting and immunofluorescence. Further supporting the effect on DNA damage, we observed an arrest of treated cells in the G0 or G1 phases of the cell cycle. Currently, we do not know what the main driver of this effect is, however several possibilities could be explored in association with our other observations. The increase in ROS levels that we observed in the mitochondria could damage DNA, generating oxidized bases and strand breaks [146]. Additionally, the known effect of CR-1-31-B on metabolic regulators could lead to a depletion of building blocks for nucleotides, causing replicative stress. To better understand how the response to DNA damage impacts AML growth in the context of CR-1-31-B, these experiments could be repeated in cells that are deficient in factors regulating this process, such as TP53, ATM, or ataxia telangiectasia and Rad3-related protein (ATR). Interestingly, the aforementioned report by Chan *et al* also observed that although CR-1-31-B increased total cellular ROS production, treatment with the ROS scavenger N-acetyl-cysteine failed to rescue cell death. Analogous to our findings, this implies that inducing ROS is likely not the primary mechanism underlying CR-1-31-B-mediated cell death.

Importantly, we found that CR-1-31-B can be synergistically combined with two standard of care agents to target chemoresistant AML cells. *In vitro*, CR-1-31-B enhances the fractional killing of AML by cytarabine and we believe that this synergy is due to the targeting by CR-1-31-B of essential adaptations of AML cells to chemotherapy. Interestingly, we also observed a strong synergy between CR-1-31-B and the novel therapy venetoclax, which is increasingly recognized as a potent treatment for AML. While we did not characterize this synergy during the timeframe of this thesis, we can hypothesize that CR-1-31-B may be synergistic through inhibition of the synthesis of other BCL-2 family members or an effect on mitochondrial activity, which is an important determinant of resistance [47, 72]. Further experiments characterizing candidate proteins and the effect on metabolism will be attempted in our models with this drug combination. In agreement with prior studies proposing residual AML cells strongly rely on oxidative

metabolism, we observed increased mitochondrial activity and mitochondrial specific ROS production post-chemotherapy in both models tested *in vitro*, as well as *in vivo* in the partially chemosensitive FM4 model. This suggests that the observed effect of CR-1-31-B as a single agent on mitochondrial activity and mitochondrial specific ROS production may be targeting an essential adaptation of AML. While earlier reports have described that AML cells often hyperactivate mTOR signaling and upregulate mTORC1 following treatment, we further used a reporter of ribosomal translation (OP-puro, which is incorporated into nascent peptides) to demonstrate that human and mouse AML cells exhibit increased levels of protein synthesis following chemotherapy (**Figure 4.10**). In addition, we also observed an upregulation of the PI3K-Akt-mTORC1 pathway after chemotherapy, suggesting that this pathway may be responsible for promoting translation, metabolic changes, and chemoresistance. Ultimately, genetic or pharmacological perturbation of the various members of this pathway would better delineate its contribution to chemoresistance as well as a better understanding of the drivers of its activation. Collectively, our results are in line with several other published reports suggesting PI3K-Akt-mTORC1-regulated translation could be a mechanism supporting regrowth post-treatment, and CR-1-31-B may be targeting an essential downstream effector [75, 78, 127, 144].

Moreover, we observed that CR-1-31-B may be cytotoxic to AML without eliminating healthy hematopoietic cells. Although previous rocaglates, such as silvestrol and rocaglamide, have demonstrated efficacy against lymphoid malignancies the effect of these compounds on normal HSC and progenitor populations has not been comprehensively examined to our knowledge. So far, it is understood that different rocaglates have varied effects on mature B-cell populations. For example, rocaglamide was described as not cytotoxic to healthy primary human B or T cells while silvestrol was found to induce apoptosis in B cells but not T cells at equal concentrations [128, 147]. Parallel to the effects of silvestrol, we observed fewer B cells in the BM and spleen with no change in the absolute number of any T cell population ($CD3^+$, $CD4^+$ or $CD8^+$) following 7 days of CR-1-31-B treatment. Further, we observed fewer CLPs within the BM and markedly fewer pre-B CFUs in CR-1-31-B treated samples. Although we observed no difference in the numbers of T cells or mature B cells following CR-1-31-B treatment, it remains possible that inhibition of eIF4A could alter the clonal expansion of lymphocytes following an antigenic challenge. To address whether CR-1-31-B impairs translation of proteins critical to clonal selection or expansion, healthy C57BL/6 mice treated with CR-1-31-B could be challenged with

a non-toxic antigen and flow cytometry could be used to profile the resulting antigen-specific expanded T cell and B cell populations.

Interestingly, we observed significantly enlarged spleens in both healthy and AML-engrafted mice treated with CR-1-31-B, with the mean spleen weight of treated leukemic mice greater than that of untreated controls (**Figure 4.16B**, **Figure 4.17C**). The parallel increase in both models suggests that neither leukemic infiltration nor recruitment of $CD11b^{+}$ $GR\text{-}1^{+}$ cells is the cause of this splenomegaly. Curiously, previous experiments involving *in vivo* treatment with silvestrol have not described significant changes to spleen size [128, 139]. Further characterization of this phenomenon could be attempted by performing histopathological analysis of sections of CR-1-31-B treated spleens. Collectively, these results indicate that CR-1-31-B is overall well tolerated by mice, with minimal systemic toxicity and few changes in mature hematopoietic cells, except for a decrease in common lymphocyte and B-progenitors. From a therapeutic standpoint, this would make this approach attractive, as agents that selectively target B-cells (such as the monoclonal antibody rituximab) are overall well tolerated and B-cell function can be compensated by transfusion of intravenous immunoglobulins.

We believe that this project is one of the first to test eIF4A inhibitors in AML *in vivo* and reveals that targeting of eIF4A has the potential to improve response to chemotherapy in cytarabine-resistant AML. Recently, a study using a different type of eIF4A inhibitor showed single-agent activity *in vivo* in a similar AML model (MOLM-13), as well as *in vitro* synergy with inhibitors of mutated FLT3 [148]. In this case, the authors proposed that the effect was due to downregulation of heat shock response factor 1 (HSF1), which depends on eIF4A. In addition, in human AML patients, inhibition of eIF4E (another member of the eIF4F complex) has been attempted with ribavirin, leading to clinical responses in a small fraction of patients [114]. However, further combination with cytarabine was accompanied by the development of resistance mechanisms, such as increased intracellular metabolism and efflux leading to subtherapeutic intracellular levels [115]. Whether similar resistance would be observed with CR-1-31-B remains to be determined using a larger array of AML samples, however, it is worth noting that ribavirin metabolism is associated with its molecular structure as a nucleoside analogue. Inhibitors of eIF4A are currently in early phase clinical trials for other types of solid malignancies (NCT04092673) [149], supporting an acceptable toxicity profile in humans and *in vivo* targeting of the pathway. This preclinical work may further support the validity of testing these drugs in AML.

While in this work we tested the combination of eIF4A inhibition and chemotherapy based on evidence that upregulation of known downstream effectors occurs in that context, we could also propose that eIF4A inhibition may be efficacious in the context of specific mutated genes. For example, RAS and FLT3 mutations in AML lead to activation of mTORC1 through crosstalk with the RAS-MAPK-ERK pathway. These mutations are also associated with chemoresistance; thus, it would be particularly relevant to test the effect of eIF4A inhibition in these molecular subgroups and examine if it enhances the effect of targeted inhibition of these pathways.

In conclusion, this thesis examined the emerging concept that AML adapts to chemotherapy through dynamic changes to cellular metabolism and protein synthesis. We also demonstrated that targeting translation initiation by inhibition of eIF4A shows anti-leukemic activity in experimental models *in vitro* and *in vivo*, and targets pathways upregulated in residual AML cells after treatment, such as mitochondrial activity. We hope that results from our ongoing metabolomic and polysome sequencing analyses will provide valuable insight into how AML resists intensive chemotherapy. Ultimately, our preclinical data provides a potential therapeutic strategy for limiting leukemic regrowth and interesting pathways to be further investigated. Although further work is required, we believe eIF4A-inhibition in AML has the potential for clinical translation and could yield novel combination therapies.

Chapter 6: Appendix

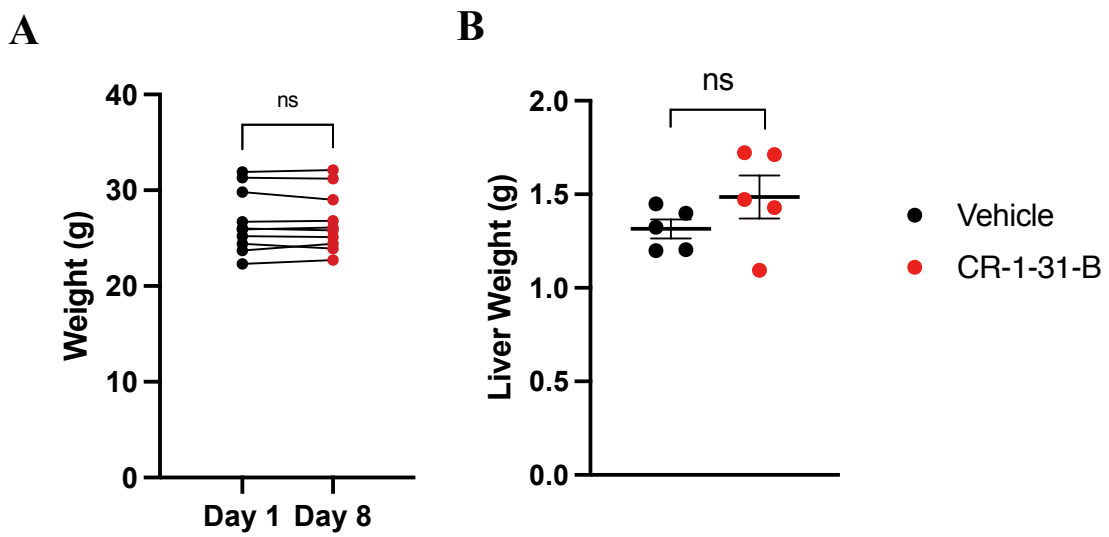

Supplemental Figure 1. CR-1-31-B treatment does not change mouse body or liver weight
(**A**) Body weight of CR-1-31-B treated mice on day 1 and day 8 of treatment in grams (paired t-test, n = 10 pairs, p = 0.9434). (**B**) Liver weight of vehicle-treated and CR-1-31-B-treated mice in grams (t-test, n = 10, p = 0.2109).

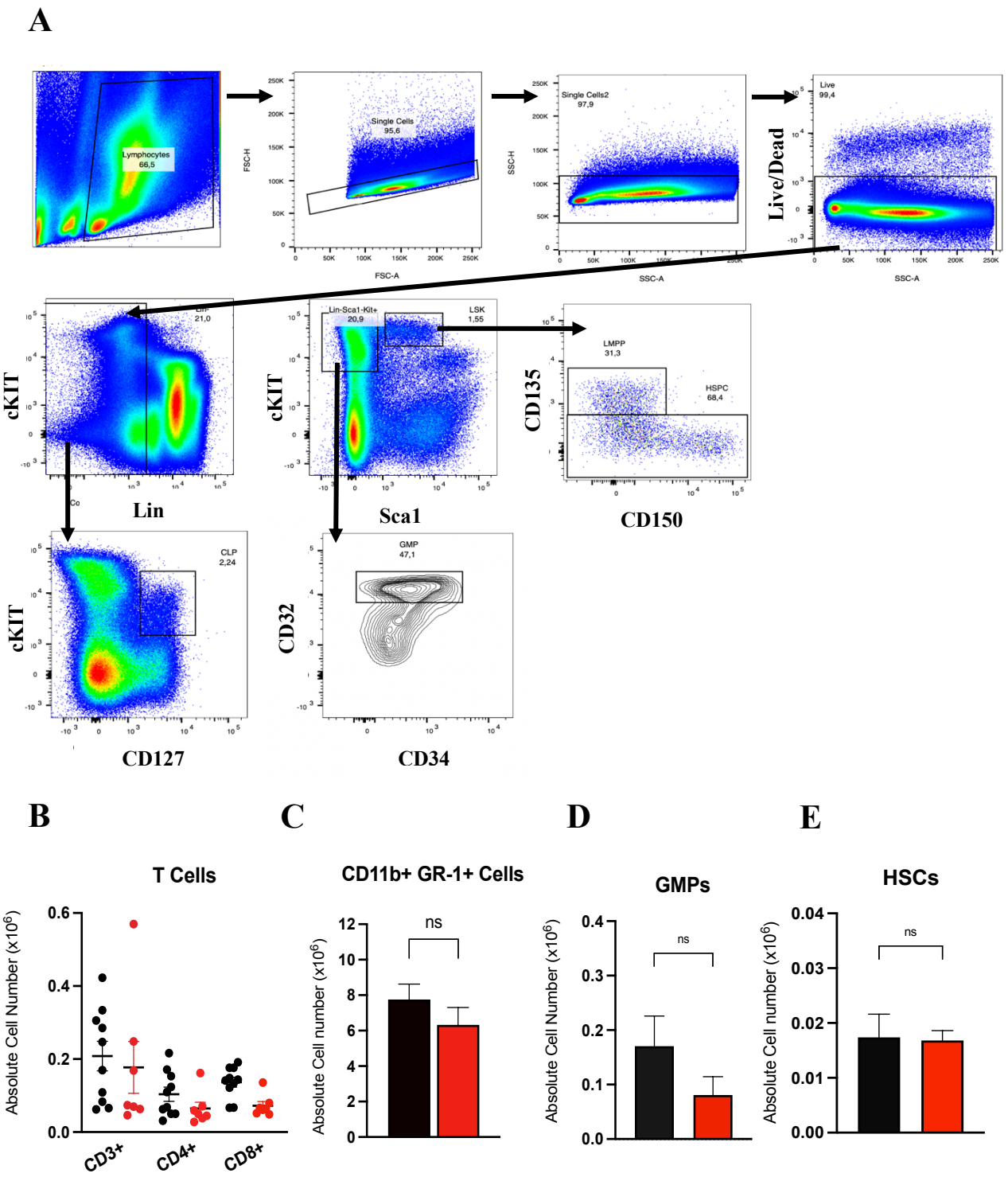

Supplemental Figure 2. Stages of B-Cell Development in Murine Bone Marrow

(**A**) Representative gating strategy of HSC and progenitor panel. (**B**) Absolute number of $CD3^{+,}$ $CD4^{+}$ and $CD8^{+}$ T cells within vehicle and CR-1-31-B treated mouse BM. (**C**) Absolute number of $CD11b^{+}$ $GR\text{-}1^{+}$ cells within vehicle and CR-1-31-B treated mouse BM. (**D**) Absolute number of GMPs within vehicle and CR-1-31-B treated mouse BM. (**E**) Absolute number of HSCs within vehicle and CR-1-31-B treated mouse BM. Abbreviations: BM HSC: bone marrow hematopoietic stem cell, CLP: common lymphocyte progenitor, GMP: granulocyte macrophage progenitor, LMPP: lymphoid-primed multipotent progenitor.

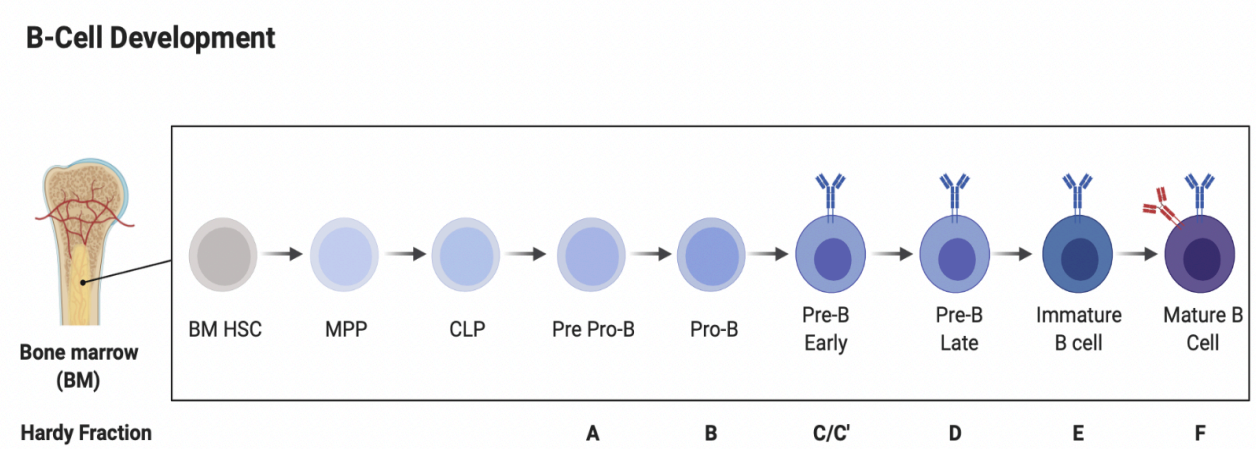

Supplemental Figure 3. Stages of B-Cell Development in Murine Bone Marrow
The broad stages of B-cell development in mice, beginning in the bone marrow with subsequent maturation in spleen. Abbreviations: BM HSC, bone marrow hematopoietic stem cell, MPP, multipotent progenitor, CLP, common lymphoid progenitor. Figure adapted from [137] and "B-1 and B-2 Cell Development" by BioRender.

References

1. Orkin, S.H. and L.I. Zon, *Hematopoiesis: an evolving paradigm for stem cell biology.* Cell, 2008. **132**(4): p. 631-44.
2. Calvi, L.M. and D.C. Link, *Cellular complexity of the bone marrow hematopoietic stem cell niche.* Calcif Tissue Int, 2014. **94**(1): p. 112-24.
3. Kondo, M., et al., *Cell-fate conversion of lymphoid-committed progenitors by instructive actions of cytokines.* Nature, 2000. **407**(6802): p. 383-6.
4. Akashi, K., et al., *A clonogenic common myeloid progenitor that gives rise to all myeloid lineages.* Nature, 2000. **404**(6774): p. 193-7.
5. Iwasaki, H., et al., *The order of expression of transcription factors directs hierarchical specification of hematopoietic lineages.* Genes Dev, 2006. **20**(21): p. 3010-21.
6. Till, J.E. and C.E. Mc, *A direct measurement of the radiation sensitivity of normal mouse bone marrow cells.* Radiat Res, 1961. **14**: p. 213-22.
7. Becker, A.J., C.E. Mc, and J.E. Till, *Cytological demonstration of the clonal nature of spleen colonies derived from transplanted mouse marrow cells.* Nature, 1963. **197**: p. 452-4.
8. Baum, C.M., et al., *Isolation of a candidate human hematopoietic stem-cell population.* Proc Natl Acad Sci U S A, 1992. **89**(7): p. 2804-8.
9. Majeti, R., C.Y. Park, and I.L. Weissman, *Identification of a hierarchy of multipotent hematopoietic progenitors in human cord blood.* Cell Stem Cell, 2007. **1**(6): p. 635-45.
10. Okada, S., et al., *In vivo and in vitro stem cell function of c-kit- and Sca-1-positive murine hematopoietic cells.* Blood, 1992. **80**(12): p. 3044-50.
11. Osawa, M., et al., *Long-term lymphohematopoietic reconstitution by a single CD34-low/negative hematopoietic stem cell.* Science, 1996. **273**(5272): p. 242-5.
12. Kondo, M., *Lymphoid and myeloid lineage commitment in multipotent hematopoietic progenitors.* Immunol Rev, 2010. **238**(1): p. 37-46.
13. Yang, L., et al., *Identification of Lin(-)Sca1(+)kit(+)CD34(+)Flt3- short-term hematopoietic stem cells capable of rapidly reconstituting and rescuing myeloablated transplant recipients.* Blood, 2005. **105**(7): p. 2717-23.
14. Ali, M.A.E., et al., *Functional dissection of hematopoietic stem cell populations with a stemness-monitoring system based on NS-GFP transgene expression.* Sci Rep, 2017. **7**(1): p. 11442.
15. De Kouchkovsky, I. and M. Abdul-Hay, *'Acute myeloid leukemia: a comprehensive review and 2016 update'.* Blood Cancer J, 2016. **6**(7): p. e441.
16. Shallis, R.M., et al., *Epidemiology of acute myeloid leukemia: Recent progress and enduring challenges.* Blood Rev, 2019. **36**: p. 70-87.
17. Hao, T., et al., *An emerging trend of rapid increase of leukemia but not all cancers in the aging population in the United States.* Sci Rep, 2019. **9**(1): p. 12070.
18. Lonetti, A., A. Pession, and R. Masetti, *Targeted Therapies for Pediatric AML: Gaps and Perspective.* Front Pediatr, 2019. **7**: p. 463.
19. Dohner, H., et al., *Diagnosis and management of AML in adults: 2017 ELN recommendations from an international expert panel.* Blood, 2017. **129**(4): p. 424-447.
20. Bennett, J.M., et al., *Proposals for the classification of the acute leukaemias. French-American-British (FAB) co-operative group.* Br J Haematol, 1976. **33**(4): p. 451-8.
21. Swerdlow, S.H., International Agency for Research on Cancer., and World Health Organization., *WHO classification of tumours of haematopoietic and lymphoid tissues*.

4th ed. World Health Organization classification of tumours. 2008, Lyon, France: International Agency for Research on Cancer. 439 p.
22. Swerdlow, S.H., World Health Organization, and International Agency for Research on Cancer, *WHO classification of tumours of haematopoietic and lymphoid tissues*. Revised 4th edition. ed. World Health Organization classification of tumours. 2017, Lyon: International Agency for Research on Cancer. 585 pages.
23. Cancer Genome Atlas Research, N., et al., *Genomic and epigenomic landscapes of adult de novo acute myeloid leukemia.* N Engl J Med, 2013. **368**(22): p. 2059-74.
24. Bullinger, L., K. Dohner, and H. Dohner, *Genomics of Acute Myeloid Leukemia Diagnosis and Pathways.* J Clin Oncol, 2017. **35**(9): p. 934-946.
25. DiNardo, C.D. and J.E. Cortes, *Mutations in AML: prognostic and therapeutic implications.* Hematology Am Soc Hematol Educ Program, 2016. **2016**(1): p. 348-355.
26. Herold, T., et al., *Validation and refinement of the revised 2017 European LeukemiaNet genetic risk stratification of acute myeloid leukemia.* Leukemia, 2020. **34**(12): p. 3161-3172.
27. Carter, J.L., et al., *Targeting multiple signaling pathways: the new approach to acute myeloid leukemia therapy.* Signal Transduct Target Ther, 2020. **5**(1): p. 288.
28. DiNardo, C.D., et al., *Azacitidine and Venetoclax in Previously Untreated Acute Myeloid Leukemia.* N Engl J Med, 2020. **383**(7): p. 617-629.
29. Lagadinou, E.D., et al., *BCL-2 inhibition targets oxidative phosphorylation and selectively eradicates quiescent human leukemia stem cells.* Cell Stem Cell, 2013. **12**(3): p. 329-41.
30. Diesch, J., et al., *A clinical-molecular update on azanucleoside-based therapy for the treatment of hematologic cancers.* Clin Epigenetics, 2016. **8**: p. 71.
31. Bonnet, D. and J.E. Dick, *Human acute myeloid leukemia is organized as a hierarchy that originates from a primitive hematopoietic cell.* Nat Med, 1997. **3**(7): p. 730-7.
32. Thomas, D. and R. Majeti, *Biology and relevance of human acute myeloid leukemia stem cells.* Blood, 2017. **129**(12): p. 1577-1585.
33. Eppert, K., et al., *Stem cell gene expression programs influence clinical outcome in human leukemia.* Nat Med, 2011. **17**(9): p. 1086-93.
34. Goardon, N., et al., *Coexistence of LMPP-like and GMP-like leukemia stem cells in acute myeloid leukemia.* Cancer Cell, 2011. **19**(1): p. 138-52.
35. Sarry, J.E., et al., *Human acute myelogenous leukemia stem cells are rare and heterogeneous when assayed in NOD/SCID/IL2Rgammac-deficient mice.* J Clin Invest, 2011. **121**(1): p. 384-95.
36. Taussig, D.C., et al., *Leukemia-initiating cells from some acute myeloid leukemia patients with mutated nucleophosmin reside in the CD34(-) fraction.* Blood, 2010. **115**(10): p. 1976-84.
37. Ho, J.M., et al., *CD200 expression marks leukemia stem cells in human AML.* Blood Adv, 2020. **4**(21): p. 5402-5413.
38. Iwasaki, M., et al., *CD93 Marks a Non-Quiescent Human Leukemia Stem Cell Population and Is Required for Development of MLL-Rearranged Acute Myeloid Leukemia.* Cell Stem Cell, 2015. **17**(4): p. 412-21.
39. Jan, M., et al., *Prospective separation of normal and leukemic stem cells based on differential expression of TIM3, a human acute myeloid leukemia stem cell marker.* Proc Natl Acad Sci U S A, 2011. **108**(12): p. 5009-14.

40. Jordan, C.T., et al., *The interleukin-3 receptor alpha chain is a unique marker for human acute myelogenous leukemia stem cells.* Leukemia, 2000. **14**(10): p. 1777-84.
41. Saito, Y., et al., *Identification of therapeutic targets for quiescent, chemotherapy-resistant human leukemia stem cells.* Sci Transl Med, 2010. **2**(17): p. 17ra9.
42. Jung, N., et al., *An LSC epigenetic signature is largely mutation independent and implicates the HOXA cluster in AML pathogenesis.* Nat Commun, 2015. **6**: p. 8489.
43. Ng, S.W., et al., *A 17-gene stemness score for rapid determination of risk in acute leukaemia.* Nature, 2016. **540**(7633): p. 433-437.
44. Ishikawa, F., et al., *Chemotherapy-resistant human AML stem cells home to and engraft within the bone-marrow endosteal region.* Nat Biotechnol, 2007. **25**(11): p. 1315-21.
45. Sriskanthadevan, S., et al., *AML cells have low spare reserve capacity in their respiratory chain that renders them susceptible to oxidative metabolic stress.* Blood, 2015. **125**(13): p. 2120-30.
46. Pei, S., et al., *AMPK/FIS1-Mediated Mitophagy Is Required for Self-Renewal of Human AML Stem Cells.* Cell Stem Cell, 2018. **23**(1): p. 86-100 e6.
47. Skrtic, M., et al., *Inhibition of mitochondrial translation as a therapeutic strategy for human acute myeloid leukemia.* Cancer Cell, 2011. **20**(5): p. 674-88.
48. Breitman, T.R., S.E. Selonick, and S.J. Collins, *Induction of differentiation of the human promyelocytic leukemia cell line (HL-60) by retinoic acid.* Proc Natl Acad Sci U S A, 1980. **77**(5): p. 2936-40.
49. Chomienne, C., et al., *All-trans retinoic acid in acute promyelocytic leukemias. II. In vitro studies: structure-function relationship.* Blood, 1990. **76**(9): p. 1710-7.
50. Jensen, H.A., et al., *Retinoic acid therapy resistance progresses from unilineage to bilineage in HL-60 leukemic blasts.* PLoS One, 2014. **9**(6): p. e98929.
51. Degos, L. and Z.Y. Wang, *All trans retinoic acid in acute promyelocytic leukemia.* Oncogene, 2001. **20**(49): p. 7140-5.
52. Boitano, A.E., et al., *Aryl hydrocarbon receptor antagonists promote the expansion of human hematopoietic stem cells.* Science, 2010. **329**(5997): p. 1345-8.
53. Pabst, C., et al., *Identification of small molecules that support human leukemia stem cell activity ex vivo.* Nat Methods, 2014. **11**(4): p. 436-42.
54. Garrido, S.M., et al., *Acute myeloid leukemia cells are protected from spontaneous and drug-induced apoptosis by direct contact with a human bone marrow stromal cell line (HS-5).* Exp Hematol, 2001. **29**(4): p. 448-57.
55. Ito, S., et al., *Long term maintenance of myeloid leukemic stem cells cultured with unrelated human mesenchymal stromal cells.* Stem Cell Res, 2015. **14**(1): p. 95-104.
56. Kohnken, R., P. Porcu, and A. Mishra, *Overview of the Use of Murine Models in Leukemia and Lymphoma Research.* Front Oncol, 2017. **7**: p. 22.
57. Geraghty, R.J., et al., *Guidelines for the use of cell lines in biomedical research.* Br J Cancer, 2014. **111**(6): p. 1021-46.
58. Brenner, A.K., et al., *The Capacity of Long-Term in Vitro Proliferation of Acute Myeloid Leukemia Cells Supported Only by Exogenous Cytokines Is Associated with a Patient Subset with Adverse Outcome.* Cancers (Basel), 2019. **11**(1).
59. Zuber, J., et al., *Mouse models of human AML accurately predict chemotherapy response.* Genes Dev, 2009. **23**(7): p. 877-89.
60. Steinhilber, D. and R. Marschalek, *How to effectively treat acute leukemia patients bearing MLL-rearrangements ?* Biochem Pharmacol, 2018. **147**: p. 183-190.

61. Krivtsov, A.V., et al., *Cell of origin determines clinically relevant subtypes of MLL-rearranged AML.* Leukemia, 2013. **27**(4): p. 852-60.
62. Krivtsov, A.V., et al., *Transformation from committed progenitor to leukaemia stem cell initiated by MLL-AF9.* Nature, 2006. **442**(7104): p. 818-22.
63. Somervaille, T.C. and M.L. Cleary, *Identification and characterization of leukemia stem cells in murine MLL-AF9 acute myeloid leukemia.* Cancer Cell, 2006. **10**(4): p. 257-68.
64. Collins, E.C., et al., *Inter-chromosomal recombination of Mll and Af9 genes mediated by cre-loxP in mouse development.* EMBO Rep, 2000. **1**(2): p. 127-32.
65. Lee, B.H., et al., *FLT3 internal tandem duplication mutations induce myeloproliferative or lymphoid disease in a transgenic mouse model.* Oncogene, 2005. **24**(53): p. 7882-92.
66. Basova, P., et al., *Aggressive acute myeloid leukemia in PU.1/p53 double-mutant mice.* Oncogene, 2014. **33**(39): p. 4735-45.
67. Shultz, L.D., et al., *Human lymphoid and myeloid cell development in NOD/LtSz-scid IL2R gamma null mice engrafted with mobilized human hemopoietic stem cells.* J Immunol, 2005. **174**(10): p. 6477-89.
68. Wunderlich, M., et al., *AML xenograft efficiency is significantly improved in NOD/SCID-IL2RG mice constitutively expressing human SCF, GM-CSF and IL-3.* Leukemia, 2010. **24**(10): p. 1785-8.
69. Dick, J.E., *Complexity of the human acute myeloid leukemia stem cell compartment: implications for therapy.* Biol Blood Marrow Transplant, 2005. **11**(2 Suppl 2): p. 9-11.
70. Vergez, F., et al., *High levels of CD34+CD38low/-CD123+ blasts are predictive of an adverse outcome in acute myeloid leukemia: a Groupe Ouest-Est des Leucemies Aigues et Maladies du Sang (GOELAMS) study.* Haematologica, 2011. **96**(12): p. 1792-8.
71. Boyd, A.L., et al., *Identification of Chemotherapy-Induced Leukemic-Regenerating Cells Reveals a Transient Vulnerability of Human AML Recurrence.* Cancer Cell, 2018. **34**(3): p. 483-498 e5.
72. Farge, T., et al., *Chemotherapy-Resistant Human Acute Myeloid Leukemia Cells Are Not Enriched for Leukemic Stem Cells but Require Oxidative Metabolism.* Cancer Discov, 2017. **7**(7): p. 716-735.
73. Moschoi, R., et al., *Protective mitochondrial transfer from bone marrow stromal cells to acute myeloid leukemic cells during chemotherapy.* Blood, 2016. **128**(2): p. 253-64.
74. Ye, H., et al., *Leukemic Stem Cells Evade Chemotherapy by Metabolic Adaptation to an Adipose Tissue Niche.* Cell Stem Cell, 2016. **19**(1): p. 23-37.
75. Oki, T., et al., *Imaging dynamic mTORC1 pathway activity in vivo reveals marked shifts that support time-specific inhibitor therapy in AML.* Nat Commun, 2021. **12**(1): p. 245.
76. Poulain, L., et al., *High mTORC1 activity drives glycolysis addiction and sensitivity to G6PD inhibition in acute myeloid leukemia cells.* Leukemia, 2017. **31**(11): p. 2326-2335.
77. Xu, Q., et al., *Survival of acute myeloid leukemia cells requires PI3 kinase activation.* Blood, 2003. **102**(3): p. 972-80.
78. Xu, Q., J.E. Thompson, and M. Carroll, *mTOR regulates cell survival after etoposide treatment in primary AML cells.* Blood, 2005. **106**(13): p. 4261-8.
79. Kasner, M.T., et al., *Sirolimus enhances remission induction in patients with high risk acute myeloid leukemia and mTORC1 target inhibition.* Invest New Drugs, 2018. **36**(4): p. 657-666.

80. Perl, A.E., et al., *A phase I study of the mammalian target of rapamycin inhibitor sirolimus and MEC chemotherapy in relapsed and refractory acute myelogenous leukemia.* Clin Cancer Res, 2009. **15**(21): p. 6732-9.
81. Sonenberg, N. and A.G. Hinnebusch, *Regulation of translation initiation in eukaryotes: mechanisms and biological targets.* Cell, 2009. **136**(4): p. 731-45.
82. Schwanhausser, B., et al., *Global quantification of mammalian gene expression control.* Nature, 2011. **473**(7347): p. 337-42.
83. Galicia-Vazquez, G., et al., *A cellular response linking eIF4AI activity to eIF4AII transcription.* RNA, 2012. **18**(7): p. 1373-84.
84. Jackson, R.J., C.U. Hellen, and T.V. Pestova, *The mechanism of eukaryotic translation initiation and principles of its regulation.* Nat Rev Mol Cell Biol, 2010. **11**(2): p. 113-27.
85. Chasse, H., et al., *Analysis of translation using polysome profiling.* Nucleic Acids Res, 2017. **45**(3): p. e15.
86. Babendure, J.R., et al., *Control of mammalian translation by mRNA structure near caps.* RNA, 2006. **12**(5): p. 851-61.
87. Pelletier, J., et al., *Targeting the eIF4F translation initiation complex: a critical nexus for cancer development.* Cancer Res, 2015. **75**(2): p. 250-63.
88. Koromilas, A.E., A. Lazaris-Karatzas, and N. Sonenberg, *mRNAs containing extensive secondary structure in their 5' non-coding region translate efficiently in cells overexpressing initiation factor eIF-4E.* EMBO J, 1992. **11**(11): p. 4153-8.
89. Svitkin, Y.V., et al., *The requirement for eukaryotic initiation factor 4A (elF4A) in translation is in direct proportion to the degree of mRNA 5' secondary structure.* RNA, 2001. **7**(3): p. 382-94.
90. Feoktistova, K., et al., *Human eIF4E promotes mRNA restructuring by stimulating eIF4A helicase activity.* Proc Natl Acad Sci U S A, 2013. **110**(33): p. 13339-44.
91. Robichaud, N., et al., *Phosphorylation of eIF4E promotes EMT and metastasis via translational control of SNAIL and MMP-3.* Oncogene, 2015. **34**(16): p. 2032-42.
92. Kraljacic, B.C., et al., *Inhibition of eIF4E with ribavirin cooperates with common chemotherapies in primary acute myeloid leukemia specimens.* Leukemia, 2011. **25**(7): p. 1197-200.
93. Modelska, A., et al., *The malignant phenotype in breast cancer is driven by eIF4A1-mediated changes in the translational landscape.* Cell Death Dis, 2015. **6**: p. e1603.
94. Wendel, H.G., et al., *Dissecting eIF4E action in tumorigenesis.* Genes Dev, 2007. **21**(24): p. 3232-7.
95. Bordeleau, M.E., et al., *Therapeutic suppression of translation initiation modulates chemosensitivity in a mouse lymphoma model.* J Clin Invest, 2008. **118**(7): p. 2651-60.
96. Rodrigo, C.M., et al., *Synthesis of rocaglamide hydroxamates and related compounds as eukaryotic translation inhibitors: synthetic and biological studies.* J Med Chem, 2012. **55**(1): p. 558-62.
97. Wolfe, A.L., et al., *RNA G-quadruplexes cause eIF4A-dependent oncogene translation in cancer.* Nature, 2014. **513**(7516): p. 65-70.
98. Elfakess, R. and R. Dikstein, *A translation initiation element specific to mRNAs with very short 5'UTR that also regulates transcription.* PLoS One, 2008. **3**(8): p. e3094.
99. Elfakess, R., et al., *Unique translation initiation of mRNAs-containing TISU element.* Nucleic Acids Res, 2011. **39**(17): p. 7598-609.
100. Mirabilii, S., et al., *Biological Aspects of mTOR in Leukemia.* Int J Mol Sci, 2018. **19**(8).

101. Zeng, Z., et al., *Targeting of mTORC1/2 by the mTOR kinase inhibitor PP242 induces apoptosis in AML cells under conditions mimicking the bone marrow microenvironment.* Blood, 2012. **120**(13): p. 2679-89.
102. Yang, H.S., et al., *The transformation suppressor Pdcd4 is a novel eukaryotic translation initiation factor 4A binding protein that inhibits translation.* Mol Cell Biol, 2003. **23**(1): p. 26-37.
103. Yee, K.W., et al., *Phase I/II study of the mammalian target of rapamycin inhibitor everolimus (RAD001) in patients with relapsed or refractory hematologic malignancies.* Clin Cancer Res, 2006. **12**(17): p. 5165-73.
104. Bertacchini, J., et al., *Feedbacks and adaptive capabilities of the PI3K/Akt/mTOR axis in acute myeloid leukemia revealed by pathway selective inhibition and phosphoproteome analysis.* Leukemia, 2014. **28**(11): p. 2197-205.
105. Bertacchini, J., et al., *Dual inhibition of PI3K/mTOR signaling in chemoresistant AML primary cells.* Adv Biol Regul, 2018. **68**: p. 2-9.
106. Bhat, M., et al., *Targeting the translation machinery in cancer.* Nat Rev Drug Discov, 2015. **14**(4): p. 261-78.
107. Cencic, R., et al., *Reversing chemoresistance by small molecule inhibition of the translation initiation complex eIF4F.* Proc Natl Acad Sci U S A, 2011. **108**(3): p. 1046-51.
108. Callahan, K.P., et al., *Flavaglines target primitive leukemia cells and enhance anti-leukemia drug activity.* Leukemia, 2014. **28**(10): p. 1960-8.
109. Cencic, R., et al., *Modifying chemotherapy response by targeted inhibition of eukaryotic initiation factor 4A.* Blood Cancer J, 2013. **3**: p. e128.
110. Cencic, R., et al., *Synergistic effect of inhibiting translation initiation in combination with cytotoxic agents in acute myelogenous leukemia cells.* Leuk Res, 2010. **34**(4): p. 535-41.
111. Masvidal, L., et al., *mTOR-sensitive translation: Cleared fog reveals more trees.* RNA Biol, 2017. **14**(10): p. 1299-1305.
112. Gandin, V., et al., *nanoCAGE reveals 5′ UTR features that define specific modes of translation of functionally related MTOR-sensitive mRNAs.* Genome Res, 2016. **26**(5): p. 636-48.
113. Sinvani, H., et al., *Translational tolerance of mitochondrial genes to metabolic energy stress involves TISU and eIF1-eIF4GI cooperation in start codon selection.* Cell Metab, 2015. **21**(3): p. 479-92.
114. Assouline, S., et al., *Molecular targeting of the oncogene eIF4E in acute myeloid leukemia (AML): a proof-of-principle clinical trial with ribavirin.* Blood, 2009. **114**(2): p. 257-60.
115. Assouline, S., et al., *A phase I trial of ribavirin and low-dose cytarabine for the treatment of relapsed and refractory acute myeloid leukemia with elevated eIF4E.* Haematologica, 2015. **100**(1): p. e7-9.
116. Borden, K.L., *Targeting the oncogene eIF4E in cancer: From the bench to clinical trials.* Clin Invest Med, 2011. **34**(6): p. E315.
117. Kentsis, A., et al., *Ribavirin suppresses eIF4E-mediated oncogenic transformation by physical mimicry of the 7-methyl guanosine mRNA cap.* Proc Natl Acad Sci U S A, 2004. **101**(52): p. 18105-10.
118. Zahreddine, H.A., et al., *The sonic hedgehog factor GLI1 imparts drug resistance through inducible glucuronidation.* Nature, 2014. **511**(7507): p. 90-3.

119. Sridharan, S., et al., *Targeting of the Eukaryotic Translation Initiation Factor 4A Against Breast Cancer Stemness.* Front Oncol, 2019. **9**: p. 1311.
120. Chu, J., et al., *Amidino-Rocaglates: A Potent Class of eIF4A Inhibitors.* Cell Chem Biol, 2019. **26**(11): p. 1586-1593 e3.
121. Shen, L. and J. Pelletier, *Selective targeting of the DEAD-box RNA helicase eukaryotic initiation factor (eIF) 4A by natural products.* Nat Prod Rep, 2020. **37**(5): p. 609-616.
122. Taroncher-Oldenburg, G., et al., *Targeting the DEAD-Box RNA Helicase eIF4A with Rocaglates-A Pan-Antiviral Strategy for Minimizing the Impact of Future RNA Virus Pandemics.* Microorganisms, 2021. **9**(3).
123. Saradhi, U.V., et al., *Characterization of silvestrol pharmacokinetics in mice using liquid chromatography-tandem mass spectrometry.* AAPS J, 2011. **13**(3): p. 347-56.
124. Gupta, S.V., et al., *Resistance to the translation initiation inhibitor silvestrol is mediated by ABCB1/P-glycoprotein overexpression in acute lymphoblastic leukemia cells.* AAPS J, 2011. **13**(3): p. 357-64.
125. Chu, J., et al., *Rocaglates Induce Gain-of-Function Alterations to eIF4A and eIF4F.* Cell Rep, 2020. **30**(8): p. 2481-2488 e5.
126. Gremke, N., et al., *mTOR-mediated cancer drug resistance suppresses autophagy and generates a druggable metabolic vulnerability.* Nat Commun, 2020. **11**(1): p. 4684.
127. Mills, J.R., et al., *mTORC1 promotes survival through translational control of Mcl-1.* Proc Natl Acad Sci U S A, 2008. **105**(31): p. 10853-8.
128. Lucas, D.M., et al., *The novel plant-derived agent silvestrol has B-cell selective activity in chronic lymphocytic leukemia and acute lymphoblastic leukemia in vitro and in vivo.* Blood, 2009. **113**(19): p. 4656-66.
129. Gandin, V., et al., *Polysome fractionation and analysis of mammalian translatomes on a genome-wide scale.* J Vis Exp, 2014(87).
130. Owen, N., et al., *Enhanced cytarabine-induced killing in OGG1-deficient acute myeloid leukemia cells.* Proc Natl Acad Sci U S A, 2021. **118**(11).
131. Kowolik, C.M., et al., *NT1721, a novel epidithiodiketopiperazine, exhibits potent in vitro and in vivo efficacy against acute myeloid leukemia.* Oncotarget, 2016. **7**(52): p. 86186-86197.
132. Copp, J., G. Manning, and T. Hunter, *TORC-specific phosphorylation of mammalian target of rapamycin (mTOR): phospho-Ser2481 is a marker for intact mTOR signaling complex 2.* Cancer Res, 2009. **69**(5): p. 1821-7.
133. Gingras, A.C., et al., *Regulation of 4E-BP1 phosphorylation: a novel two-step mechanism.* Genes Dev, 1999. **13**(11): p. 1422-37.
134. Ianevski, A., A.K. Giri, and T. Aittokallio, *SynergyFinder 2.0: visual analytics of multi-drug combination synergies.* Nucleic Acids Res, 2020. **48**(W1): p. W488-W493.
135. Mi, Q., et al., *Silvestrol regulates G2/M checkpoint genes independent of p53 activity.* Anticancer Res, 2006. **26**(5A): p. 3349-56.
136. Kong, T., et al., *eIF4A Inhibitors Suppress Cell-Cycle Feedback Response and Acquired Resistance to CDK4/6 Inhibition in Cancer.* Mol Cancer Ther, 2019. **18**(11): p. 2158-2170.
137. Hardy, R.R., P.W. Kincade, and K. Dorshkind, *The protean nature of cells in the B lymphocyte lineage.* Immunity, 2007. **26**(6): p. 703-14.
138. Duy, C., et al., *Chemotherapy Induces Senescence-Like Resilient Cells Capable of Initiating AML Recurrence.* Cancer Discov, 2021. **11**(6): p. 1542-1561.

139. Cencic, R., et al., *Antitumor activity and mechanism of action of the cyclopenta[b]benzofuran, silvestrol.* PLoS One, 2009. **4**(4): p. e5223.
140. Wilmore, S., et al., *Targeted inhibition of eIF4A suppresses B-cell receptor-induced translation and expression of MYC and MCL1 in chronic lymphocytic leukemia cells.* Cell Mol Life Sci, 2021. **78**(17-18): p. 6337-6349.
141. Raineri, S. and J. Mellor, *IDH1: Linking Metabolism and Epigenetics.* Front Genet, 2018. **9**: p. 493.
142. Jones, C.L., et al., *Inhibition of Amino Acid Metabolism Selectively Targets Human Leukemia Stem Cells.* Cancer Cell, 2019. **35**(2): p. 333-335.
143. Stevens, B.M., et al., *Fatty acid metabolism underlies venetoclax resistance in acute myeloid leukemia stem cells.* Nat Cancer, 2020. **1**(12): p. 1176-1187.
144. Chan, K., et al., *eIF4A supports an oncogenic translation program in pancreatic ductal adenocarcinoma.* Nat Commun, 2019. **10**(1): p. 5151.
145. Rogakou, E.P., et al., *DNA double-stranded breaks induce histone H2AX phosphorylation on serine 139.* J Biol Chem, 1998. **273**(10): p. 5858-68.
146. Maynard, S., et al., *Base excision repair of oxidative DNA damage and association with cancer and aging.* Carcinogenesis, 2009. **30**(1): p. 2-10.
147. Zhu, J.Y., et al., *The traditional Chinese herbal compound rocaglamide preferentially induces apoptosis in leukemia cells by modulation of mitogen-activated protein kinase activities.* Int J Cancer, 2007. **121**(8): p. 1839-46.
148. Nishida, Y., et al., *Inhibition of translation initiation factor eIF4a inactivates heat shock factor 1 (HSF1) and exerts anti-leukemia activity in AML.* Leukemia, 2021. **35**(9): p. 2469-2481.
149. ClinicalTrials.gov[Internet]. *Bethesda (MD): National Library of Medicine (US). Identifier: NCT04092673. Study of eFT226 in Subjects With Selected Advanced Solid Tumor Malignancies (Zotatifin).* . 2021.
150. Cheng, H., Z. Zheng, and T. Cheng, *New paradigms on hematopoietic stem cell differentiation.* Protein Cell, 2020. **11**(1): p. 34-44.
151. Langlais, D., et al., *Rocaglates as dual-targeting agents for experimental cerebral malaria.* Proc Natl Acad Sci U S A, 2018. **115**(10): p. E2366-E2375.